The design and optimization of sustainable biopolymer-based adsorbents for the removal of a model aromatic naphthenic acid from aqueous solution

by

Patrick J. Quinlan

A thesis
presented to the University of Waterloo
in fulfillment of the
thesis requirement for the degree of
Master of Applied Science
in
Chemical Engineering (Nanotechnology)

Waterloo, Ontario, Canada, 2015

AUTHOR'S DECLARATION

I hereby declare that I am the sole author of this thesis. This is a true copy of the thesis, including any required final revisions, as accepted by my examiners.

I understand that my thesis may be made electronically available to the public.

ABSTRACT

During the extraction of bitumen from the Alberta oil sands, a wide range of contaminants are concentrated in oil sands process-affected water (OSPW), among which is a family of organic carboxylic acids known collectively as naphthenic acids (NAs). NAs have shown to be both corrosive toward process equipment and acutely toxic toward a number of aquatic organisms. Therefore, for oil sands producers to either recycle OSPW or reintroduce it back into the environment, the concentration of NAs must be reduced to acceptable levels. Adsorption is one technique that has been investigated for their removal. This thesis reports on the removal of a model aromatic NA from aqueous solution using sustainable quaternized chitosan hydrogel adsorbents. Using optimized processing conditions to prepare the adsorbent material, an adsorption efficiency of 315 mg g^{-1} was observed. The kinetic and equilibrium adsorption characteristics were investigated by performing several batch adsorption experiments under a range of conditions. To improve the compressive strength of the hydrogel, cellulose nanocrystals (CNC) and quaternized cellulose nanocrystals (QCNC) were incorporated into the adsorbent formulation. Improvements in compressive strength of up to 179% were observed. However, this improvement was coupled with reductions in the efficiency of model NA adsorption. To the best of our knowledge, this work is one of very few studies to investigate the adsorption of NAs using polymeric resins and is the first to report the use of biopolymer based hydrogels and nanocomposite hydrogels for this application. When compared to other adsorbent materials reported in the literature, the adsorption efficiency of the presently reported material was on par if not superior.

ACKNOWLEDGEMENTS

I would like to express my deepest gratitude towards my supervisor, Professor Michael K. C. Tam, for his constant guidance and support throughout my time in the Laboratory for Functional Colloids and Sustainable Nanomaterials.

I would also like to thank the members of my committee, Drs. Boxin Zhao and Leonardo Simon, for their insightful comments and constructive criticism. Their guidance helped to strengthen the quality of this thesis.

I would also like to extend my sincere gratitude to Drs. Boxin Zhao and Juewen Liu for granting me access to their equipment to provide better characterization of my work. Compression testing was performed using Dr. Zhao's mechanical testing apparatus and zeta potential analysis was performed using Dr. Liu's Malvern Nano ZS Zetasizer DLS system.

Special thanks are due to all of my lab mates who made the past two years such an enjoyable time. Thank you for the many invaluable discussions and support throughout my studies.

Finally, I would like to thank my parents and my partner Jen for their continual love, generosity, and support.

TABLE OF CONTENTS

LIST OF FIGURES

LIST OF TABLES

LIST OF SCHEMES

CHAPTER 1

Introduction

1.1 Background information and motivation for research

1.1.1 Alberta oil sands

Located in northeastern Alberta are three of the world's largest oil deposits. Identified as the Athabasca, Cold Lake, and Peace River deposits based on their geographical location, the three are referred to collectively as the Alberta oil sands. Together they cover approximately 140200 km^2, with estimates of up to 1.7 trillion barrels of oil in place. This places Canada's total oil reserve third in the world, just behind Saudi Arabia and Venezuela, in known volume of crude oil (Schramm, Stasiuk and MacKinnon 2000).

The Alberta oil sands reserves differ significantly from more traditional oil sources. While conventional oil and gas reserves, such as those in the United States and the Middle East, contain crude oil that can under most circumstances flow with ease, the Alberta oil sands bitumen is typically composed of long chain hydrocarbons and contains an interspersed solid particulate matrix, both of which give it an extremely high viscosity (~10000 Pa s at 25°C). This makes the extraction of bitumen a much more challenging process, requiring either heating or solvation or both (Hein, et al. 2013).

Broken down into its three components, oil sands ore is a combination of fine solid particulate (75-85 wt. %), bitumen (1-18 wt. %), and water (5-10 wt. %) (Schramm, Stasiuk and MacKinnon 2000).

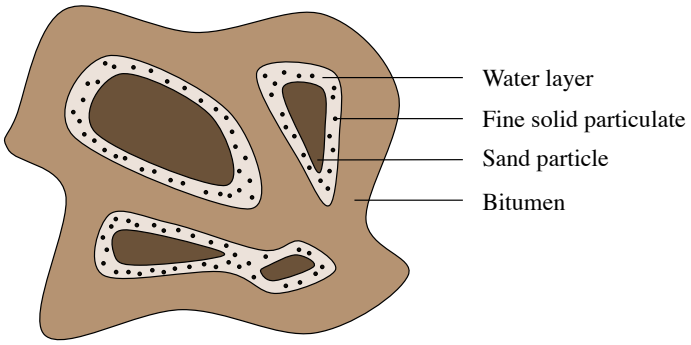

Figure 1.1 General composition of oil sands ore.

The bitumen phase is continuous, but is heavily dispersed with the solid phase, of which approximately 80-90 wt. % is quartz. Surrounding the solid phase, in most cases, is a very thin aqueous layer on the order of 10 nm (Takamura 1982). Due to the particular chemical composition of the solid phase, the solid particles in the Alberta oil sands reserves possess hydrophilic qualities. This important trait is what allows for the use of water as an extraction solvent, making the extraction process economically feasible (Schramm, Stasiuk and Turner 2001).

1.1.2 Acid extractable organic compounds

Naturally present in Alberta oil sands and other oil reserves throughout the world are a family of saturated aliphatic and alicyclic carboxylic acids known collectively as NAs (NAs) (Fan 1991) (Schramm, Stasiuk and MacKinnon 2000). NAs are weak acids with a pK_a in the range of 5-6 (Havre, et al. 2002) (Headley and McMartin 2004) and in alkaline conditions, such as those present in oil sands process-affected water (OSPW), NAs are preferentially soluble in the water phase or at hydrophilic-hydrophobic interphases (Schramm, Stasiuk and MacKinnon 2000).

Studies have shown that NAs present a significant health risk to aquatic and mammalian species upon exposure and may result in both acute and chronic toxicity (MacKinnon and Boerger 1986) (Schramm, Stasiuk and MacKinnon 2000) (Madill, et al. 2001) (Rogers, et al. 2002) (Frank, et al. 2009). As well, NAs have been identified as one of the primary causes of corrosion towards process equipment during bitumen extraction unit operations (Derungs 1956) (Schramm, Stasiuk and MacKinnon 2000) (Fan 1991). While NAs are proven to be toxic and corrosive compounds, their presence is essential for the extraction of bitumen from sand particles (Sanford 1983) (Schramm, Smith and Stone 1984) (Humphries 2008). It has been demonstrated that their concentration in process water directly correlates to extraction efficiency through a parabolic relationship, resulting in an efficiency maximum within a certain concentration range (Sanford 1983) (Schramm and Smith 1984). Therefore, if the concentration of NAs in OSPW is excessively high, bitumen extraction suffers.

As a result, for oil sands producers to (a) remediate OSPW and reintroduce it into the local environment or (b) recycle OSPW and reduce freshwater intake, the concentration of NAs in OSPW must be reduced.

1.1.3 Remediation techniques

A number of novel technologies, spanning advanced oxidation, biodegradation, coagulation/flocculation, membrane filtration, and adsorption, have been developed over the past decade and their ability to remove NAs from OSPW has been demonstrated with relative success. However, each class of technologies possesses limitations. For instance,

many of the works involving advanced oxidation processes reviewed in this article report on the preferential oxidative degradation of bulkier, polycyclic NAs (Legrini, Oliveros and Braun 1993) (Neyens and Baeyens 2003) (Afzal, et al. 2012). Conversely, reports of NA bioremediation often conclude that lower molecular weight NAs with less rings and branching are more easily biodegraded by microbial cultures (Clemente, MacKinnon and Fedorak 2004) (Scott, MacKinnon and Fedorak 2005) (Smith, et al. 2008) (Han, Scott, et al. 2008). In both cases, this selective degradation often leaves behind a number of recalcitrant NAs that persist in OSPW. Coagulation/flocculation processes are often cited as significant producers of sludge (Pourrezaei, et al. 2011) (De Philippis and Micheletti 2009) and the high ionic strength of OSPW often disrupts the destabilization mechanisms that cause flocculant-contaminant complex to settle out of solution (Allen 2008). Meanwhile, fouling, high pressure drop, and low throughput are commonly encountered for membrane filtration processes (Peng, et al. 2004) (Allen 2008). Adsorption, while being a well-developed technology for wastewater treatment, allows for high throughput and, in most cases, comprehensive NA removal.

1.2 Research scope

The research presented in this thesis is concentrated on three main regions:

(a) The optimization of quaternized chitosan hydrogel adsorbents.

The effects of polymer density, degree of crosslinking, and degree of quaternization of quaternized chitosan hydrogels on their swelling and equilibrium adsorption characteristics were investigated. The equilibrium adsorption experiments involved the removal of 2-

naphthoxyacetic acid, a model NA, from aqueous solution. Based on the modeled adsorption efficiencies of the formulations using the Langmuir adsorption isotherm, a formulation in which adsorption efficiency was maximized was obtained.

(b) Investigation of the kinetic, equilibrium, and thermodynamic characteristics involved with the adsorption of a model NA from aqueous solution using quaternized chitosan hydrogel adsorbents.

The optimized adsorbent formulation was used to remove 2-naphthoxyacetic acid, a model aromatic NA, from alkaline aqueous solution. The effects of adsorbate concentration, adsorbent dosage, agitation rate, solution pH, monovalent ionic strength, and temperature on the kinetics of adsorption were modeled using the pseudo second order rate equation. The equilibrium adsorption characteristics for the optimized adsorbent formulation were modeled using the Langmuir adsorption isotherm. The thermodynamic parameters associated with the adsorption process were also determined. The regenerability and cyclability of the adsorbent material was demonstrated.

(c) The development of novel quaternized cellulose nanocrystal-chitosan nanocomposite hydrogels for the adsorption of a model NA from aqueous solution.

CNC and QCNC were incorporated at different loadings into the quaternized chitosan hydrogel matrix of the optimized adsorbent formulation to improve the mechanical strength of the material. The effects on swelling behaviour, adsorption efficiency, and compressive strength were reported.

1.3 Thesis outline

This thesis consists of seven chapters. Chapter 1 provides background information describing the motivation behind this research, as well as the scope of the work presented herein. Chapter 2 provides an in depth literature review describing some of the current practices used for NA removal or remediation. Special attention is paid to adsorbent materials used to remove NAs from aqueous solution. Chapter 3 discusses some of the general theory surrounding adsorption. Chapter 4 addresses the first two objectives outlined in the research scope and is titled, "Optimized adsorption of a model aromatic naphthenic acid from aqueous solution using sustainable quaternized chitosan hydrogels". Chapter 5 addresses the last objective outlined in the research scope and is titled, "The development of novel quaternized cellulose nanocrystal-chitosan nanocomposite hydrogels for the adsorption of a model aromatic naphthenic acid from aqueous solution". Chapter 6 provides a general summary of the findings reported in Chapters 4 and 5. Chapter 7 highlights recommendations for future work based on the conclusions of this research. Following Chapter 7 are, in order, an alphabetical list of references used throughout the entire report, Appendix A, providing secondary data for Chapter 4, and Appendix B, providing secondary data for Chapter 5.

CHAPTER 2

Literature review

2.1 Oil sands mining operations

While crude oil reservoirs can be mined using traditional drilling methods that take advantage of oil displacement and capillary forces (Sah 2003), the high viscosity and mixed composition of oil sands bitumen limits their extraction to specialized mining techniques, the most common being surface and in situ mining (Hein, et al. 2013).

2.1.1 Surface mining

Surface mining is the more traditional approach to isolating bitumen from oil sands ore. The bituminous ore, including bitumen, solid particulate, and water, is removed from shallow deposits using either large draglines or shovels and is transported to a separate site for processing and separation. The ore is combined with high temperature alkaline water and is mixed to create a slurry. Thermal and mechanical energy are employed to overcome the forces holding the ore together in clusters (Schramm, Stasiuk and Turner 2001). Air is sparged into the mixing tank and the bitumen rich froth, which accumulates at the top of the tank, is skimmed off. This process is often repeated a number of times before the froth is further separated using centrifugation and additional filtration units. Distillation is then used to isolate a purified bitumen product for upgrading (Schramm, Stasiuk and MacKinnon 2000) (Humphries 2008). While the extraction processes amongst different surface mining operations typically vary, they all loosely follow this general procedure.

2.1.2 In situ mining

In situ mining is a less conventional approach to isolating bitumen from oil sands ore, but, over the past 25 years, has become much more widespread in Alberta. For in situ

recovery, a three-stage process is used: (1) alkaline steam is injected approximately 100 metres underground to the reservoir using a pipeline; (2) the steam and condensed water heat the bitumen ore, reducing its viscosity and allowing the bitumen to flow like conventional oil; and (3) the heated mixture of water, bitumen, and dissolved fine solids are pumped to the surface for separation by centrifugation and distillation. While in situ mining typically requires less water and results in less ground clearance, an elevated level of greenhouse gas and SO_2 emissions often accompanies it (Humphries 2008).

2.2 Naphthenic acids (NAs)

2.2.1 Molecular structure and physical properties

Naturally present in Alberta oil sands and other oil reserves throughout the world are a family of saturated aliphatic and alicyclic carboxylic acids known collectively as NAs (NAs) (Fan 1991) (Schramm, Stasiuk and MacKinnon 2000). Produced by the oxidation of hydrocarbons, NAs are amphiphilic compounds, in which the hydrophobic segment is often composed of saturated 5- or 6-carbon rings in a variety of combinations, and the hydrophilic segment is present in a carboxyl group, separated from the ring structure by a carbon chain of at least two units in length. Acyclic NAs also exist, but are more likely to be branched (Clemente, Prasad, et al. 2003).

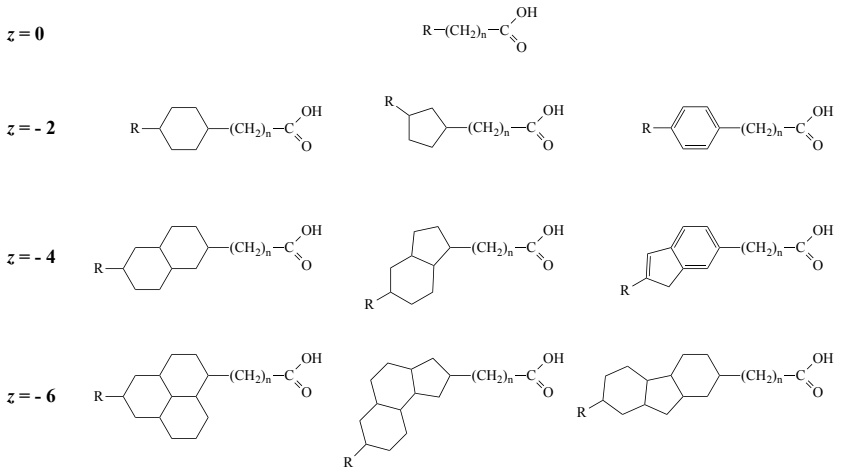

Figure 2.1 Generalized molecular structure of some monoacidic NAs.

NAs may be defined by the general chemical formula $C_mH_{2m+n}O_xN_yS_z$, where *m* is the carbon number, *n* is a negative even integer corresponding to hydrogen deficiency resulting from ring formation in the organic segment, and *x*, *y*, and *z*, are the oxygen, nitrogen, and sulphur numbers (Schramm, Stasiuk and Turner 2001), which for 'classical' NAs are equal to 2, 0, and 0, respectively (Headley and McMartin 2004) (Mapolelo, et al. 2011). The carbon number (*m*) for most NAs is typically in the range of C_{13} to C_{27} (Clemente, Prasad, et al. 2003). Aromatic, steroidal, and multi-acidic NAs have also been documented (Jones, et al. 2012) (Rowland, et al. 2011) (Frank, et al. 2009).

NAs are weak acids with a pK_a in the range of 5-6 (Havre, et al. 2002) (Headley and McMartin 2004). Therefore, below pH 5, NAs are preferentially soluble in the hydrophobic phase and above pH 6, NAs are preferentially soluble in the hydrophilic phase. Compared to synthetic anionic surfactants, NAs have a lower preference for the aqueous phase, but remain water soluble in alkaline conditions, nonetheless (Schramm, Stasiuk and MacKinnon 2000).

During the extraction of bitumen from oil sands ore, NAs are solubilized and concentrated in slightly alkaline (pH ~ 8.5) OSPW (Schramm, Stasiuk and MacKinnon 2000). The ambient concentration of NAs in rivers and waterways in northern Alberta is typically below 1 mg l^{-1}, while the concentration of NAs may be as high as 110 mg l^{-1} (Conrad Environmental Aquatics Technical Advisory Group (CEATAG) 1998). In aged tailings pond water, NAs are usually present in concentrations ranging from 40 to 70 mg l^{-1}, a figure slightly reduced by the natural microbial biodegradation processes present (Allen 2008).

Table 2.1 General physical and chemical properties of acid extractable organic compounds.

Parameter	General characteristics	References
Color	Pale yellow to dark amber	(Brient, Wessner and Doyle 1995)
State	Viscous liquid	(Brient, Wessner and Doyle 1995)
Molecular weight	140-450 g mol^{-1}	(Schramm, Stasiuk and MacKinnon 2000) (Kannel and Gan 2012)
Density	0.97-0.99 g cm^{-3}	(Armstrong 2008)
Water solubility	< 50 mg l^{-1}	(Brient, Wessner and Doyle 1995)
Dissociation constant	5 – 6	(Havre, et al. 2002) (Headley and McMartin 2004)
Boiling point	250 – 350°C	(Brient, Wessner and Doyle 1995)
Acid number	150 – 310 mg KOH g^{-1}	(Brient, Wessner and Doyle 1995) (Pyhälä 1914)
Refractive index	~ 1.5	(Armstrong 2008)

2.2.2 Origin

NAs originate in petroleum deposits and are believed to be a result of two natural phenomena: (a) partial aerobic biodegradation (Watson, et al. 2002) and (b) incomplete catagenesis (Clemente and Fedorak 2005) of bituminous compounds. Natural geological events, such as earthquakes and erosion, expose bitumen to environments that are ideal for aerobic biodegradation and the high pressure and temperatures found in some petroleum deposits may result in catagenesis of organic matter.

2.2.3 Corrosivity

NAs are of interest to those associated with bitumen production for a number of reasons. In the early twentieth century, it was discovered that NAs played a major role in the corrosion of process equipment used in the upgrading and refining stages of petroleum processing (Derungs 1956) (Schramm, Stasiuk and MacKinnon 2000). NAs present in the liquid phase have been reported to induce corrosion when process temperatures lie within the range of approximately 200-400°C (Fan 1991) (Brient, Wessner and Doyle 1995). The corrosion mechanism involving NAs is poorly understood. It has been proposed, however, that at high temperatures, NA multimers in solution disassociate into their monomeric form and those present at the surface of equipment materials form metal carboxylates with nearby metal ions (Scheme 2.1) (Chakravarti, et al. 2013). The mobilization of these complexes away from the metal surface and into the bulk fluid leads to local degradation of the metal surface. The rate of corrosion by this process is hastened by increases in the flowrate and turbulence of the bulk fluid phase, as well as increases in overall process

temperature, all of which participate in the rate of mass transfer from the surface to the bulk (Lochte and Littmann 1955) (Gutzeit 1977) (Schramm, Stasiuk and MacKinnon 2000).

Scheme 2.1 NA corrosion mechanism proposed by Chakravarti et al. (2013).

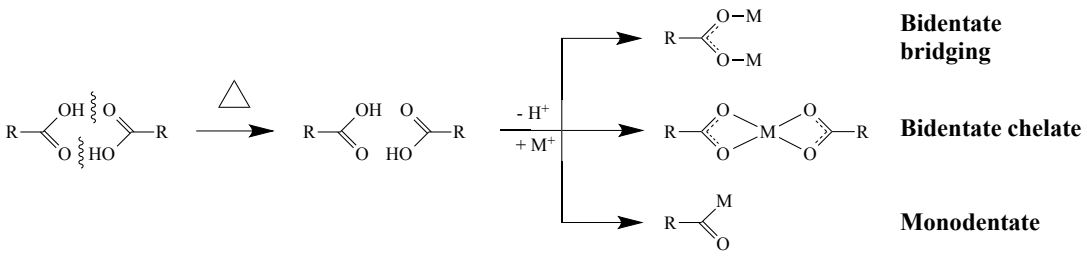

2.2.4 Toxicity

Aside from corrosivity, there is also concern regarding the toxicity of NAs. In fact, NAs are believed to be the most toxic compounds present in OSPW (MacKinnon and Boerger 1986) (Schramm, Stasiuk and MacKinnon 2000) (Madill, et al. 2001). Their toxicity is often attributed to their surface-active behaviour (Rogers, et al. 2002), with the primary mode of toxicity suggested to be non-specific narcosis via cell membrane disruption (Frank, et al. 2009). In a study by MacKinnon and Boerger (1986), the removal of NAs alone from OSPW significantly reduced its acute lethality towards rainbow trout (*Onchorhynchus mykiss*) and water fleas (*Daphnia magna*). Rogers et al. (2002) found the acute toxicity of NAs present in the drinking water of Wistar rats (*Rattus norvegicus*) at concentrations commonly observed in OSPW to be relatively low. Still, they did observe adverse health affects from repeated low doses, suggesting the subchronic toxicity of low-dose NAs towards mammalian species similar in size and habit to the Wistar rat.

Frank et al. (2009) suggested that NA toxicity is in close relation to the hydrophobicity of the compound. In controlled studies using individual surrogate NAs of varying structure, it was observed that toxicity of monoacidic NAs increased with molecular weight, but that the introduction of additional carboxylic acid groups on the NA molecule resulted in lower toxicity. Interestingly, they also observed that, in general, NAs of higher molecular weight often possessed more than one carboxylic acid groups, which lead to a reduced overall toxicity when compared with smaller monoacidic NAs.

2.2.5 Role of NAs in bitumen recovery

While NAs are proven to be toxic and corrosive compounds, their presence is essential for the extraction of bitumen from sand particles (Sanford 1983). Under basic conditions, the carboxylic acids of NAs are present as the carboxylate salts, giving the molecule strong amphiphilic behaviour. The negatively charged carboxylates are soluble in water, while the hydrophobic segment preferentially adsorbs to the air-water interface or, under certain conditions, causes the NAs to self-assemble into micelles (Havre, et al. 2002) (Havre, Sjöblom and Vindstad 2003) (Mohamed, Wilson and Peru, et al. 2013). Because of these qualities, NAs are classified as surface-active components.

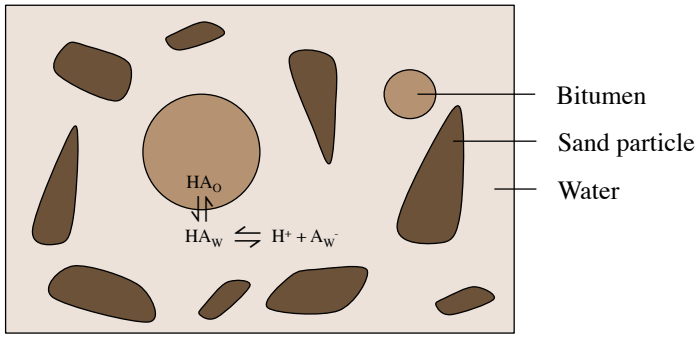

Figure 2.2 NA equilibrium in oil sands slurry under alkaline conditions.

The surface-active behaviour associated with NAs has proven to be of significant aid in primary bitumen recovery, especially in low-grade bitumen ore (i.e. ore with a low bitumen fraction). From early research in the Alberta oil sands, it was understood that the addition of NaOH to the process water improved bitumen recovery (Humphries 2008), but it was not until the latter half of the twentieth century that the effect of NAs and their ability to aid in oil recovery were specifically identified and recognized (Schramm, Smith and Stone 1984). The addition of NaOH neutralizes NAs to carboxylates, which, at a critical concentration, allows for optimal oil recovery (Sanford 1983) (Schramm and Smith 1984), as shown in Figure 2.3.

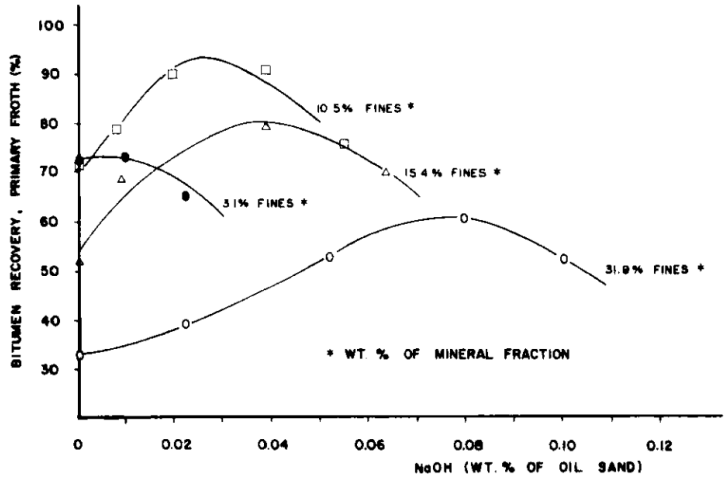

Figure 2.3 Processability curves as a function of NaOH concentration for oil sands of different composition (Sanford 1983).

The recovery of bitumen from oil sands is, generally, a two-stage process (Schramm, Stasiuk and MacKinnon 2000). The first step, which takes place in the flooding of oil sands ore with alkaline water, is bitumen-solid separation. This involves the adsorption of anionic NAs at the interface between the solid sand particles and the bituminous coating that

surrounds them. The adsorbed NAs act as a wedge between the two phases, causing them to electrostatically repel one another. This eventually results in the ejection of bitumen droplets into the aqueous phase. The second step, bitumen-air adhesion, occurs during the flotation process. The efficiency of this stage hinges on the degree of adhesion between solubilized bitumen droplets and the bubbles of air sparged into the system. However, NAs may also adsorb on the surface of the air bubbles, introducing undesired electrostatic repulsive forces that counter bitumen-air adhesion. Therefore, there is an optimal concentration of NAs in OSPW. There must be enough NAs present to promote repulsion and separation between the bitumen droplets and sand particles, but not so much so as to hinder the bitumen-air adhesion process (Schramm, Stasiuk and MacKinnon 2000).

2.3 Methods of NA removal or remediation

In an effort to improve the recyclability and/or reduce the acute toxicity of OSPW, several methods have been developed to remove or remediate NAs. These include but are not limited to advanced oxidation, biodegradation, flocculation, membrane filtration, and adsorption (Allen 2008).

2.3.1 Advanced oxidation

Advanced oxidation is a broad term for processes in which chemical compounds are partially or completely degraded through oxidation reactions with hydroxyl radicals (Andreozzi, et al. 1999). There is a wide range of advanced oxidation processes used in wastewater treatment, such as photocatalysis and Fenton's peroxidation, which are

characterized by the system of reactions used to produce reactive hydroxyl radicals that go on to decompose compounds (Hendricks 2006).

Perez-Estrada et al. (2011) investigated the use of ozonation to oxidize NAs from OSPW. In alkaline conditions, they found that ozone decomposed to form hydroxyl radicals, which in turn reacted with NAs. It was determined that NAs of greater molecular weight more readily decomposed. Using this process, up to 61% removal was accomplished. The same group, in 2012, also investigated the relative reactivity of NAs using a UV/H_2O_2 advanced oxidation process (Afzal, et al. 2012). Similar to the previous study, NAs of greater molecular wright were preferentially oxidized. Degradation rates of up to 99% were achieved under some experimental conditions.

In many cases, advanced oxidation processes only partially degrade their chemical precursors (Legrini, Oliveros and Braun 1993) (Neyens and Baeyens 2003). In the case of OSPW treatment, this could pose as a significant hurdle, as it may result in products of greater toxicity than the initial NAs (Afzal, et al. 2012). As well, advanced oxidation processes are often resource intensive, resulting in high operating costs (Oller, Malato and Sánchez-Pérez 2011). This becomes especially true when aiming to achieve complete oxidation because reaction intermediates are often more resistant to degradation, requiring a greater amount of resources (energy or chemical reactants, depending on the oxidation method) (Muñoz, et al. 2005).

2.3.2 Biodegradation

Similar to advanced oxidation processes, certain microbes possess the ability to naturally metabolize soluble organic matter, resulting in either partial or complete degradation. Products of biodegradation are often carbon dioxide and new biomass (Grady, Daigger and Lim 1999). Complete mineralization of precursor chemicals would result in only carbon dioxide evolution.

A number of microorganisms have been shown to metabolize NAs, including *Acinetobacter anitratum*, *Alcaligenes faecalis*, and *Pseudomonas putida* (Del Rio, et al. 2006). It is believe that the degradation pathway is dominated by β-oxidation, but α-oxidation and aromatization may also play a contributing role (Han, Scott, et al. 2008). Clemente et al. (2004) illustrated the biodegradation of commercial NA preparations using microorganisms native to tailings ponds. Microbes native to OSPW were selected for the study, as they are often resistant to the toxic effects of NAs. They observed that within 10 days of incubation under aerobic conditions, the concentration of NA declined by more than 90%, from approximately 100 mg l^{-1} to less than 10 mg l^{-1}. They also observed that NAs of lesser molecular weight were more prone to biodegradation, which opposes the trend observed for most advanced oxidation processes. Scott et al. (2005) compared the biodegradation of commercial NA preparations with actual OSPW extracts containing native NAs. Their findings suggested that native NAs present in OSPW are much less biodegradable than solutions prepared using commercial NAs. For commercial NA preparations, removal rates of 77-93% were observed within 10 days of incubations. Conversely, only approximately 25% of the native NAs were removed within 40-49 days.

The authors indicate that the disparity is likely a result of the fact that the commercial NAs were of much lesser molecular weight compared to the native NAs.

One of the primary issues relating to NA biodegradation is the structure selectivity. Aside from the size selectivity observed by Clemente et al. (2004) and Scott et al. (2005), studies have also demonstrated that NAs with more rings and alkyl chain branching are often less prone to biodegradation (Smith, et al. 2008) (Han, Scott, et al. 2008). As well, biodegradation in some cases is a very slow process, taking months or even years to degrade some recalcitrant species (Scott, MacKinnon and Fedorak 2005) (Han, MacKinnon and Martin 2009). As a result, biodegradation may play a role in the remediation of OSPW, but would likely require the use of alternative remediation techniques in combination (Clemente, MacKinnon and Fedorak 2004).

2.3.3 Flocculation

Flocculation processes involve the collision of small particles to form larger particles, which are then separated from solution by either flotation or settling. It is usually a two-stage process, where dissolved particles or suspended solids first coagulate to form what are known as microflocs. These microflocs then agglomerate to form flocs. The formation of microflocs is typically a result of electrostatic attraction between the compound of interest and a polyelectrolyte. The combination results in charge neutralization and instability in aqueous solution (Hendricks 2006).

Pourrezaei et al. (2011) demonstrated the removal of NAs from OSPW using a two-step flocculation process. First, a metallic salt was dispersed in the OSPW under rapid mixing to

form microflocs with the dissolved NAs via electrostatic interaction. Then, a cationic polymer was added under slow mixing to bridge between microflocs and form larger flocs that could settle out of solution. Using this treatment method, the authors were able to achieve 37% removal of NAs and 86% removal of oxidized NAs. NAs of higher molecular weight were preferentially removed. Bjornen (2014) removed NAs from wastewater using an electrocoagulation method, where a sacrificial anode made of iron or aluminum was oxidized under high current density to produce metal cations in solution. The production of positively charged species caused the coagulation and subsequent flocculation of NAs dissolved in the water. Up to 93% removal was obtained using this method.

While flocculation processes are often energy efficient and simple to maintain (Hendricks 2006), there are associated limitations. Typically, for flocculation processes to effectively remove dissolved contaminants, a surplus of chemical flocculants is required. This is often accompanied by excessive operating costs for the materials consumed. As well, once settling has occurred within the process, large volumes of sludge are produced as a waste product (De Philippis and Micheletti 2009).

2.3.4 Membrane filtration

Membrane filtration is a broad term describing a process wherein a fluid is passed through a porous immobilized solid material, allowing for the removal of select solutes from the fluid stream (Hendricks 2006). The mechanism of removal may include electrostatic attraction or size exclusion. Membrane technologies are often categorized depending on the size of the smallest solute they are capable of rejecting (Taylor and Duranceau 2000).

Peng et al. (2004) explored the use of three commercial polymeric nanofiltration membranes for the removal of NAs from OSPW. Maintaining a commercially acceptable permeate flux of 15 l m^{-2} h^{-1} at a trans-membrane pressure of 10.3 bar, they were able to achieve greater than 95% removal. While significant fouling was observed during the course of the 18 h experiment, it was found to be reversible, allowing for continued use of the membranes. Alpatova et al. (2014) investigated the use of a commercial ceramic ultrafiltration membrane to remove dissolved organic and inorganic solutes from OSPW. First, aluminum sulphate was added to the OSPW to coagulate dissolved species and was then passed through the membrane with a pressure of 2.8 bar. While relatively high removal rates were observed for particulates and chemical oxygen demand, only 12.4% of NAs were removed under the conditions studied.

An apparent limitation of membrane filtration processes is fouling. Fouling not only limits the removal efficiency of the membrane, but also reduces the flux through the membrane (Hendricks 2006). Therefore, to maintain a constant effluent flowrate under fouling conditions, the trans-membrane pressure must be increased. However, the pressure across the membrane is also limited by the mechanical strength of the membrane material (Riffat 2013).

2.3.5 Adsorption

Adsorption is a physical or chemical process wherein an adsorbate, a solution-based solute, preferentially concentrates at an interface (Hendricks 2006). This results in a concentration profile, where the solute concentration increases towards the interface. The adsorption process is exothermic and is driven by the unique surface energetics of bulk

materials, a result of the bonding deficiencies experienced by atoms at a material's external surface (Israelachvilli 2011). Depending on the mode of adsorption, the adsorbate may accumulate on the interface in a monolayer or multilayer.

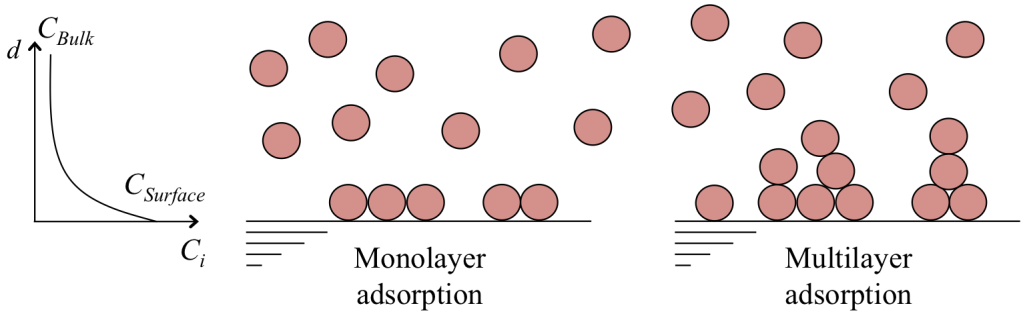

Figure 2.4 Monolayer and multilayer adsorption.

The most common adsorbent investigated for the removal of NAs from OSPW is activated carbon (Hendricks 2006). Mohamed et al. (2008) explored the use of commercial granular activated carbon for NA removal and, under the experimental conditions used, observed a maximum adsorption efficiency of 159 mg g^{-1}, as estimated by the Langmuir equilibrium adsorption isotherm. Sarkar (2013) studied the adsorption of a single-ring model NA from simulated process water using petroleum coke-derived activated carbons that varied in both overall surface area and functionality. It was observed that activated carbons with higher surface area and ammonia surface functionality offered optimal adsorption with removal rates of up to 98%. Gong and Yao (2012) investigated the use of spent fluid catalytic cracking catalyst for the adsorption of NAs from OSPW. The exterior and pore surfaces of the zeolite-based catalyst, after exposure to hydrocarbon cracking, was coated with carbon and provided the material with an active surface for adsorption. Under the experimental conditions studied, an adsorption efficiency of approximately 52 mg g^{-1}

was achieved. Most recently, Iranmanesh et al. (2014) produced activate carbons from sawdust using both chemical and physical activation processes for the removal of NAs from OSPW. The chemically activated carbon possessed a higher surface area and, thus, resulted in greater adsorption efficiency (up to 35 mg g^{-1}). While activated carbons tend to possess high porosity and specific surface area that lend to their adsorption efficiency, the cost of commercial activated carbons may be prohibitive (Sarkar 2013). Small et al. (2012) also found that activated carbons derived from coke tend to leach heavy metals, such as magnesium, nickel, cobalt, vanadium, and copper, which could result in the secondary concern of inorganic toxicity in reclaimed OSPW. As well, the activation process, while necessary to achieve suitable specific surface areas, is often energy intensive and may produce air emissions that contain particulate matter and volatile organic compounds (Cecen and Aktas 2012). The use of activated carbons derived from waste products may remain economical, though, depending on their removal efficiencies.

Other adsorbent materials explored for the removal of NAs from wastewater include clay and synthetic resins (Zou, et al. 1997) (Mohamed, Wilson and Headley, et al. 2008) (Gaikar and Maiti 1996). Zou et al. (1997) investigated the adsorption process of NAs onto the surfaces of montmorillonite, kaolinite, and illite using calorimetry. They observed that the process was driven by two surface interactions. First, the carboxylate group of the NA molecules participated with polar atoms or water molecules bound to the clay surface by hydrogen bonding. Second, the hydrophobic segment of NA molecules was found to bond to the clay surface through van der Waals interactions. They concluded that clays with a greater specific surface area performed better as adsorbents. Mohamed et al. (2008)

prepared synthetic polymer networks with β-cyclodextrin (β-CD) functionality. The ability of the β-CD to complex with hydrophobic molecules allowed for the adsorption of NAs, with the hydrophobic segment of the NAs centred within the β-CD. Under the conditions studies, adsorption efficiencies of 20-30 mg g^{-1} were achieved. As suggested by the authors, the specific surface area of the adsorbent limited the removal efficiency. Gaikar and Maiti (1996) studied the use of commercial anion exchange resins with tertiary or quaternary amine functionality to remove NAs from a continuous water stream. To achieve adequate rates of adsorption using the resins with tertiary amine functionality, the inlet water stream required acidification. Conversely, the resins with quaternary amine functionality performed well in the native alkaline conditions. These findings suggested that the mode of adsorption between NAs and anion exchange resins was primarily electrostatic. However, structural factors, such as porosity and functional group accessibility, dictated the overall adsorption efficiency, which, among the resins studies, ranged from 15.5-92 mg g^{-1}.

2.4 Chitosan as a sustainable adsorbent

2.4.1 Chitosan

Chitosan (CS) is a random linear copolysaccharide constituted of β-linked D-glucosamine and N-acetyl-D-glucosamine (Rinaudo 2006). It is a deacetylated derivative of chitin, the second most abundant polymer in the world, after cellulose (Tharanathan and Kittur 2003). CS is defined as having a degree of deacetylation (DD) of 50% or greater, i.e. the molar fraction of D-glucosamine units is greater than the molar fraction of N-acetyl-D-glucosamine units present within the copolymer chain. The opposite is true for chitin. The

deacetylation process involves mixing chitin in 40% sodium hydroxide at 120°C for 1 to 3 hours (M. N. Kumar 2000). The source of most of the chitin and, consequently, CS used for practical applications is the exoskeleton of marine crustaceans, such as shrimp and crab (M. N. Kumar, A review of chitin and chitosan application 2000) (Rinaudo 2006). Other sources include fungi (Teng, et al. 2001) and yeast (Roelofsen and Hoette 1951).

Chitosan is an attractive material for functional applications in wastewater treatment for a number of reasons. Being an abundant, natural biopolymer derived from food industry waste makes its production feasible (M. N. Kumar 2000). Also, its solubility properties allow for processing and modification reactions to be carried out in aqueous media (pH < 5). Simple crosslinking reactions with chitosan have been well studied (Monteiro and Airoldi, Some studies of crosslinking chitosan - glutaraldehyde interaction in a homogenous system 1999) (Mi, Sung and Shyu 2000) (Berger, et al. 2004) (Hudson and Jenkins 2004), as has its use as a matrix material in hydrogels (Chatterjee, Lee and Woo 2010) (Baysal, et al. 2013) (Chen, et al. 2013).

Scheme 2.2 Deacetylation reaction of chitin to form chitosan.

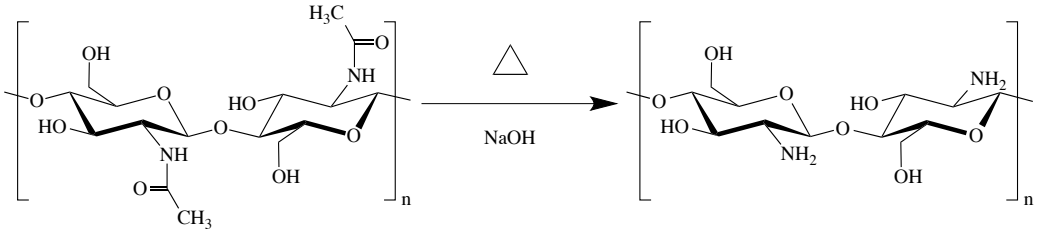

2.4.2 Chitosan hydrogel adsorbents

Hydrogels are highly porous three-dimensional polymer networks, which, in the presence of water, swell to many times their dry mass (Hoffman 2002). Their high porosity lends to their exceptional ability as adsorbents (Baysal, et al. 2013). Li and Bai (2005) investigated the use of covalently crosslinked chitosan hydrogel beads for the adsorption of metal ions from aqueous solution. The authors proposed a novel crosslinking method that involved the shielding of the amine groups of chitosan by reaction with formaldehyde to limit the crosslinking of the polymer to only the hydroxyl groups. The crosslinking agent used was ethyleneglycol diglycidyl ether (EGDE). This crosslinking approach maintained a high degree of free amine groups to participate as active sites for adsorption, which could be protonated by the addition of hydrochloric acid. While this approach did improve the adsorption capacity of the hydrogel beads, the production process was resource intensive. Yan and Bai (2005) studied the adsorption of lead ions and humic acid onto non-crosslinked chitosan hydrogel beads under mildly acidic and neutral conditions. The authors observed that the hydrogels remained intact even under mildly acidic conditions due to the low deprotonation of the amine group and the strong hydrogen bonding that existed between chitosan chains. The lead ions were observed to complex with the nitrogen atoms on chitosan and the humic acid was observed to locally protonate amine groups and bind electrostatically. It is likely that this system would lack the robustness found in covalently gelled systems, limiting the useful lifetime and regenerability of the material. Chiou and coworkers (2004) studied the adsorption of anionic dyes in acidic solution using chitosan hydrogel beads covalently crosslinking with epichlorohydrin. The covalent

crosslinking allowed the hydrogels to avoid solubilization under acidic condition, regardless of protonation of the amine groups. Adsorption capacities of up to 2498 mg g^{-1} were observed for the high molecular weight dyes studied.

Electrostatic adsorption of solute onto chitosan is limited by the pH of the solution. At low pH, the C_2 amine groups of chitosan exit in their protonated and, thus, positively charged state. This charge allows it to electrostatically bind with anionic chemical species in solution. At high pH, above the pK_a of chitosan, the amine group exists primarily in the deprotonated state. As a result, the polymer loses its hydrophilicity and its positive charge, barring the material from electrostatically bonding with anions. To combat this circumstance and permit chitosan-based materials to electrostatically adsorb anionic solute under neutral and alkaline conditions, a number of groups have reported the functionalization of chitosan with quaternary ammonium moieties (Qin, et al. 2003) (Wang, et al. 2008) (Zhang, et al. 2011) (Sowmya and Meenakshi 2013). Qin et al. (2003) prepared epichlorohydrin crosslinked chitosan microspheres with the amine groups of chitosan covalently shielded. The amine groups were unshielded and quaternized by reaction with glycidyltrimethylammonium chloride. The quaternized chitosan microspheres were used to remove chromium (VI) ions from aqueous solutions via electrostatic adsorption. While the adsorption of chromium onto the non-quaternized chitosan was limited to acidic pH, the functionality of the quaternized derivative was extended over the pH range of 3 to 11. The high ionic strength of solution under extremely acidic or basic conditions limited the adsorption efficiency of the adsorbent material due to electrostatic charge screening. In more recent work by Sowmya and Meenakshi (2013) investigated the adsorption of

inorganic anionic solutes onto quaternized chitosan hydrogel beads. The chitosan hydrogel beads were first crosslinked using glutaraldehyde, then quaternized by reaction with glycidyltrimethylammonium chloride. The authors observed adsorption capacities of 67.5 and 59.0 mg g^{-1} toward nitrate and phosphate anions, respectively, from highly concentrated solutions. The adsorbent material was also demonstrated to be regenerable for more than 10 cycles.

CHAPTER 3

Adsorption theory

3.1 Theoretical overview of adsorption

Adsorption is a phase transfer process wherein a chemical species preferentially concentrates at an interface (Hendricks 2006). In the treatment of wastewater, adsorption processes are used to remove dissolved compounds (adsorbate) from an inlet water stream and localize them on the surface of a solid substrate (adsorbent), yielding water of higher purity in the effluent.

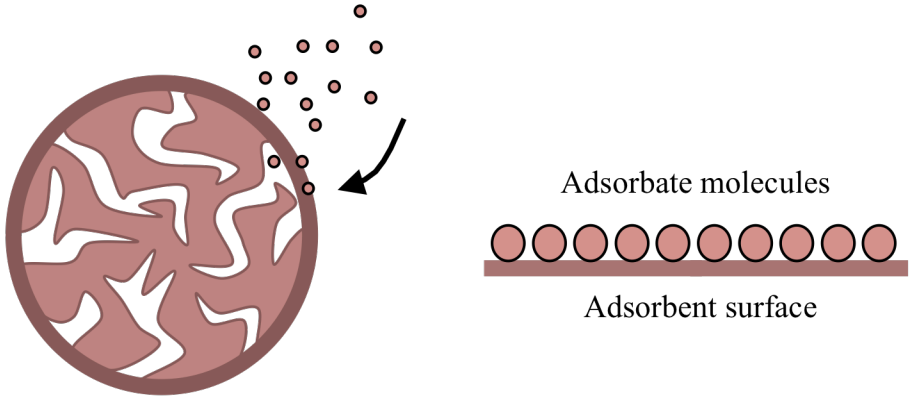

Figure 3.1 Adsorption of adsorbate molecules onto a solid adsorbent surface.

As a result of this concentration of like species, the entropy of the system decreases, i.e. $dS < 0$. If we consider the following:

$$dG = dH - TdS \tag{3.1}$$

where dG is the change in Gibbs free energy of the system (J mol^{-1}), dH is the change in enthalpy of the system (J mol^{-1}), T is the temperature of the system (K), and dS is the change in entropy of the system (J mol^{-1} K^{-1}), then we observe that for an adsorption process to proceed spontaneously, i.e. $dG < 0$, the system must be exothermic, i.e. $dH < 0$.

Therefore, as temperature increases, we expect the maximum adsorption efficiency to decrease.

Another very important concept in adsorption processes is the specific adsorption of an adsorbent, q (mg g^{-1}). In a liquid-solid system, it is defined as the amount of adsorbate removed from the bulk liquid phase and adsorbed to the adsorbent surface per mass of adsorbent (Hendricks 2006). For a batch system of constant volume, the specific adsorption may be calculated as follows:

$$q = \frac{(C_o - C)V}{m} \tag{3.2}$$

where C_o is the initial concentration of solute in the bulk liquid (mg l^{-1}), C is the concentration of the solute in the bulk liquid at time t (mg l^{-1}), V is the volume of the system (l), and m is the mass of the adsorbent (g). The specific adsorption alludes to the adsorption efficiency of an adsorbent, that is, how much solute can be adsorbed by a given mass of adsorbent. At equilibrium, Eq. 2 may be modified to give the specific adsorption of an adsorbent at equilibrium, q_e (mg g^{-1}):

$$q_e = \frac{(C_o - C_e)V}{m} \tag{3.3}$$

where C_e is the concentration of the solute in the bulk liquid at equilibrium (mg l^{-1}).

3.2 Modes of adsorption

The driving force for adsorption may differ between processes and is dependent on the adsorbate-adsorbent interaction (Hendricks 2006) (Worch 2012). Most adsorption

processes can be grouped into one of three categories, though: (a) physical adsorption, (b) chemical adsorption, and (c) electrostatic adsorption (Inglezakis and Poulopoulos 2006).

3.2.1 Physical adsorption

Physical adsorption, often referred to as physisorption, is driven by weak intermolecular interactions, such as van der Waals and hydrogen bonding, between the adsorbate and the surface of the adsorbent (Worch 2012). These interactions are not site-specific and allow the adsorbate to adsorb at any point on the surface of the adsorbent. The interaction energy for this process is comparable to the heat of vapourization (Inglezakis and Poulopoulos 2006). The adsorbate may adsorb in a monolayer fashion, wherein the depth of the adsorbed molecules is limited to one molecule, or in a multilayer fashion, characterized by the stacking of adsorbate molecules on the surface of the adsorbent (Hendricks 2006). Due to the relative weakness of the interactions in physical adsorption processes, the adsorbate is free to migrate across the surface of the adsorbent. Typically, physical adsorption processes are characterized by an enthalpy change of -25 kJ mol^{-1} or less and may be reversed by reducing the concentration of the adsorbate in the bulk (Worch 2012). Due to the low heat of adsorption, physical adsorption processes are only stable at temperatures below 150°C (Inglezakis and Poulopoulos 2006).

3.2.2 Chemical adsorption

The adsorption of adsorbate to an adsorbent surface via a chemical bond is referred to as chemical adsorption, or chemisorption (Worch 2012). Chemical adsorption typically only occurs at specific sites on the surface of the adsorbent due to localized surface energetics or

chemical functionality. The interaction energy for chemical adsorption processes is comparable to the strength of chemical bonds and are quite stable at high temperatures (Inglezakis and Poulopoulos 2006). As a result of the site specificity, chemical adsorption usually occurs only in monolayer fashion and is often a non-reversible process (Davis 2012). The enthalpy change associated with chemical adsorption typically lies in the range of -40 – 800 kJ mol^{-1} (Inglezakis and Poulopoulos 2006). The rate of chemical adsorption processes may be much greater than physical adsorption and, thus, it may take much longer periods of time to approach equilibrium (Davis 2012).

3.2.3 Electrostatic adsorption (ion exchange)

Electrostatic adsorption is another class of adsorption processes and is driven by Coulombic attraction between the adsorbate and adsorbent (Worch 2012). Similar to chemical adsorption processes, electrostatic adsorption relies on specific sites on the adsorbent surface to host adsorbate molecules driven from the bulk. These sites are typically of either amine or carboxyl functionality, imparting a positive or negative electrostatic charge on the adsorbate surface, respectively (Davis 2012). The electrostatic adsorption process is often referred to as ion exchange because it involves the stoichiometric displacement of a counter ion from the adsorption sites when the adsorption process occurs (Hendricks 2006). This separates electrostatic adsorption from physical and chemical adsorption, which do not involve the release of any chemical species from the adsorbent. In most cases, the associated enthalpy change in electrostatic adsorption processes is very small, often less than -10 kJ mol^{-1}. Electrostatic adsorption may be

reversed by exposing the saturated adsorbent to a bulk solvent concentrated with a different ionic species of the same charge (Inglezakis and Poulopoulos 2006).

3.3 Equilibrium adsorption isotherms

If an adsorbent is exposed to adsorbate for sufficiently long periods of time, equilibrium between adsorption and desorption will be established. For the development of an adsorption process, it is necessary to have a sound understanding of the equilibrium properties of the system, as they will influence many design and operational parameters (Hendricks 2006). An adsorption isotherm is a model used to describe the equilibrium of an adsorption system at a constant temperature by relating the concentration of adsorbate in the bulk to the specific adsorption of the adsorbent. Some of the most frequently used isotherms in practice are the Langmuir, Freundlich, and Temkin models (Worch 2012).

3.3.1 Langmuir model

The Langmuir isotherm is the simplest and most commonly used model to describe equilibrium adsorption data (Foo and Hameed 2010) (Howe, et al. 2012). It was initially derived in 1916 for a gas-solid system (Langmuir 1916), but has since been adapted for liquid-solid systems, as well (Inglezakis and Poulopoulos 2006) (Worch 2012). The isotherm is presented as follows:

$$q_e = \frac{q_m k_l C_e}{1 + k_l C_e} \tag{3.4}$$

where q_e is the specific adsorption of an adsorbent at equilibrium (mg g^{-1}), q_m is the maximum specific adsorption of an adsorbent (mg g^{-1}), k_l is the Langmuir affinity

coefficient (l mg^{-1}), and C_e is the concentration of the solute in the bulk liquid at equilibrium (mg l^{-1}). At low concentrations, the Langmuir isotherm reduces to Henry's law:

$$\lim_{C_e \to 0} q_e = q_m k_l C_e \tag{3.5}$$

wherein the surface adsorption is linearly proportional to the adsorbate concentration in the bulk.

Linearization of the Langmuir isotherm yields the following:

$$\frac{C_e}{q_e} = \frac{1}{q_m} C_e + \frac{1}{q_m k_l} \tag{3.6}$$

The model parameters, q_m and k_l, may be determined by performing one of two batch experiments: (a) vary the initial adsorbate concentration and measure the specific adsorption at equilibrium, while keeping all other parameters constant or (b) vary the adsorbent loading and measure the specific adsorption at equilibrium, while keeping all other parameters constant. Both methods will yield data sets of C_e and q_e, which may then be used to calculate the model parameters through linear regression. Non-linear regressive techniques may also be applied.

There are many assumptions associated with the Langmuir isotherm (Inglezakis and Poulopoulos 2006). One is that the surface of the adsorbent is uniform. This implies that the surface is perfectly flat and without imperfection. It also implies that the active sites for adsorption on the adsorbent surface are energetically equivalent. Further, this isotherm only accounts for monolayer adsorption, wherein adsorbate molecules stoichiometrically occupy the active sites. Lastly, it is assumed that there is negligible interaction between adjacent

adsorbed molecules. In practical situations, many of these assumptions are rarely satisfied (Langmuir 1916). Nonetheless, the Langmuir model often provides adequate fit of experimental adsorption data (Foo and Hameed 2010).

Because the Langmuir isotherm is so frequently used in the literature, q_m is the most commonly reported figure to represent the adsorption efficiency of a specific adsorbent material (Foo and Hameed 2010). As a result, q_m may be used to compare between different materials with caution.

3.3.2 Freundlich model

The Freundlich isotherm, while not as commonly used as the Langmuir isotherm, is the older of the two. Like the Langmuir isotherm, the Freundlich isotherm is a two-parameter model (Freundlich 1906). Unlike the Langmuir isotherm, however, its foundation is strictly empirical and lacks a thermodynamic basis. It is often used to model adsorbents with heterogeneous surfaces or multilayer adsorption (Patel and Vashi 2014). The isotherm is as follows:

$$q_e = k_F C_e^{\frac{1}{n}} \tag{3.7}$$

where k_F is an index for adsorption capacity ((mg g^{-1})(l mg^{-1})$^{1/n}$) and *1/n* is a measure of the adsorption intensity. An increase in k_F indicates an increase in the maximum adsorption capacity of the adsorbent, while an increase in *1/n* indicates a more favourable adsorption process. It is also referred to as the heterogeneity factor because a deviation from unity signifies a deviation from the Langmuir model for homogenous adsorption sites (Foo and Hameed 2010). The value of *n* may also be used to determine whether an adsorption

process is favourable or not under certain conditions. If $n > 1$, then the process is favourable (Patel and Vashi 2014).

The Freundlich model inherently assumes that the heat of adsorption decays exponentially as the fractional surface coverage increases. In other words, it assumes that the strongest binding sites are occupied first, followed by those of weaker energy (Foo and Hameed 2010). Its ability to account for site heterogeneity, as well as its general simplicity makes the Freundlich isotherm an attractive modeling tool.

Linearization of the isotherm permits parameter determination:

$$\log q_e = \log k_F + \frac{1}{n} \log C_e \tag{3.8}$$

Similar to the procedure used for the Langmuir isotherm, data sets of q_e and C_e may be plotted to determine the model parameters. Non-linear regressive techniques may also be applied.

One of major limitations associated with the Freundlich isotherm is that the lower limit as C_e approaches zero does not reduce to Henry's law. Similarly, at high concentrations, the upper limit for q_e is not bound. Therefore, as concentration increases, there is no limit to the amount of solute that may be adsorbed on the adsorbent surface. Because of this, the Freundlich isotherm tends to fail at high concentrations. One advantage, however, is that a well-defined relationship can often be obtained with limited data sets (Foo and Hameed 2010).

3.3.3 Temkin model

Similar to the Freundlich isotherm, the Temkin isotherm assumes that the heat of adsorption decreases as the fractional surface coverage of the adsorbent increases (Temkin and Pyzhev 1940). As a result, the Temkin isotherm also retains the ability to account heterogeneous adsorption processes, where the assumption of constant heat of adsorption may not be valid (Foo and Hameed 2010). While the Freundlich isotherm assumes an exponential reduction, the Temkin isotherm assumes a linear reduction in the heat of adsorption. The two-parameter model is as follows:

$$q_e = \frac{RT}{b_T} \ln A_T C_e \tag{3.9}$$

where R is the universal gas constant (8.314 J mol^{-1} K^{-1}), T is the temperature of the system (K), b_T is a model parameter related to the heat of adsorption (g J mg^{-1} mol^{-1}), and A_T is a model parameter related to the equilibrium binding constant (l g^{-1}).

The Temkin isotherm is expressed below in its linear form:

$$q_e = \frac{RT}{b_T} \ln A_T + \frac{RT}{b_T} \ln C_e \tag{3.10}$$

Again, data sets of q_e and C_e may be plotted to determine the model parameters using linear regression. Non-linear regressive techniques may also be applied.

3.4 Kinetic adsorption models

In order to design and implement an adsorption column in a process, a thorough understanding of the kinetics involved with the system is required (Ho and McKay, The

kinetics of sorption of basic dyes from aqueous solution by sphagnum moss peat 1998). By studying the kinetics of adsorption, one may elucidate the effect of different parameters on the overall rate of the adsorption process (K. V. Kumar 2006). These parameters may include system parameters, such as the adsorbent composition and the type of adsorbate, or environmental parameters, such as solution pH, salt concentration, and temperature. By having a reliable estimation of the rate and mechanism of adsorption, one can then begin to safely design for a column's dimensions and desired residence time (Ho 2004).

As in the study of adsorption equilibrium, there have many models developed to aid in the understanding and prediction of adsorption kinetics. Some of the more commonly used models are described below.

3.4.1 Pseudo first order model

The pseudo first order model is an empirical model derived by Lagergren in 1898 to study the adsorption of organic acids onto charcoal (Lagergren 1898) and is one of the most-widely applied techniques for modeling the kinetics of aqueous liquid-solid adsorption systems. The equation is presented below:

$$\frac{dq}{dt} = k_1(q_e - q) \tag{3.11}$$

where t is time (min) and k_1 is the pseudo first order rate constant (min^{-1}). While the rate law may be defined in terms of the number of active sites free for adsorption, in Equation. 3.11 it is instead defined using the adsorption efficiency, q, as the two are assumed to be proportional (Ho and McKay 1999). By integrating the above equation with the boundary conditions $q = 0$ at $t = 0$ and $q = q$ at $t = t$, we may arrive at the following linear form:

$$\log(q_e - q) = \log q_e - \frac{k_1}{2.303} t \tag{3.12}$$

By measuring the specific adsorption efficiency as a function of time in a batch experiment, linear regression may be used to obtain the rate constant. Non-linear regressive techniques may also be applied.

3.4.2 Pseudo second order model

The pseudo second order model is also very commonly used to model liquid-solid adsorption processes (Ho and McKay 1999). Similar to the pseudo first order model, the rate law is defined in terms of the adsorption efficiency, q:

$$\frac{dq}{dt} = k_2(q_e - q)^2 \tag{3.13}$$

where k_2 is the pseudo second order rate constant (min^{-1}). By integrating with the boundary conditions $q = 0$ at $t = 0$ and $q = q$ at $t = t$, we again arrive at a linear form:

$$\frac{t}{q} = \frac{1}{k_2 q_e^2} + \frac{1}{qe} t \tag{3.14}$$

Through a thorough review of the literature, Ho and McKay (1999) found that while the pseudo first order model is simplest, the pseudo second order model was more accurate in modeling solid-liquid adsorption kinetics beyond its initial stages.

3.4.3 Intraparticle diffusion model

The intraparticle diffusion model takes a mechanistic approach to describing adsorption kinetics (Weber and Morris 1963). By doing so, the model may assist in elucidating the effect of boundary layer diffusion on the rate of adsorption for a given system. The

intraparticle diffusion model, sometimes referred to as the Weber and Morris model, is presented below:

$$q = kt^{0.5} + C \tag{3.15}$$

where k is the intraparticle diffusion rate constant (mg g^{-1} $min^{-0.5}$) and C is a constant reflecting the external boundary layer effects (mg g^{-1}). If C approaches *0*, then the adsorption process is entirely diffusion controlled.

3.5 Summary of adsorption models

Presented below is a clear and concise tabular summary of the equilibrium and kinetic models discussed, as well as their linearized forms.

Table 3.1 Summary of equilibrium adsorption models presented.

Model	Equation	Linear form	Reference
Langmuir	$q_e = \frac{q_m k_l C_e}{1 + k_l C_e}$	$\frac{C_e}{q_e} = \frac{1}{q_m} C_e + \frac{1}{q_m k_l}$	(Langmuir 1916)
Freundlich	$q_e = k_F C_e^{\frac{1}{n}}$	$\log q_e = \log k_F + \frac{1}{n} \log C_e$	(Freundlich 1906)
Temkin	$q_e = \frac{RT}{b_T} \ln A_T C_e$	$q_e = \frac{RT}{b_T} \ln A_T + \frac{RT}{b_T} \ln C_e$	(Temkin and Pyzhev 1940)

Table 3.2 Summary of kinetic adsorption models presented.

Model	Equation	Linear form	Reference
Pseudo first order	$\frac{dq}{dt} = k_1(q_e - q)$	$\log(q_e - q) = \log q_e - \frac{k_1}{2.303} t$	(Lagergren 1898)

Pseudo second order	$\frac{dq}{dt} = k_2(q_e - q)^2$	$\frac{t}{q} = \frac{1}{k_2 q_e^2} + \frac{1}{qe}t$	(Ho and McKay 1999)
Intraparticle diffusion model	$q = kt^{0.5} + C$	N/A	(Weber and Morris 1963)

CHAPTER 4

Optimized adsorption of a model aromatic naphthenic acid from aqueous solution using sustainable quaternized chitosan hydrogels

---

4.1 Introduction

For each barrel of bitumen produced in the Alberta, Canada's oil sands development, approximately 0.5 to 2.5 barrels of freshwater must be drawn in from local waterways to aid in the processing of the mined ore (Allen 2008). This equates to approximately 2.9 million barrels of freshwater per day. Upon the mining and extraction of bitumen from oil sands ore, a number of contaminants are solubilized and concentrated in oil sands process-affected water (OSPW), where they prompt several environmental and process-related concerns. Among these contaminants is a very broad family of saturated aliphatic and alicyclic carboxylic acids known collectively as naphthenic acids (NAs). NAs are surface-active compounds (Havre, et al. 2002) (Headley and McMartin 2004) that have proven to be both corrosive toward process equipment (Derungs 1956) (Schramm, Stasiuk and MacKinnon 2000) (Fan 1991) and acutely toxic toward a number of aquatic organisms (MacKinnon and Boerger 1986) (Schramm, Stasiuk and MacKinnon 2000) (Madill, et al. 2001) (Rogers, et al. 2002) (Frank, et al. 2009).

A range of novel technologies, spanning advanced oxidation, biodegradation, coagulation/flocculation, membrane filtration, and adsorption, have been developed over the past decade and their ability to remove NAs from OSPW has been demonstrated with relative success. However, each class of remediation techniques possesses certain limitations. For instance, many of the works involving advanced oxidation processes report on the preferential oxidative degradation of bulkier, polycyclic NAs (Legrini, Oliveros and Braun 1993) (Neyens and Baeyens 2003) (Afzal, et al. 2012). Conversely, reports of NA bioremediation often conclude that lower molecular weight NAs with less rings and

branching are more easily biodegraded by microbial cultures (Clemente, MacKinnon and Fedorak 2004) (Scott, MacKinnon and Fedorak 2005) (Smith, et al. 2008) (Han, Scott, et al. 2008). In both cases, this selective degradation often leaves behind a number of recalcitrant NAs that persist in OSPW. Coagulation/flocculation processes are often cited as significant producers of sludge (Pourrezaei, et al. 2011) (De Philippis and Micheletti 2009) and the high ionic strength of OSPW often disrupts the destabilization mechanisms that cause flocculant-contaminant complex to settle out of solution (Allen 2008). Meanwhile, fouling, high pressure drop, and low throughput are commonly encountered for membrane filtration processes (Peng, et al. 2004) (Allen 2008). Adsorption, while being a well-developed technology for wastewater treatment, allows for high throughput and, in most cases, comprehensive NA removal.

The most common adsorbent material investigated for the removal of NAs from OSPW is activated carbon. Mohamed et al. (2008) explored the use of commercial granular activated carbon for NA removal and, under the experimental conditions used, observed a maximum adsorption efficiency of 159 mg g^{-1}, as estimated by the Langmuir equilibrium adsorption isotherm. Sarkar (2013) studied the adsorption of a single-ring model NA from simulated process water using petroleum coke-derived activated carbons that varied in both overall surface area and functionality. It was observed that activated carbons with higher surface area and ammonia surface functionality offered optimal adsorption with removal rates of up to 98%. Gong and Yao (2012) investigated the use of spent fluid catalytic cracking catalyst for the adsorption of NAs from OSPW. The exterior and pore surfaces of the zeolite-based catalyst, after exposure to hydrocarbon cracking, was coated with carbon

and provided the material with an active surface for adsorption. Under the experimental conditions studied, an adsorption efficiency of approximately 52 mg g^{-1} was achieved. Most recently, Iranmanesh et al. (2014) produced activate carbons from sawdust using both chemical and physical activation processes for the removal of NAs from OSPW. The chemically activated carbon possessed a higher surface area and, thus, resulted in greater adsorption efficiency (up to 32 mg g^{-1}). In comparison with commercial activated carbon whose maximum NA adsorption capacity was 21 mg g^{-1}, both the physically and chemically activated carbons were an improvement. While activated carbons tend to possess high porosity and specific surface area that lend to their adsorption efficiency, the cost of commercial activated carbons may be prohibitive (Sarkar 2013). As well, the activation process, while necessary to achieve suitable specific surface areas, is often energy intensive and may produce gaseous emissions that contain particulate matter and volatile organic compounds (Cecen and Aktas 2012). The use of activated carbons derived from waste products (Sarkar 2013) (Gong and Yao 2012) (Iranmanesh, et al. 2014) (Islam, Zhang, et al. 2015) (Islam, Dong, et al. 2014) may remain economical, though, depending on their removal efficiencies.

Other adsorbent materials explored for the removal of NAs from wastewater include clays and synthetic resins (Zou, et al. 1997) (Mohamed, Wilson and Headley, et al. 2008) (Gaikar and Maiti 1996). Zou et al. (1997) investigated the adsorption process of NAs onto the surfaces of montmorillonite, kaolinite, and illite using calorimetry. They observed that the process was driven by two surface interactions. First, the carboxylate groups of the NA molecules participated with polar atoms or water molecules bound to the clay surface by

hydrogen bonding. Second, the hydrophobic segment of NA molecules was found to bond to the clay surface through van der Waals interactions. They concluded that clays with a greater specific surface area performed better as adsorbents. Mohamed et al. (Mohamed, Wilson and Headley, et al. 2008) (Mohamed, Wilson, et al. 2011) prepared synthetic supramolecular polyurethane adsorbents with β-cyclodextrin (β-CD) functionality. The ability of the β-CD to complex with hydrophobic molecules allowed for the adsorption of NAs, with the hydrophobic segment of the NAs centered within the β-CD and the carboxylate directed away from the adsorbent material. Under the conditions studies, adsorption efficiencies of 20-30 mg g^{-1} were achieved. As suggested by the authors, the specific surface area of the adsorbent limited the removal efficiency.

In a recent report published by Sowmya and Meenakshi (2013), regenerable quaternized chitosan hydrogel adsorbents were used for the selective removal of phosphate and nitrate anions from aqueous solutions. Chitosan (CS) is a random linear copolysaccharide constituted of β-linked *D*-glucosamine and *N*-acetyl-*D*-glucosamine (Rinaudo 2006). It is a deacetylated derivative of chitin, the second most abundant polymer in the world, after cellulose (Tharanathan and Kittur 2003). Chitosan is an attractive material for functional applications in wastewater treatment for a number of reasons. First, being an abundant, natural biopolymer derived from food industry waste makes its production economical (M. N. Kumar 2000). Further, its solubility properties allow for processing and modification reactions to be carried out in aqueous media (pH < 5). The ISO 14000 family of standards addresses the concept of industrial sustainability in businesses and organizations, offering guidelines for environmental management systems (EMS) (Internation Organization for

Standardization (ISO) 2004). The potential benefits of implementing and abiding by such systems include reduction in waste production and the avoidance of use and disposal of hazardous or potentially polluting materials. By using chitosan as the bulk material for the adsorbent and carrying out reactions in aqueous media, the work described herein aims to approach the industrial ideals and standards outlined in ISO 14001.

Simple crosslinking reactions with chitosan have been well studied (Monteiro and Airoldi 1999) (Mi, Sung and Shyu 2000) (Berger, et al. 2004) (Hudson and Jenkins 2004), as has its use as a matrix material in hydrogels (Chatterjee, Lee and Woo 2010) (Baysal, et al. 2013) (Chen, et al. 2013). In their study, Sowmya and Meenakshi (2013) observed adsorption capacities of 67.5 and 59.0 mg g^{-1} toward nitrate and phosphate anions, respectively, from highly concentrated solutions. The hydrogels were also demonstrated to be regenerable for more than 10 cycles.

The present study investigates the use of similar quaternized chitosan hydrogels for the adsorption of an organic anion, 2-naphthoxyacetic acid, to demonstrate the applicability of this type of material towards the removal of NAs from OSPW. The effects of varying three processing parameters on the physical and adsorption characteristics of the resulting adsorbent material were investigated. This included studying the density of chitosan, the degree of crosslinking, and the degree of quaternization of the hydrogels. Their effects on the swelling behaviour and Langmuir adsorption capacity for the model NA were reported. From the results of this optimization study, an optimal adsorbent formulation was produced and the batch equilibrium and kinetic adsorption processes were characterized. The Langmuir adsorption isotherm provided adequate fit for the equilibrium adsorption data,

while the pseudo second order rate equation modeled the kinetic adsorption data quite well. The effects of adsorbate concentration, adsorbent dosage, agitation rate, ionic strength, pH, and temperature on the adsorption process were studied. Under optimal conditions, up to 91% of the model NA was adsorbed. The optimized quaternized chitosan hydrogel adsorbents reported in this study possessed a maximum adsorption efficiency of 315 mg g^{-1}, as estimated by the Langmuir adsorption isotherm from batch equilibrium adsorption data. This is a significant improvement from the hydrogel adsorbents reported by Sowmya and Meenakshi (2013), as well as many of the activated carbon adsorbents used for the removal of NAs from OSPW (Sarkar 2013) (Gong and Yao 2012) (Iranmanesh, et al. 2014) (Mohamed, Wilson and Headley, et al. 2008) (Mohamed, Wilson, et al. 2011).

4.2 Experimental section

4.2.1 Materials

Medium molecular weight chitosan (CS, 75-85% deacetylated), sodium hydroxide (NaOH, pellets, ≥ 99.0%), hydrochloric acid (HCl, 37%), glutaraldehyde (GA, 50% w/w in water), glycidyltrimethylammonium chloride (GTMAC, ≥ 90%), 2-naphthoxyacetic acid (mNA, ≥ 98.0%), and sodium chloride (NaCl, ≥ 99.0%) were purchased from Sigma-Aldrich and used without further purification. Water (≥ 18 MΩ cm) used in all procedures was filtered through a Millipore Milli-Q Purification System.

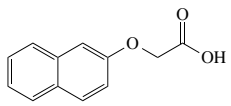

Figure 4.1 Chemical structure of 2-naphthoxyacetic acid (mNA, MW = 202.21 g mol^{-1}, λ_{max} = 325 nm).

4.2.2 Methods

4.2.2.1 Synthesis of quaternized chitosan hydrogel adsorbents

The procedure for preparing the QCHA was adapted from the recent work of Sowmya and Meenakshi (Sowmya and Meenakshi 2013). First, aqueous chitosan solutions were prepared by dissolving 200-400 mg CS in 19.6-19.8 ml 1% w/w HAc solution, depending on the desired CS concentration (1, 1.25, 1.5, 1.75, and 2% w/w). The solutions were shaken at 500 rpm on an orbital plate shaker for 1 h to ensure complete dissolution. Spherical CS hydrogels were then prepared by slowly drop casting the mildly acidic CS solution into 100 ml of a gently stirring 0.5 M aqueous NaOH solution. A peristaltic pump was used to dispense the solution through a 22G hypodermic needle at a rate of approximately 2 drops per second. The tip of the needle was maintained at a height of 3 cm above the liquid surface. The hydrogels were stirred in the NaOH solution for 30 minutes to allow for complete coagulation. The beads were then carefully filtered from the NaOH solution and placed in 100 ml water to remove the NaOH from the pores of the beads. The beads were stirred for 5 minutes before carefully filtering them from the solution. This wash process was repeated until the pH of the water approached neutral values (pH 6-7) and remained consistent (approximately 5 to 7 total iterations).

The CS hydrogel beads were then added to 20 ml water in a 100 ml conical flask. Next, 50-250 µl GA was added, depending on the desired aldehyde to amine molar ratio on the GA and CS, respectively (0.5:1, 1:1. 1.5:1, 2:1, and 2.5:1). The solution was shaken at 250 rpm for 1 h to allow for the crosslinking reaction to occur, after which the beads were

carefully filtered from the reaction solution and were washed using the previously described procedure.

The crosslinked CS hydrogel beads were then added to 30 ml water in a 100 ml round bottom flask. Next, 0.82-2.88 ml GTMAC was added, depending on the desired epoxy to amine molar ratio on the GTMAC and CS, respectively (5:1, 7.5:1, 10:1, 12.5:1, 15:1, and 17.5:1). The contents were then heated to 55ºC under gentle stirring and allowed to react for 12 h. The resulting quaternized chitosan hydrogel adsorbent (QCA) were then carefully filtered from the reaction solution and were washed using the previously described procedure. The beads were stored in their hydrated state.

Scheme 4.1 Crosslinking and quaternization of chitosan hydrogels.

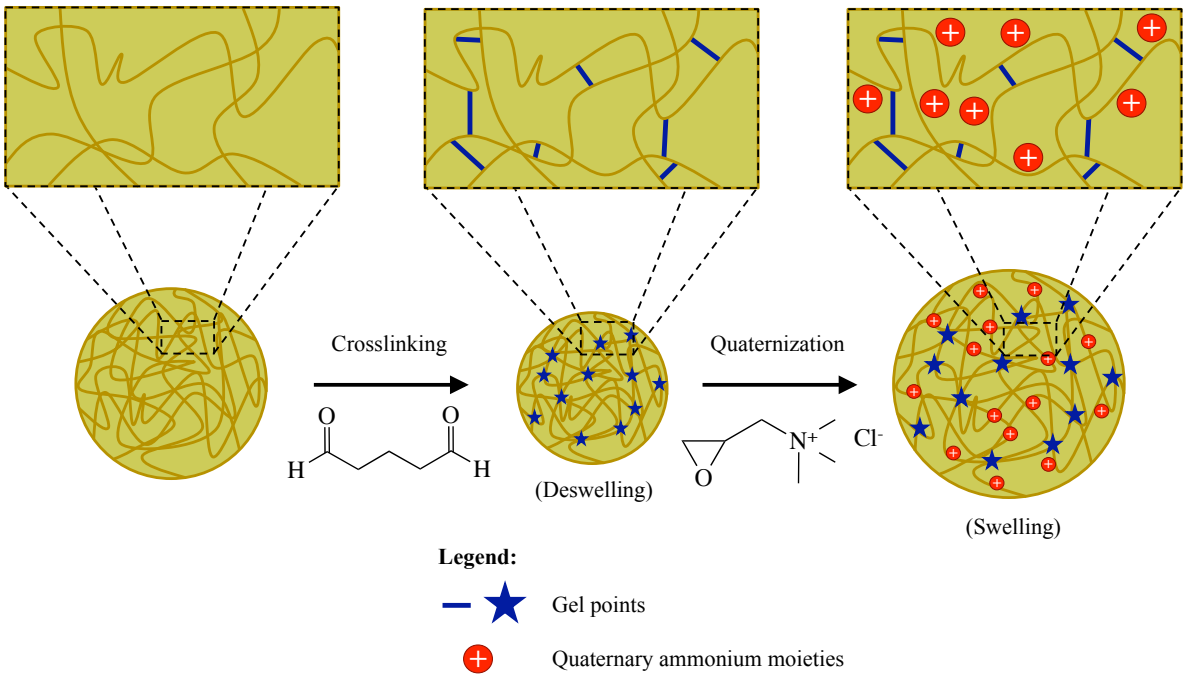

4.2.2.2 Optimization of quaternized chitosan hydrogel adsorbents

The effects of varying a number of reaction and processing parameters on the swelling behaviour and adsorption performance of the resulting QCA were studied. The parameters investigated were (A) the amount of CS in the initial suspension, (B) the molar ratio of aldehyde to amine on the GA and CS, respectively, in the crosslinking reaction, and (C) the molar ratio of epoxy to amine on the GTMAC and CS, respectively, in the quaternization reaction. The variations in conditions are outlined in Table 1, below. An optimized formulation for use in thorough kinetic and equilibrium adsorption experiments was determined based on the results of this parameter study.

Table 4.1 Experimental conditions for QCA reaction and processing parameter study.

Sample	Amount of CS (% w/w)	Aldehyde: amine ratio (molar)	GTMAC: amine ratio (molar)
A1[†]	1	1	10
A2	1.25	1	10
A3	1.5	1	10
A4	1.75	1	10
A5	2	1	10
B1	1	0.5	10
B2[†]	1	1	10
B3	1	1.5	10
B4	1	2	10
B5	1	2.5	10
C1	1	1	5
C2	1	1	7.5
C3[†]	1	1	10
C4	1	1	12.5
C5	1	1	15
C6	1	1	17.5

[†] A1, B2, and C3 are replicates.

4.2.3 Characterization

4.2.3.1 Swelling ratio

The swelling ratio of the QCA was determined gravimetrically. The hydrated beads were placed on cellulose filter paper to remove any excess water and the mass of 15 beads was measured. The beads were dried under vacuum pressure at room temperature for 12 h and the mass of the dehydrated beads was measured. The swelling ratio, *SR* (g g^{-1}), was determined as the ratio of hydrated mass, m_w (g), to dehydrated mass, m_d (g):

$$SR = \frac{m_w}{m_d} \tag{4.1}$$

Each measurement was recorded in triplicate.

4.2.3.3 Equilibrium adsorption

A 1 l stock solution of 1 mM mNA was prepared, with the pH adjusted to 8 using 0.1M NaOH to relate to the pH of OSPW. The same stock solution was used throughout the course of all adsorption experiments. UV-vis absorbance with a range in wavelength of 300-350 nm was used to measure the concentration of mNA in solution (Varian Cary 100 Bio) (Figure 4.2a). A calibration plot was prepared by diluting the stock mNA solution to five different concentrations using water (pH adjusted to 8) and measuring the corresponding peak UV-vis absorbance (325 nm) for each concentration (Figure 4.2b). The same calibration plot was used throughout the course of the adsorption experiments.

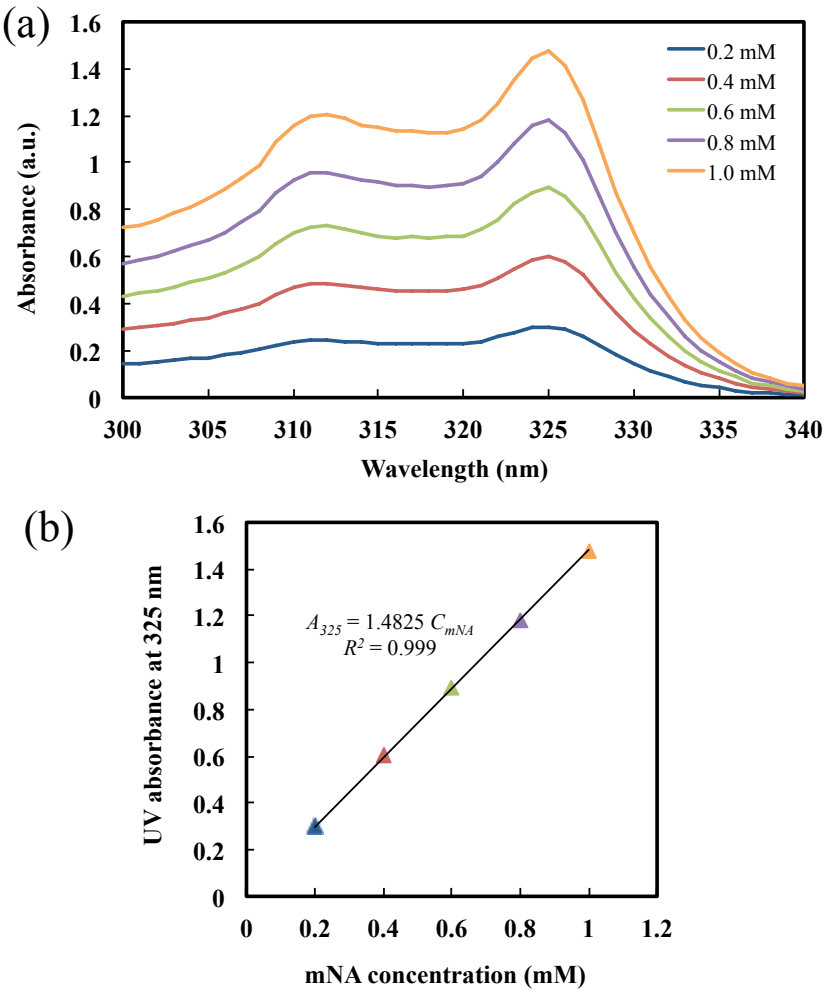

Figure 4.2 (a) UV-vis absorbance of the mNA for a wavelength range of 300 to 340 nm and (b) a calibration plot demonstrating the relationship between mNA concentration and UV absorbance at 325 nm.

10 mg dry equivalent QCA were added to a series of five 20 ml polypropylene vials. To each, 10 ml of mNA stock solution was added and the vials were immediately placed on a temperature controlled orbital shaker at 25ºC and shaken at 300 rpm. After 4 h, equilibrium had been reached and 2.5 ml aliquots of mNA solution were removed from each vial. The concentration of mNA was measured using UV-vis absorbance. Five initial adsorbate concentrations were studied: 0.2, 0.4, 0.6, 0.8, and 1.0 mM.

These experiments were used to determine the equilibrium adsorption characteristics for the QCA parameter study and the optimized QCA formulation. The equilibrium adsorption of mNA onto the various QCA was modeled using the Langmuir isotherm (Langmuir 1916):

$$q_e = \frac{q_m k_l C_e}{1 + k_l C_e} \tag{4.2}$$

where q_e is the specific adsorption of an adsorbent at equilibrium (mg g^{-1}), q_m is the maximum specific adsorption of an adsorbent (mg g^{-1}), k_l is the Langmuir affinity coefficient (l mg^{-1}), and C_e is the concentration of the mNA in the bulk liquid at equilibrium (mg l^{-1}). q_e may be calculated using at equilibrium using the following relationship:

$$q_e = \frac{(C_o - C_e)V}{m} \tag{4.3}$$

where C_o is the initial mNA concentration, V is the volume of the system, and m is the adsorbent dosage.

The parameters to the Langmuir equation, q_m and k_l were evaluated nonlinearly using the MATLAB built-in function *nlinfit*.

4.2.3.2 Kinetic adsorption

A certain mass of dry equivalent QSCHB was added to a series of 20 ml polypropylene vials. To each, 10 ml of mNA stock solution was added and the vials were immediately placed on a temperature controlled orbital shaker and shaken at a particular rate. At predefined time intervals, 2.5 ml aliquots of mNA solution were removed from each vial and the concentration of mNA was measured using UV absorbance. The solution was then placed back into its respective vial and the adsorption experiment was allowed to continue for a total of 4 h.

The effect of the initial adsorbate concentration on the adsorption kinetics was studied by varying the amount of mNA in each batch adsorption experiment. Five initial adsorbate concentrations were studied: 0.2, 0.4, 0.6, 0.8, and 1.0 mM. The adsorbent mass, agitation rate, initial solution pH, NaCl concentration, and temperature were maintained at 10 mg, 300 rpm, pH 8, 0 mM, and 25ºC, respectively.

The effect of adsorbent dosage on the adsorption kinetics was studied by varying the mass of adsorbent in each batch adsorption experiment. Five adsorbent dosages were studied: 5, 7.5, 10, 12.5, and 15 mg. The initial adsorbate concentration, The initial adsorbate concentration, agitation rate, initial solution pH, NaCl concentration, and temperature were maintained at 1 mM, 300 rpm, pH 8, 0 mM, and 25ºC, respectively.

The effect of agitation rate on the adsorption kinetics was studied by varying the rotational speed of the orbital shaker used throughout the batch adsorption experiments. Three agitation rates were studied: 100, 300, and 500 rpm. The initial adsorbate

concentration, adsorbent mass, initial solution pH, NaCl concentration, and temperature were maintained at 1 mM, 10 mg, pH 8, 0 mM, and 25ºC, respectively.

The effect of solution pH on the adsorption kinetics was studied by varying the initial pH of solution in each batch adsorption experiment. This was done by preparing five 50 ml mNA solutions from the original stock and adjusting the pH using very small volumes of 1.0 and 0.1 M HCl and 1.0 and 0.1 M NaOH. The mNA solutions for this set of experiments were then drawn from the corresponding pH adjusted stock solutions. Five initial pH values were studied: pH 2, 4, 6, 8, and 10. The initial adsorbate concentration, adsorbent mass, agitation rate, NaCl concentration, and temperature were maintained at 1 mM, 10 mg, 300 rpm, 0 mM, and 25ºC, respectively.

The effect of ionic strength on the adsorption kinetics was studied by varying the concentration of NaCl in each batch adsorption experiment. This was done by preparing five 50 ml mNA solutions from the original stock and adjusting the salt concentration by adding 29.2-116.9 mg NaCl to each solution. Five NaCl concentrations were studied: 0, 10, 20, 30, and 40 mM. The initial adsorbate concentration, adsorbent mass, agitation rate, initial solution pH, and temperature were maintained at 1 mM, 10 mg, 300 rpm, 8, and 25ºC, respectively.

The effect of temperature on the adsorption kinetics was studied by varying the water bath temperature in each batch adsorption experiment. Three temperatures were studied: 25, 35, and 45ºC. The initial adsorbate concentration, adsorbent mass, agitation rate, initial solution pH, and NaCl concentration were maintained at 1 mM, 10 mg, 300 rpm, 8, and 0 mM, respectively.

These experiments were used to determine the kinetic adsorption characteristics for the optimized HTCC hydrogel formulation. The kinetic adsorption of mNA onto the optimized QCA under a variety of process conditions was modeled using the pseudo second order rate equation (Ho and McKay 1999):

$$\frac{dq}{dt} = k_2(q_e - q)^2 \tag{4.4}$$

where k_2 is the pseudo second order rate constant. Integration of Equation 4.4 for the boundary conditions $q = 0$ at $t = 0$ and $q = q$ at $t = t$ yields the integrated pseudo second order rate law:

$$q = \frac{q_e^2\ t\ k_2}{1 + \ k_2\ q_e} \tag{4.5}$$

The parameters to the pseudo second order rate equation, q_e and k_2 were also evaluated nonlinearly using the MATLAB built-in function *nlinfit*.

4.2.3.4 Adsorbent regeneration

To study the recyclability of the optimized QCA formulation, a series of equilibrium adsorption and desorption experiments were performed. For these experiments, 10 mg dry equivalent QCA were added to a 20 ml polypropylene vial. Then, 10 ml of 1 mM mNA stock solution was added and the vial was immediately placed on an orbital shaker at 25ºC and shaken at 300 rpm. After 4 h, equilibrium had been reached and a 2.5 ml aliquot of mNA solution was removed from the vial. The concentration of mNA was measured using

UV absorbance. The remaining solution mNA solution was then strained from the beads and 10 ml 50 mM NaCl was added. The vial was then immediately placed back on the orbital shaker and shaken at 300 rpm. At predefined time intervals, 2.5 ml aliquots of regeneration solution were removed from the vial and the concentration of desorbed mNA was measured using UV absorbance. The solution was then placed back into the vial and the desorption experiment was allowed to continue until equilibrium was reached (2 h). Once desorbed, the hydrogel beads were strained from the regeneration solution and washed five times with water to remove any excess NaCl. This procedure was then repeated for a total of five cycles. Each measurement was recorded in triplicate.

4.3 Results and discussion

4.3.1 Optimization of quaternized chitosan hydrogel adsorbents

4.3.1.1 Effect of chitosan density

Adsorbents are typically housed in fixed bed adsorption columns, the capital cost of which is proportional to the volume required for the specified design (Faust and Aly 1987) (Hendricks 2011). After a certain period of time, the adsorbent must either be regenerated by desorbing the adsorbed solute using an eluent or disposed of and replaced by unused adsorbent material. The regeneration or replacement of adsorbent material results in significant operating costs. By increasing the effective density of the adsorbent material, one may be able to achieve more functional surface area for adsorption per unit volume and/or improve the lifetime of the material, resulting in a reduced regeneration or replacement frequency (Li, et al. 2014). For example, if two hydrogel adsorbent beads are

of similar volume, but one has twice the potential adsorption sites due to an increased density of the gel network, then an adsorption column of half the volume could be used to provide the same overall adsorption efficiency. Alternatively, if the same volume of adsorbent were used, the adsorbent with twice the density of adsorption sites could have potentially twice the active lifetime. However, it is possible that by increasing the density of the gel, access to the innermost adsorption sites may be limited by effective mass transfer, making those sites unusable. By investigating the impact of density of the QCA on the material's adsorption capacity, we may confirm or reject the above hypotheses.

The hydrogel density could be easily controlled by varying the concentration of chitosan in the initial polymer solution (1.0 to 2.0% w/w) prior to bead formation. In terms of processing, the more concentrated chitosan solutions were of higher viscosity, resulting in slower and slightly more tortuous pumping through the narrow needle used to drop cast the solution into NaOH solution throughout the hydrogel preparation stage. Upon drop casting, the clear-yellow chitosan solution was observed to immediately congeal into white coloured spheres. The gels remained at the air-water interface of the NaOH solution until complete coagulation (approximately 2 minutes), after which they were observed to submerge to the bottom of the vessel. Although the solution viscosity differed between samples, the size of the resulting spherical hydrogels remained relatively consistent at approximately 2.5-3.0 mm in diameter.

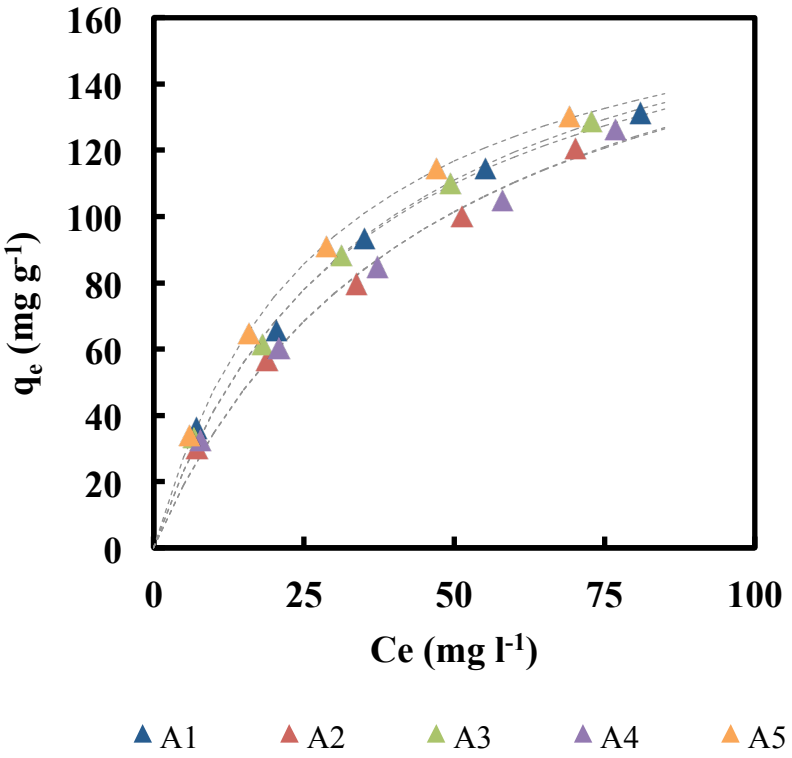

Figure 4.3 Langmuir adsorption isotherms for the adsorption of mNA onto QCA samples A1 to A5 at 25°C. The experimental data is represented by the triangles and the modeled data is represented by the dashed line.

The effect of varying the density of chitosan on the swelling ratio and adsorption efficiency of the QCA is depicted in Figure 4.4. The swelling ratio of the adsorbents was observed to decay somewhat exponentially as the chitosan density was increased from 1.0 to 2.0% w/w. The lowest density hydrogels possessed a swelling ratio of 57.0 ± 2.55 g g^{-1}, while the swelling ratio for the highest density hydrogels was 30.0 ± 0.94 g g^{-1}, an almost 50% reduction. This was to be expected because, although the hydrogel volume remained relatively constant throughout this series of experiments, the effective mass of polymer

within the gels continually increased. Therefore, there is less volume available for water sorption in the higher density hydrogels.

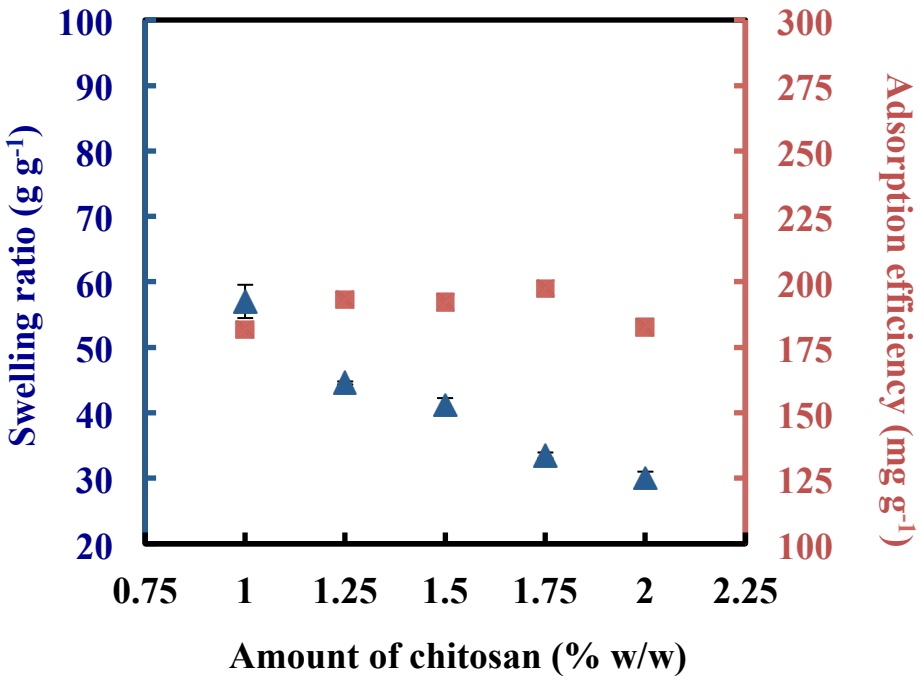

Figure 4.4 The effect chitosan density on the swelling ratio (blue triangles) and mNA adsorption efficiency (red squares) of the resulting QCA samples.

While the swelling ratio was observed to decrease, the adsorption efficiency of the hydrogels towards the mNA remained relatively constant throughout the series, ranging from 181.8 mg g^{-1} on the low end to 197.3 mg g^{-1} on the high end. This means that regardless of density, a given mass of hydrogels permits the same removal efficiency of mNA from water. This observation persuades one to conclude that the higher density hydrogels, with more mass per volume, possess more effective adsorption sites for a given volume. As well, one may conclude that limitations to mass transfer within the hydrogels are either non-observable or non-existent for the applied experimental conditions. This is

likely a result of the porous nature of the non-glassy gels, which permits the flow of water and dissolved solutes relatively easily within the gel structure (Hoch, Chauhan and Radke 2003).

4.3.1.2 Effect of the amount of crosslinking agent

To improve the robustness of the QCA and to avoid aqueous dissolution of the chitosan polymer after quaternization, heterogeneous covalent crosslinking was introduced to the hydrogels prior to the quaternization step. The most common crosslinking agents investigated for covalently crosslinking chitosan are glutaraldehyde, a five carbon dialdehyde, (Roberts and Taylor 1989) (Argüelles-Monal, et al. 1998) (Monteiro and Airoldi, Some studies of crosslinking chitosan–glutaraldehyde interaction in a homogeneous system 1999) and genipin, a naturally occurring protein crosslinker (Butler, Ng and Pudney 2003) (Muzzarelli 2009) (Espinosa-García, et al. 2007). While genipin is considered to be a more biocompatible, non-toxic alternative (Lai 2012), glutaraldehyde is low cost, commercially available, and highly reactive (Migneault, et al. 2004). In this investigation, where the proposed application of the hydrogels is non-biological, glutaraldehyde was used for economical reasons.

Almost immediately upon introduction of the glutaraldehyde to the chitosan hydrogels, the slightly translucent beads were observed to turn completely opaque. Correspondingly, the size of the beads was observed to decrease slightly. Throughout the reaction, the beads had taken on a very light yellow colour. Similar colour change has been previously reported for glutaraldehyde crosslinked chitosan systems (Roberts and Taylor 1989) (Monteiro and Airoldi, Some studies of crosslinking chitosan–glutaraldehyde interaction in a

homogeneous system 1999) (Schiffman and Schauer 2007). Roberts and Taylor (1989) suggested that the change in colour is likely a result of the formation of a chromophore as one of the stable crosslinking products. After 1 h, the hydrogels appeared sufficiently crosslinked and the reaction was terminated. Monteiro and Airoldi (1999) suggest that 1 h is more than enough time to allow for ample imine formation between the primary amines of chitosan and the aldehydes on glutaraldehyde. A schematic for the reaction between GA and CS under neutral conditions is shown in Scheme 2. Since the crosslinking of chitosan with glutaraldehyde is well reported in the literature and the in depth examination of the crosslinking mechanism remains out of the scope of this study, no quantitative analysis or the crosslinking process, other than the investigation of the effect on swelling ratio and mNA adsorption efficiency, was performed for the present study.

Scheme 4.2 Reaction between glutaraldehyde and chitosan under neutral conditions.

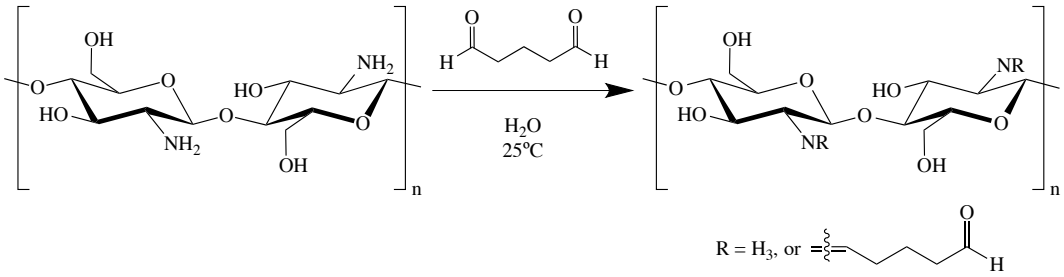

The effect of varying the amount of glutaraldehyde crosslinking agent used on the swelling ratio and adsorption efficiency of the QCA is shown in Figure 4.6. This series of crosslinking reactions was carried out under neutral pH. As the molar ratio of aldehyde groups on GA to amine groups of CS increased from 0.5 to 2.5, an exponential decay is observed for the swelling ratio. It is believed that as the amount of crosslinker used

increases, the number of gel points correspondingly also increases up to a certain point. Mirzaei and coworkers (2013) reported similar observations, claiming that increasing the amount of glutaraldehyde used to crosslink chitosan resulted in reduced chain flexibility and water sorption. The most drastic reduction in the swelling ratio is reported between ratios 0.5 and 1.0, wherein a more than 25% reduction from 77.6 ± 2.43 g g^{-1} to 57.4 ± 0.72 g g^{-1} was observed. This indicates that the majority of extra GA introduced into the system results in new gel points. Further increase in the amount of crosslinker from ratios of 1.0 to 2.5 resulted in a reduction of less than 20%, from to 57.4 ± 0.72 g g^{-1} to 46.6 ± 0.49 g g^{-1}. It is apparent that above a certain ratio of crosslinker to chitosan, excess GA likely results in incomplete crosslinking, wherein only one aldehyde group per molecule is reacted with the chitosan matrix. Therefore, although the amount of GA reacted with the chitosan increases, it is probable that many of the reacted GA molecules do not contribute to the overall gelation of the hydrogel.

As the amount of crosslinker used increased from 0.5 to 2.5, the adsorption efficiency of the system towards mNA was observed to linearly decrease from 185.3 to 159.6 mg g^{-1}. This may be a result of the reduced mass transfer through the hydrogel beads due to the increased crosslinking, but due to the results discussed for increasing chitosan density, it is believed that mass transfer is likely not limiting for the conditions used for the equilibrium adsorption experiments. Instead, it is believed that by increasing the degree of reaction between the aldehyde groups on GA and the amine groups on CS, the number of potential sites for adsorption is reduced. For the QCA under investigation, the chief sites for adsorption are the quaternary ammonium moieties that primarily react with primary amine

groups of CS. However, with GA also reacting with the same primary amines, the total amount of amine groups available for quaternization for a given mass of adsorbent is significantly reduced. Ultimately, it is believed that this chain of events is what prompts the reduced mNA adsorption efficiency of the more densely crosslinked hydrogel adsorbents.

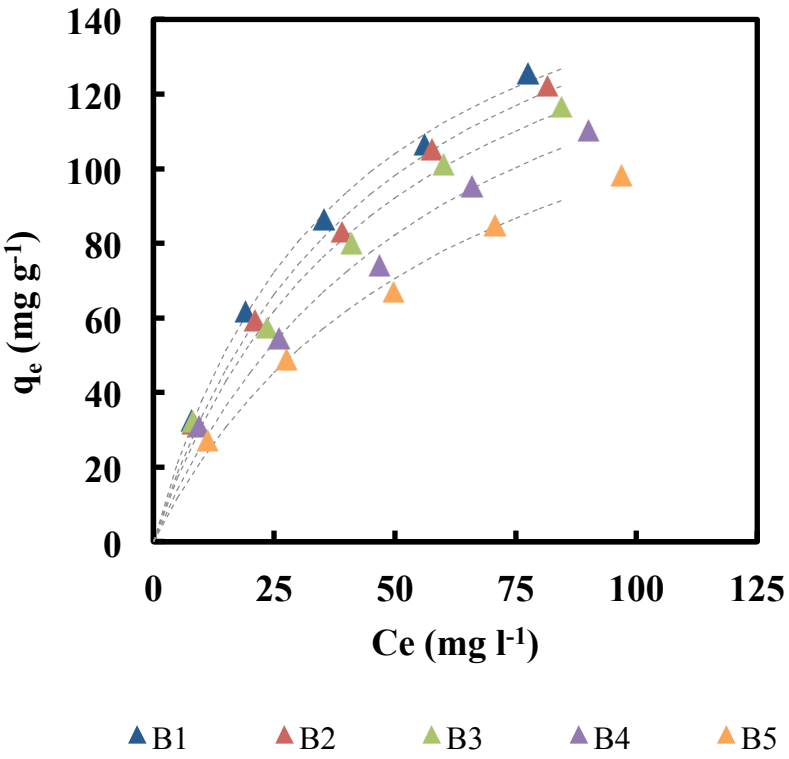

Figure 4.5 Langmuir adsorption isotherms for the adsorption of mNA onto QCA samples B1 to B5 at 25°C. The experimental data is represented by the triangles and the modeled data is represented by the dashed line.

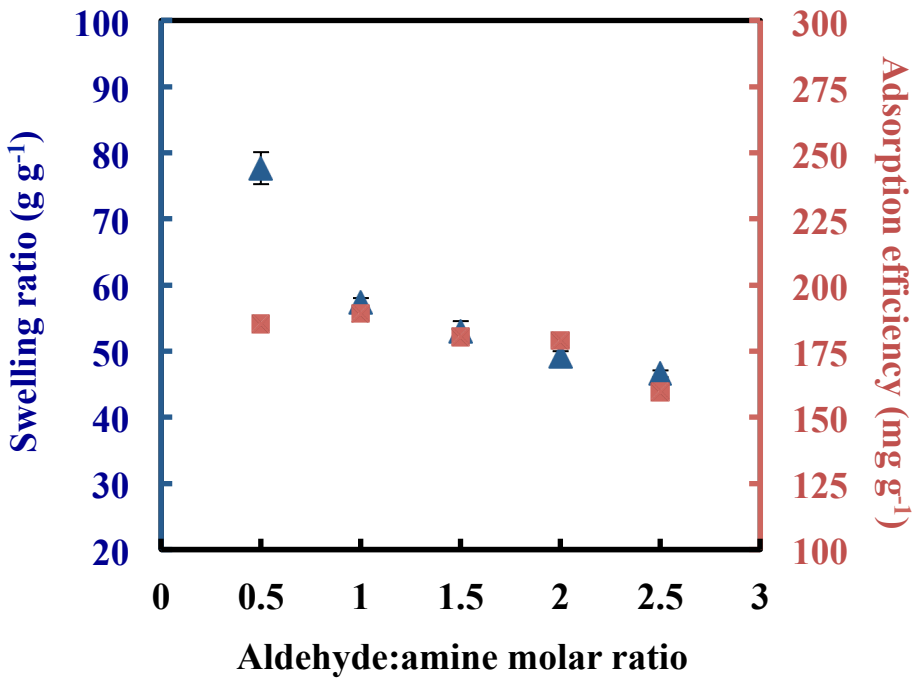

Figure 4.6 The effect of varying the amount of crosslinking agent on the swelling ratio (blue triangles) and mNA adsorption efficiency (red squares) of the resulting QCA samples.

4.3.1.3 Effect of the amount of quaternizing agent

The application of the presently investigated QCA is directed towards the removal of NAs from alkaline OSPW. Since the C_2 primary amine groups of chitosan have a pK_a of approximately 6.5-7 (Yao, et al. 2012) and are naturally deprotonated under alkaline conditions, a permanent positive charge, such as that of a quaternary ammonium group, must be introduced onto the polymer to permit the electrostatic adsorption of the anionic mNA in alkaline conditions.

Quaternized chitosan is typically prepared using one of two methods. One route is the methylation of the primary C_2 amine group on chitosan by reaction with a methylated halogen, such as iodomethane (Domard, Rinaudo and Terrassin 1986). The product is a

trimethylammonium halide pendant group. Another common route is by reaction with GTMAC to yield *N*-(2-hydroxy)-propyl-3-trimethylammonium chitosan chloride (Lim and Hudson 2004), herein referred to as QCS. The second approach was taken due to its relatively fast reaction kinetics and resulting chloride salt. The reaction schematic for GTMAC and CS under neutral conditions is depicted in Scheme 4.3.

Scheme 4.3 Reaction between glycidyltrimethylammonium chloride and chitosan under neutral conditions.

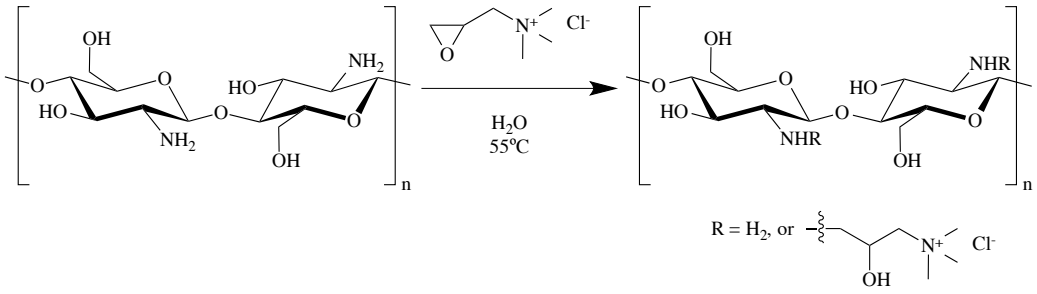

Upon reaction of the GTMAC and CS, a deep yellow colouration was observed. Also, upon introduction of positive charge, the beads were observed to swell. This was likely a result of electrostatic repulsion between trimethylammonium moieties and increased water sorption due to the increased hydrophilicity of the hydrogels.

The effect of varying the amount of GTMAC quaternizing agent used on the swelling ratio and adsorption efficiency of the QCA is shown in Figure 4.8. This series of quaternization reactions was carried out under neutral pH. An almost linear increase in the swelling ratio was observed for CS hydrogels reacted with more GTMAC. A swelling ratio of 49.5 ± 1.43 g g^{-1} was detected for QCA produced using a GTMAC:amine molar ratio of 5, while an increased swelling ratio of 59.1 ± 0.67 g g^{-1} was observed when the

GTMAC:amine molar ratio was increased to 17.5. This was likely a result of electrostatic repulsion between trimethylammonium moieties that increased as the degree of quaternization also increased. Further, it may result from increased water sorption due to the increased overall hydrophilicity of the hydrogels.

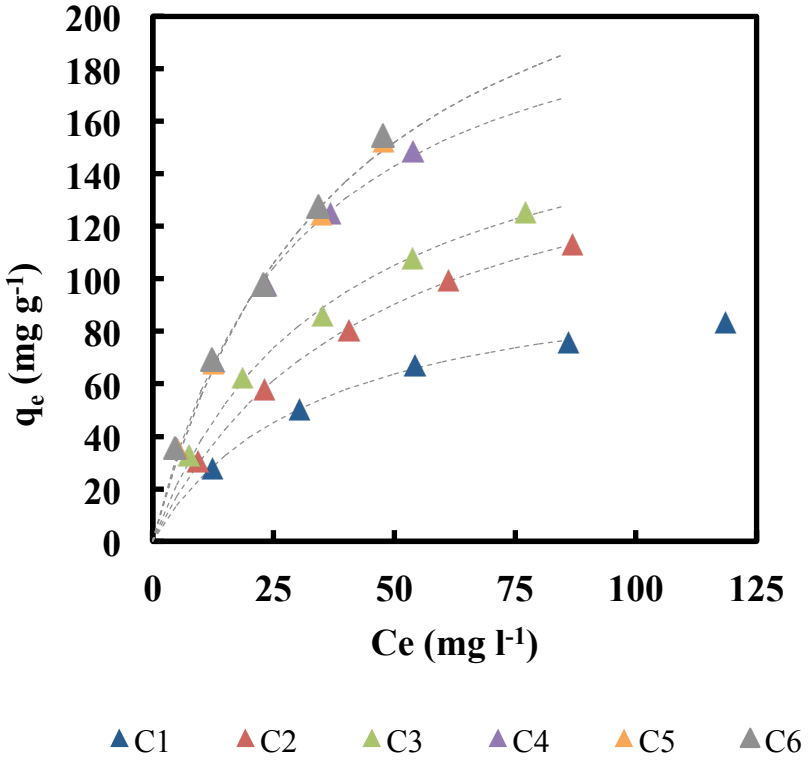

Figure 4.7 Langmuir adsorption isotherms for the adsorption of mNA onto QCA samples C1 to C6 at 25°C. The experimental data is represented by the triangles and the modeled data is represented by the dashed line.

A corresponding increase in adsorption efficiency was also increased as the ratio of GTMAC:amine increased. A sharp improvement in the mNA adsorption efficiency from 107.3 to 227.8 mg g^{-1} was observed as the ratio of GTMAC to amine groups increased from 5 to 12.5. Further increase in the amount of quaternizing agent resulted in only a minor

improvement in adsorption efficiency, from 227.8 to 266.4 mg g^{-1}. This saturation is believed to correspond to a maximal degree of quaternization, wherein all available primary amine groups have undergone quaternization.

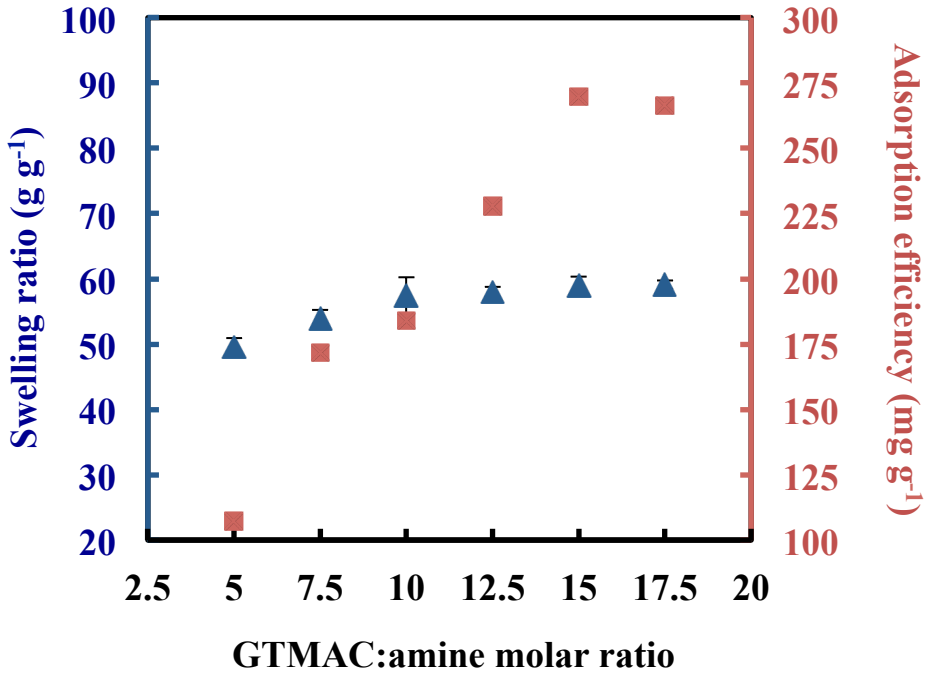

Figure 4.8 The effect of varying the amount of quaternizing agent on the swelling ratio (blue triangles) and mNA adsorption efficiency (red squares) of the resulting QCA samples.

In aqueous conditions, it is well known that GTMAC hydrolysis by water is a prevalent side reaction, yielding the non-reactive species 2,3-dihydroxypropyl trimethylammonium chloride (Zaman, et al. 2012) (Bendoraitiene, et al. 2006). While more dominant under alkaline reaction conditions, it remains significant under neutral conditions, as well (Ruihua, et al. 2012). Further, it has been suggested that in aqueous or alcoholic reaction media, GTMAC also undergoes self-polymerization, making it unreactive towards the CS (Ruihua, et al. 2012).

Scheme 4.4 Hydrolysis side reaction between glycidyltrimethylammonium chloride and water under neutral and alkaline conditions.

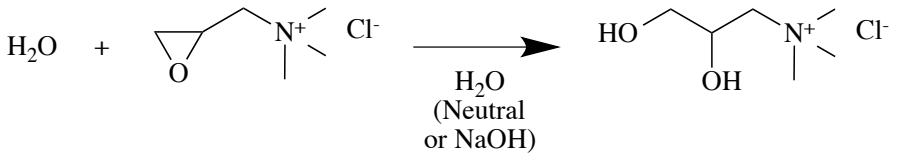

However, for the heterogeneous conditions used for the quaternization reaction, a certain volume of water was required to allow the QCA to stir easily and reduce the boundary layer effects that limit the mass transfer of reactant radially into the core of the spherical hydrogel beads. Further, the presence of ample water allowed for minimal contact between the QCA and the stir bar, avoiding any potential shear damage inflicted upon the material. For these reasons, GTMAC was required in relatively high excess to achieve a reasonable degree of quaternization.

Table 4.2 Summary of the effects of chitosan density (A1-A5), amount of crosslinking agent used (B1-B5), and amount of quaternizing agent used (C1-C6) on the swelling ratio, percent mNA removal from 1 mM aqueous solution, Maximum adsorption capacity, and Langmuir affinity coefficient of the resulting QCA adsorbents.

Sample	Swelling ratio (g g^{-1})	Percent mNA removal (C_o = 1 mM)	Maximum adsorption capacity, q_m (mg g^{-1})*	Langmuir affinity coefficient, k_l (l mg^{-1})*	Adequacy of regression, R^2*
A1†	57.0 ± 2.55	60.0	181.8	0.0286	0.995
A2	44.6 ± 0.26	65.3	193.3	0.0216	0.994
A3	41.2 ± 1.06	64.0	192.4	0.0273	0.997
A4	33.5 ± 0.44	62.0	197.3	0.0212	0.991
A5	30.0 ± 0.94	65.8	182.8	0.0353	0.999

B1	77.6 ± 2.43	61.6	185.3	0.0256	0.997
B2†	57.4 ± 0.72	59.7	189.2	0.0216	0.996
B3	53.0 ± 1.51	58.2	180.4	0.0209	0.991
B4	49.2 ± 0.78	55.5	179.0	0.0170	0.985
B5	46.6 ± 0.49	52.1	159.6	0.0159	0.993
C1	49.5 ± 1.43	41.4	107.3	0.0292	0.999
C2	53.8 ± 1.37	57.0	171.8	0.0222	1.000
C3†	57.4 ± 2.78	61.8	184.0	0.0267	0.997
C4	58.0 ± 0.78	73.4	227.8	0.0337	0.997
C5	58.9 ± 1.44	76.4	269.7	0.0259	0.995
C6	59.1 ± 0.67	76.4	266.4	0.0276	0.993

† A1, B2, and C3 are replicates. * As determined by Langmuir adsorption isotherm.

4.3.2 Adsorption equilibrium using optimized adsorbent

Based on the adsorption efficiencies of the parameter study for the QCA, optimal chitosan density, aldehyde:amine molar ratio, and GTMAC:amine molar ratio were used to produced an optimal QCA. A chitosan concentration of 1.5% w/w was selected for preparing the initial hydrogels. This allowed for increased hydrogel density, while also permitting relatively easy pumping during the bead production stage due to the relatively low solution viscosity. An aldehyde:amine molar ratio of 1:1 was selected for the crosslinking reaction to provide a moderate structural robustness to the beads, while leaving the majority of the amine groups on CS available for quaternization. Lastly, a GTMAC:amine molar ratio of 15:1 was used for the quaternization reaction. This allowed for optimal degree of quaternization of the CS, resulting in the most potential adsorption sites for mNA removal. An objective function was not applied for this parametric optimization study, as statistical optimization was not the primary goal. Instead, the goals of the study lied in using a systematic approach to understanding the effects of individual

process parameters on the performance of the QCA. The relevant variables were determined qualitatively through screening experiments.

Using the optimized QCA, a batch equilibrium adsorption study was used to determine its effectiveness in removing mNA from water. The resulting Langmuir adsorption isotherm at 25°C is presented in Figure 4.9. The Langmuir isotherm provided adequate fit to the data, with an R^2 value of 0.990. The predicted adsorption capacity for the optimized QCA was 314.9 mg g^{-1}. Under optimal conditions and a naphthenic acid concentration of 100 mg l^{-1}, this equates to approximately 317 g of adsorbent to treat 1 m^3 of OSPW. The adsorption capacity of the presently reported adsorbent is compared to that of other reported adsorbents for the removal of NAs from OSPW in Table 4.3.

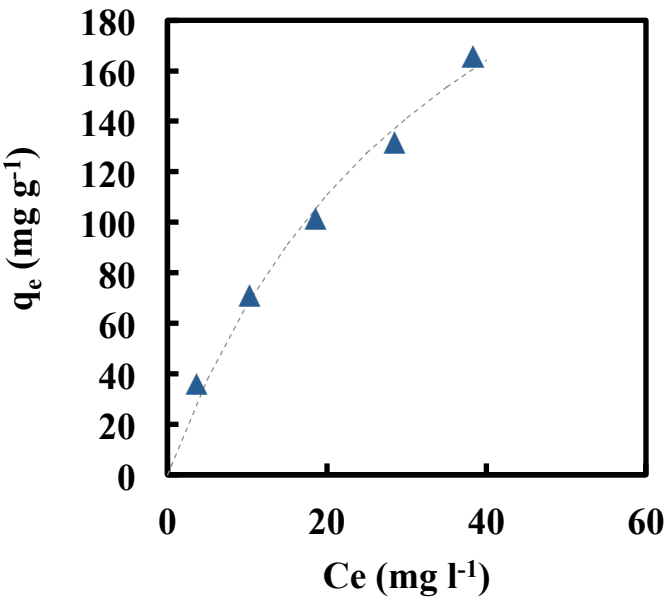

Figure 4.9 Langmuir isotherm for the removal of mNA from water at 25°C using the optimized QCA. The experimental data is represented by the blue triangles and the modeled data is represented by the dashed line.

Table 4.3 Comparison of the adsorption efficiency of common adsorbents used to remove NAs from aqueous solution.

Material	Adsorption efficiency, q_m (mg g^{-1})	Reference
Commercial granular activated carbon	159	(Mohamed, Wilson and Headley, et al. 2008)
Petroleum coke-derived activated carbon	25-300	(Sarkar 2013)
Carbon coated Al_2O_3 and SiO_2 zeolite	52	(Gong and Yao 2012)
Sawdust-derived activated carbon	35.5	(Iranmanesh, et al. 2014)
Biomass-derived aromatic material	100	(Berlin and Myroshynchenko 2013)
Clay	20-50	(Zou, et al. 1997)
Commercial anion exchange resin	15.5-92	(Gaikar and Maiti 1996)
Cyclodextrin-based synthetic resin	20-30	(Mohamed, Wilson and Headley, et al. 2008)
Quaternized chitosan hydrogel adsorbents	315	Present study

4.3.3 Adsorption kinetics using optimized adsorbent

4.3.3.1 Effect of initial adsorbate concentration

The effect of varying the initial mNA concentration on the kinetics of adsorption is depicted in Figure 4.10. For all initial concentrations, it may be observed that equilibrium had been achieved within 1 h. The percent mNA removal at equilibrium decreased linearly from 91.2% to 82.0%, as the initial mNA concentration increased, which was expected because the same amount of QCA was used for each. Figure 4.11 shows the effect of the initial mNA concentration on the pseudo second order rate parameters, as determined by

non-linear regression. The rate constant was observed to exponentially decay from 1.06×10^{-2} to 7.97×10^{-3} g mg^{-1} min^{-1}, while the equilibrium adsorption efficiency increased linearly from 38.5 to 179.4 mg g^{-1} as the initial mNA concentration increased from 0.2 to 1.0 mM. By increasing the bulk mNA concentration, the concentration gradient between the inner pores of the QCA and the bulk solution, which drives the diffusion process, also increases. With improved diffusion of mNA towards to QCA surface, an enhanced adsorption efficiency results.

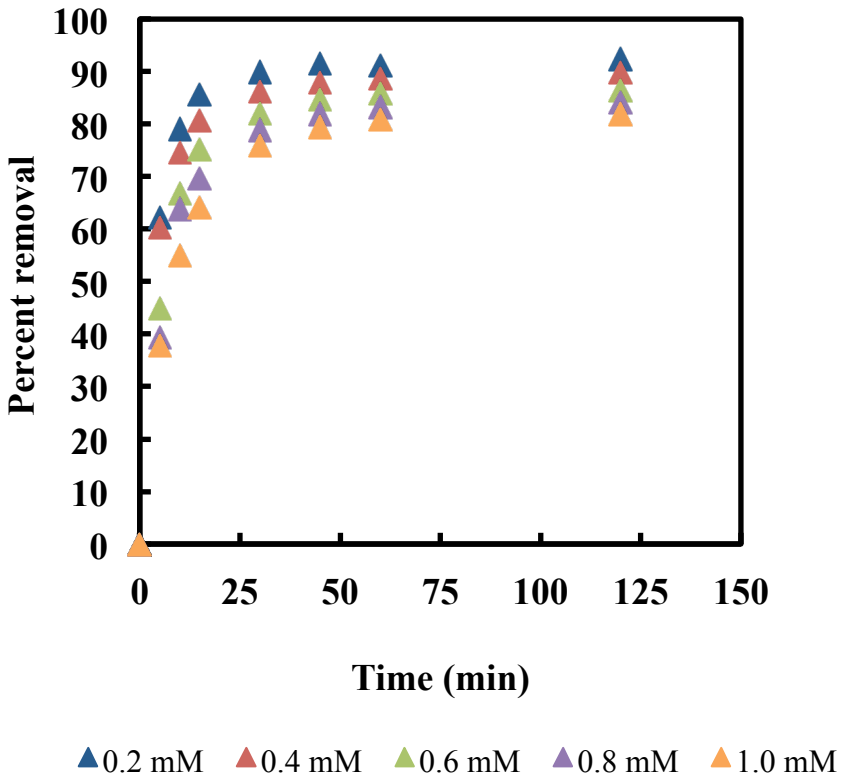

Figure 4.10 Effect of initial adsorbate concentration on the percent mNA removal by QCA.

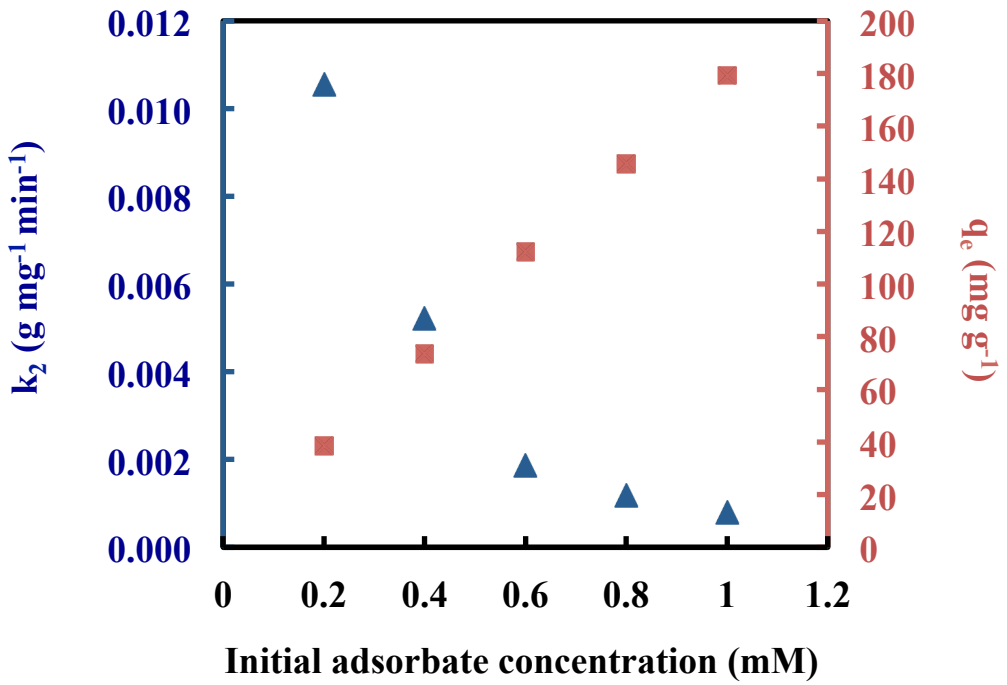

Figure 4.11 Effect of initial adsorbate concentration on the pseudo second order kinetic model parameters k_l and q_e for mNA removal by QCA.

4.3.3.2 Effect of adsorbent dosage

The effect of varying the adsorbent dosage on the kinetics of adsorption is depicted in Figure 4.12. For dosages of 5 and 7.5 mg, it may be observed that equilibrium was achieved within 2 h. However, for dosages of 10 to 15 mg, equilibrium was achieved within just 1 h. For lower adsorbent dosages, the contact between solute and adsorbent surface is limited, resulting in a greater amount of time for the adsorbent surface to reach saturation. An increase in the QCA dosage resulted in an improved percent mNA removal. The increase was almost linear, from 71.5% to 85.5%. With more adsorbent available for at higher dosages for the adsorption of the same amount of mNA in solution, it is rational that the percent removal increases upon increasing QCA dosage. Figure 4.13 demonstrates the

effect of QCA dosage on the rate parameters. By increasing the adsorbent dosage, the ratio of mNA to adsorption sites decreases. In contrast to increasing the initial mNA concentration, as discussed above, the diffusion of solute into each hydrogel is reduced because there is increased competition from other hydrogels. As a result, the equilibrium adsorption efficiency is observed to decrease from 308.2 to 118.9 mg g^{-1} as the QCA dosage increased from 5 to 15 mg. The pseudo second order rate constant was observed to increase from 4.20×10^{-4} to 4.51×10^{-3} g mg^{-1} min^{-1}.

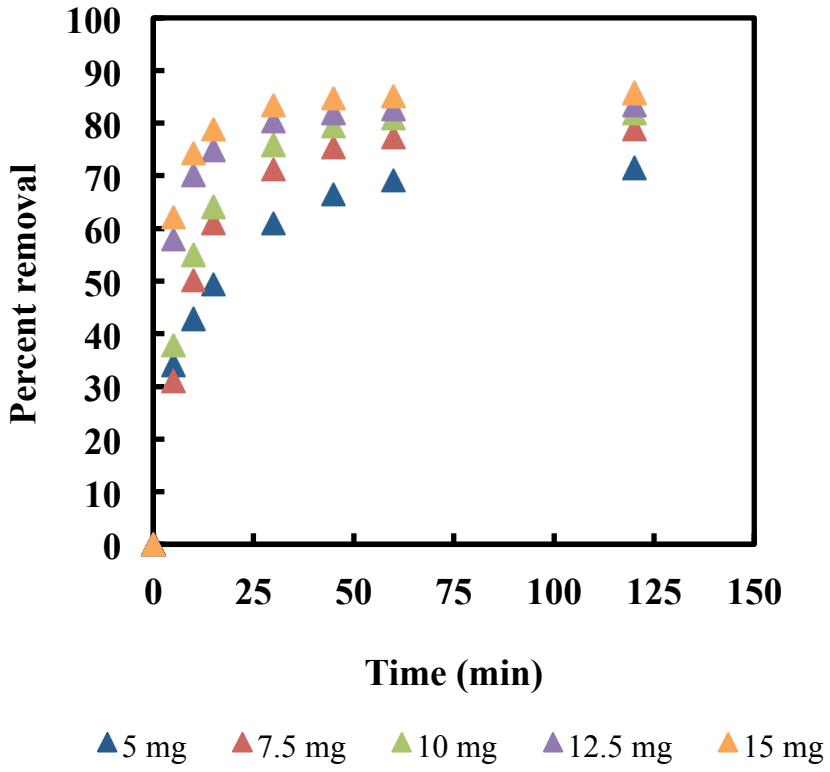

Figure 4.12 Effect of adsorbent dosage on the percent mNA removal by QCA.

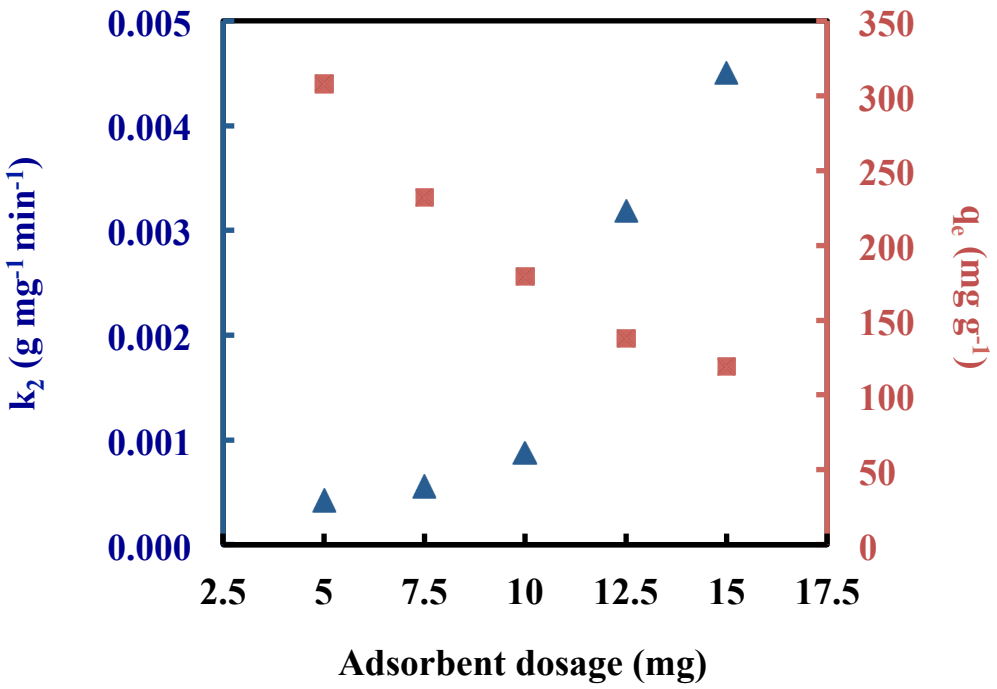

Figure 4.13 Effect of adsorbent dosage on the pseudo second order kinetic model parameters k_1 and q_e for mNA removal by QCA.

4.3.3.3 Effect of agitation rate

The effect of varying the agitation rate of the adsorption system on the kinetics of adsorption is illustrated in Figure 4.14. For agitation rates of 300 and 500 rpm, it may be observed that equilibrium was achieved within 1 h. However, much slower kinetics was observed for the agitation rate of 100 rpm. This slower mixing system took over 4 h to reach equilibrium. Increasing the rate of mixing between the QCA and the mNA solute helped to reduce the thickness of the stagnant boundary layer that surrounds the adsorbent material and limits the rate of diffusion of molecules into the hydrogel pores. Above 300 rpm, the diffusive limitations due to boundary layer effects had already been minimized, so there only minimal improvement in the rate of the system. For all mixing rates, the percent

mNA removal at equilibrium was approximately equal, at 82.3%, 82.0%, and 80.7% for agitation rates of 100, 300, and 500 rpm, respectively. Figure 5.15 shows the effect of the agitation rate on the pseudo second order rate parameters. The rate constant may be observed to increase from 3.74×10^{-5} to 2.22×10^{-3} g mg^{-1} min^{-1} as the agitation rate increased from 100 to 500 rpm. The equilibrium adsorption efficiency for the system decreased as a function of agitation rate, from 291.1 to 167.5 mg g^{-1}.

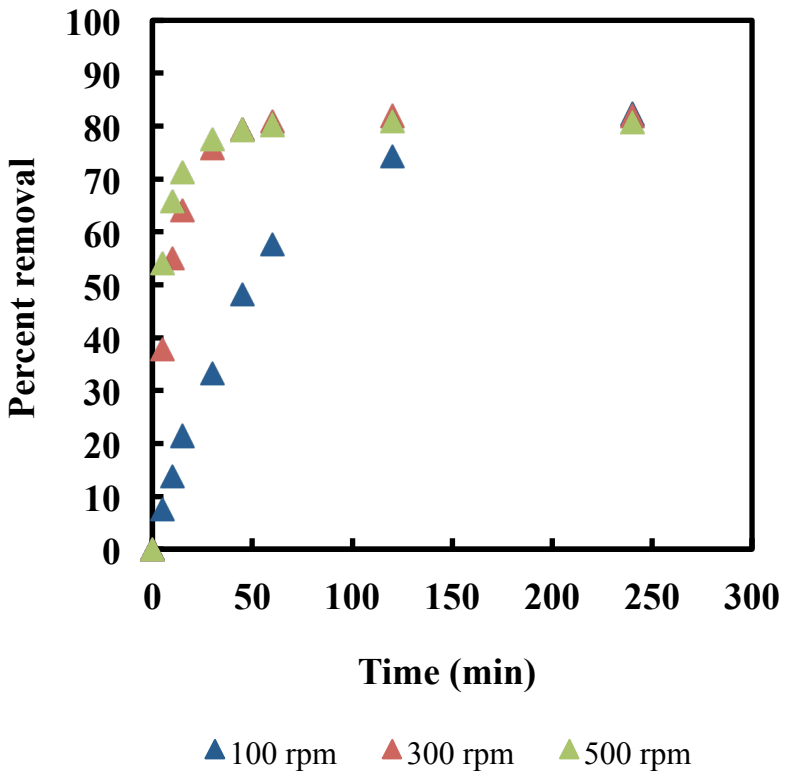

Figure 4.14 Effect of agitation rate on the percent mNA removal by QCA.

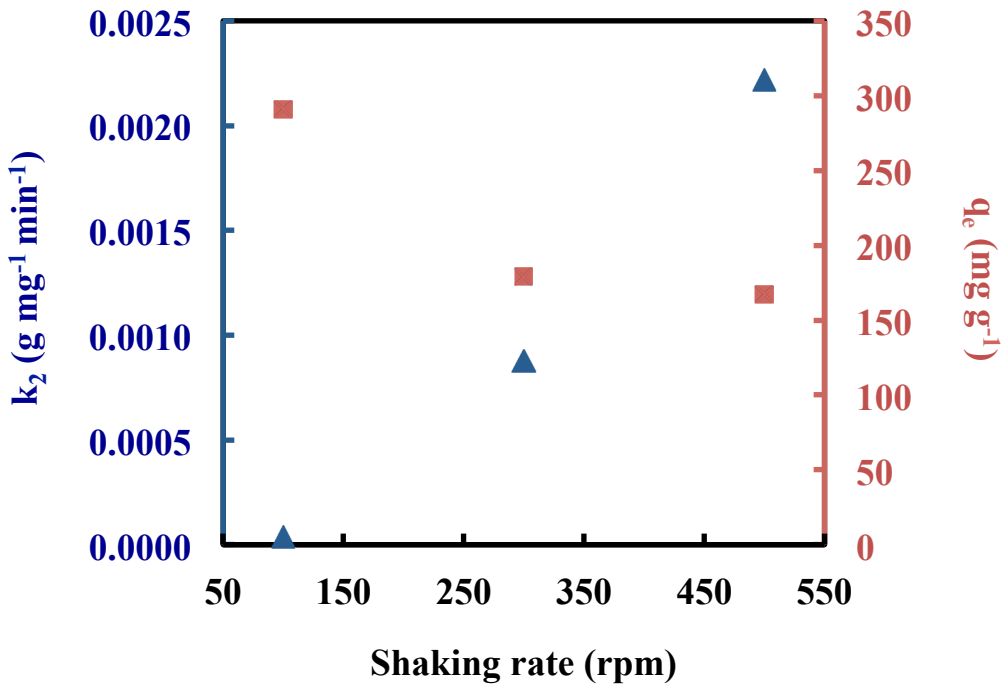

Figure 4.15 Effect of agitation rate on the pseudo second order kinetic model parameters k_1 and q_e for mNA removal by QCA.

4.3.3.4 Effect of initial pH

The effect of varying the initial solution pH on the kinetics of adsorption is depicted in Figure 4.16. For all pH levels, it may be observed that equilibrium had been achieved within 1 h. For pH 4, 6, and 8, the percent mNA removal at equilibrium was approximately equal. It was measured to be 80.6%, 81.6%, and 82.0% for pH 4, 6, and 8, respectively. The most significant reduction in the percent mNA removal at equilibrium was observed for pH 2. Under these conditions, the percent removal was limited to just 17.8%. Sowmya and Meenakshi (2013) reported similar observations for their system. They suggested that the reduced solute adsorption is a result of competitive adsorption by the highly concentrated chloride ions introduced when acidifying the solution with HCl. The chloride ions compete

for adsorption on the positively charged quaternary ammonium groups on QCA. Similarly, a slight reduction in the percent mNA removal to 76.9% was observed for pH 10. This is believed to be a result of the competitive adsorption of hydroxide ions introduced into the system after adding NaOH solution to increase the pH. The observed reduction in percent mNA removal is not as apparent as it was for the system at pH 2, however, because at pH 2 the concentration of chloride ions is ten-fold greater than the concentration of hydroxide ions at pH 10. Further, the majority of carboxylate groups present on the mNA exist in their protonated, non-charged state at pH 2, eliminating the electrostatic attractive forces that exist between mNA and QCA. Figure 4.17 illustrates the effect of initial solution pH on the pseudo second order rate parameters. The rate constant decreases from 1.61×10^{-2} to 2.28×10^{-3} g mg^{-1} min^{-1} as the pH increased from 2 to 4. Further increase in the pH resulted in no drastic changes observed for the rate constant. Contrastingly, the equilibrium adsorption efficiency for the system increased from 14.5 to 169.1 mg g^{-1} as the pH of the system increased from 2 to 4. Again, no drastic changes in q_e were observed for additional increases in pH.

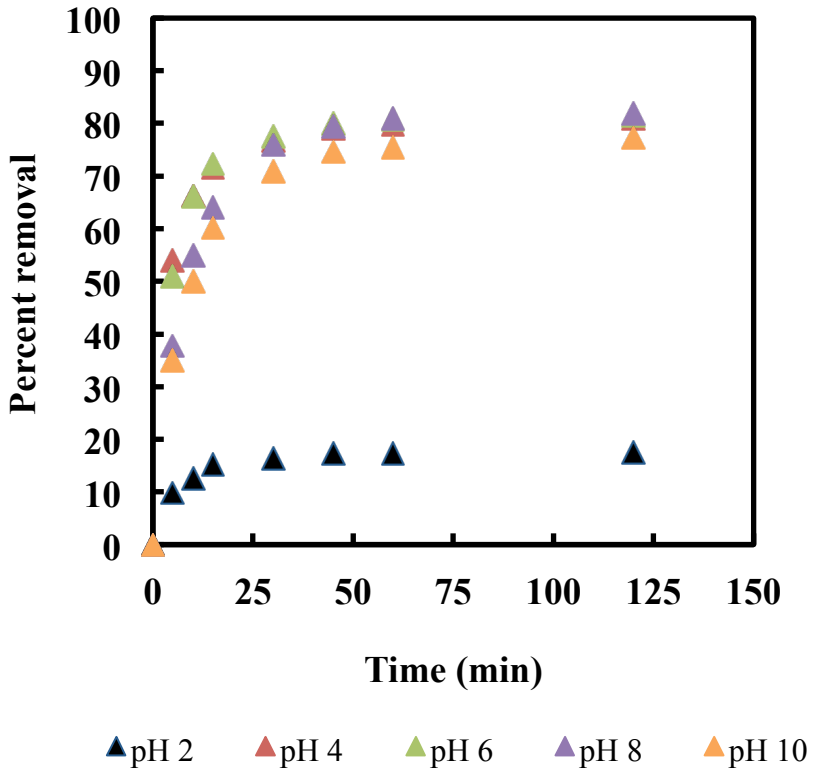

Figure 4.16 Effect of initial pH on the percent mNA removal by QCA.

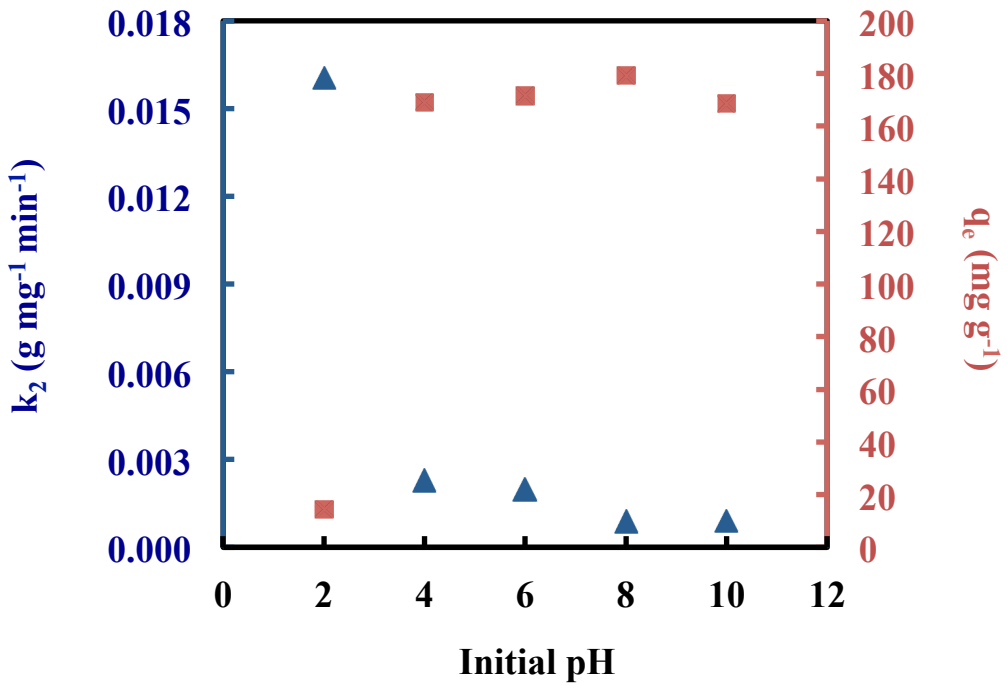

Figure 4.17 Effect of initial pH on the pseudo second order kinetic model parameters k_l and q_e for mNA removal by QCA.

4.3.3.5 Effect of monovalent ionic strength

The effect of varying the ionic strength of the system on the kinetics of adsorption is depicted in Figure 4.18. For all NaCl concentrations, it may be observed that equilibrium had been achieved within 1 h. The percent mNA removal at equilibrium was observed to decay exponentially from 82.0% to 17.7% as the concentration of NaCl increased from 0 to 40 mM. As was observed for especially low and high pH, there is an apparent competition between solutes for adsorption onto the QCA surface. In this case, it is between the added chloride ions and the mNA. At 40 mM NaCl, the concentration of chloride ions in solution is 40 times that of mNA, resulting in a very significant reduction in the efficiency of the mNA adsorption process. Figure 4.19 shows the effect of ionic strength on the constants k_l

and q_e. It is evident that as the concentration of free NaCl in solution increases, as does the rate constant. Further, the equilibrium adsorption efficiency was observed to decay exponentially from 179.4 to 37.9 mg g^{-1} as the concentration of NaCl increased from 0 to 40 mM.

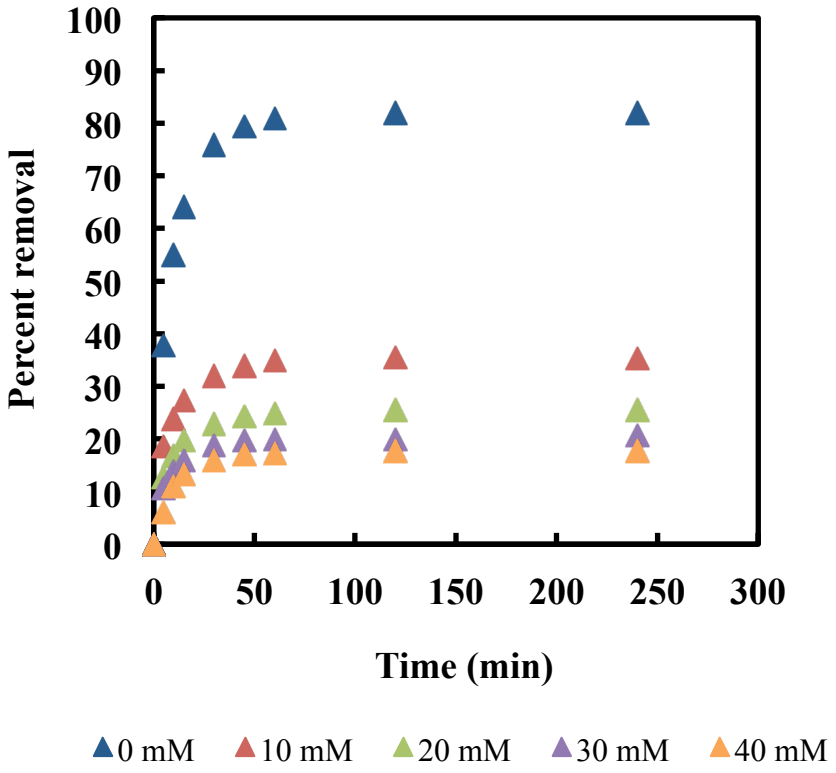

Figure 4.18 Effect of ionic strength on the percent mNA removal by QCA.

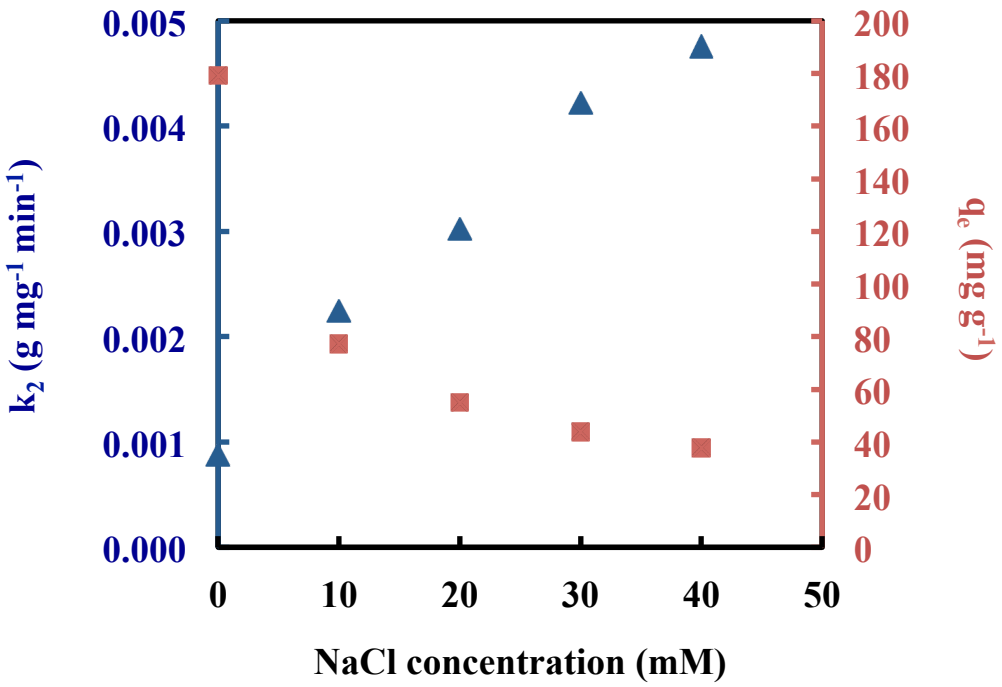

Figure 4.19 Effect of ionic strength on the pseudo second order kinetic model parameters k_l and q_e for mNA removal by QCA.

4.3.3.6 Effect of temperature

The effect of varying the temperature of the system on the kinetics of adsorption is depicted in Figure 4.20. For all temperatures, it may be observed that equilibrium had been achieved within 1 h. An increase in the temperature of the system resulted in a reduction in the time required to reach equilibrium. Figure 4.21 shows the effect of the temperature on the pseudo second order rate parameters. The rate constant was observed to increase linearly from 8.78×10^{-4} to 4.22×10^{-3} g mg^{-1} min^{-1}, while the equilibrium adsorption efficiency decreased slightly from 179.4 to 165.3 mg g^{-1} as the temperature of the system increased from 25 to 45ºC.

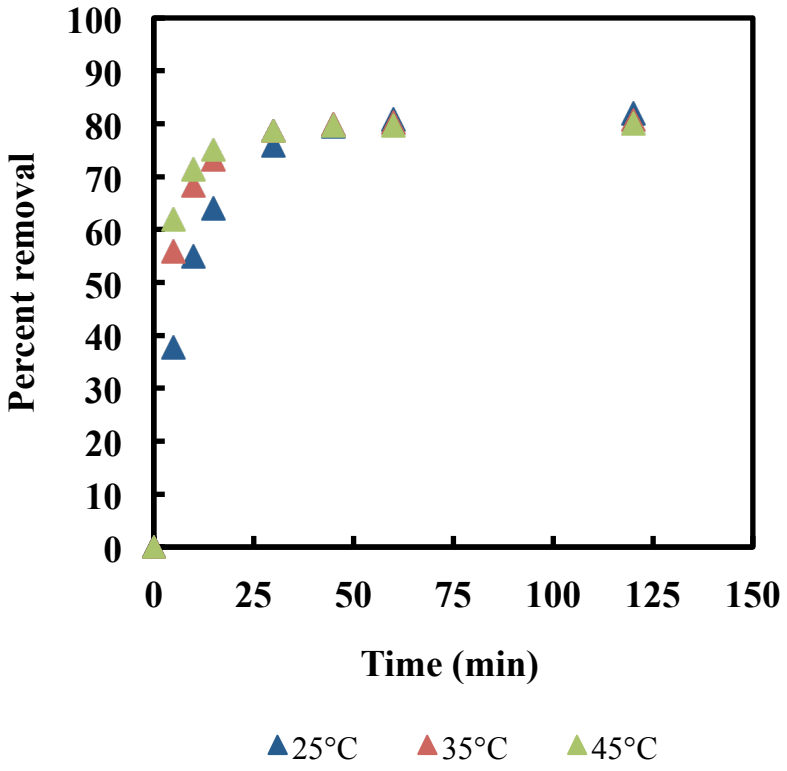

Figure 4.20 Effect of temperature on the percent mNA removal by QCA.

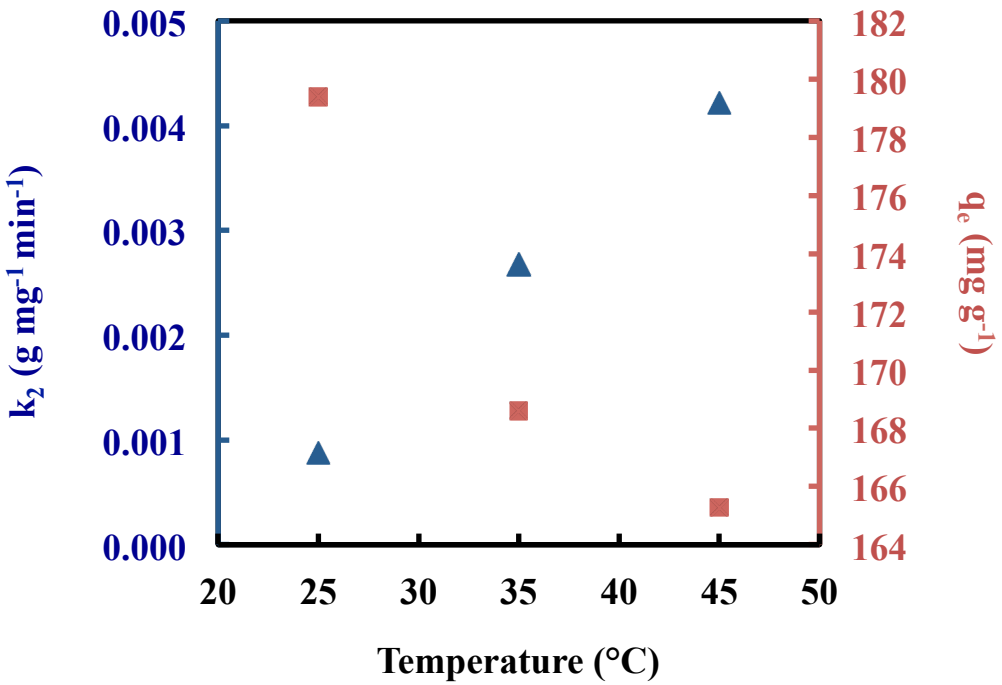

Figure 4.21 Effect of temperature on the pseudo second order kinetic model parameters k_l and q_e for mNA removal by QCA.

Using the pseudo second order rate constants for the three temperatures studied, an Arrhenius plot was constructed to analyze the thermodynamics of the adsorption process of mNA onto QCA (Figure 4.22). The relationship between temperature and rate first described by Arrhenius (1889) is as follows:

$$k = A \exp \frac{-E_a}{RT} \tag{4.6}$$

where k is the rate constant for the process (g mg^{-1} min^{-1}), A is the pre-exponential factor (g mg^{-1} min^{-1}), E_a is the activation energy of the adsorption process (kJ mol^{-1}), R is the universal gas constant (8.314 J mol^{-1} K^{-1}), and T is the temperature of the process (K). By taking the natural logarithm of both sides of Equation 4.6, one may obtain a linear

relationship between the inverse temperature, $1/T$, and the natural logarithm of the rate constant, $\ln k$:

$$\ln k = \frac{-E_a}{R}\frac{1}{T} + \ln A \tag{4.7}$$

The above equation was used to evaluate the temperature effects of the present adsorption system. Linear regression of the data presented in Figure 4.22, yields an activation energy of 62.1 kJ mol^{-1}, which, while towards the upper end of the spectrum, is in alignment with the activation energies for ion exchange systems (Saha and Chowdhury 2011) (Inglezakis and Zorpas 2012). The relatively high activation energy observed suggests that the adsorption system for the given batch experiments is surface adsorption controlled instead of diffusion controlled (Saha and Chowdhury 2011). This is in agreement with the conclusion that for agitation rates of 300 rpm or greater, the effects of external and film diffusion are negligible.

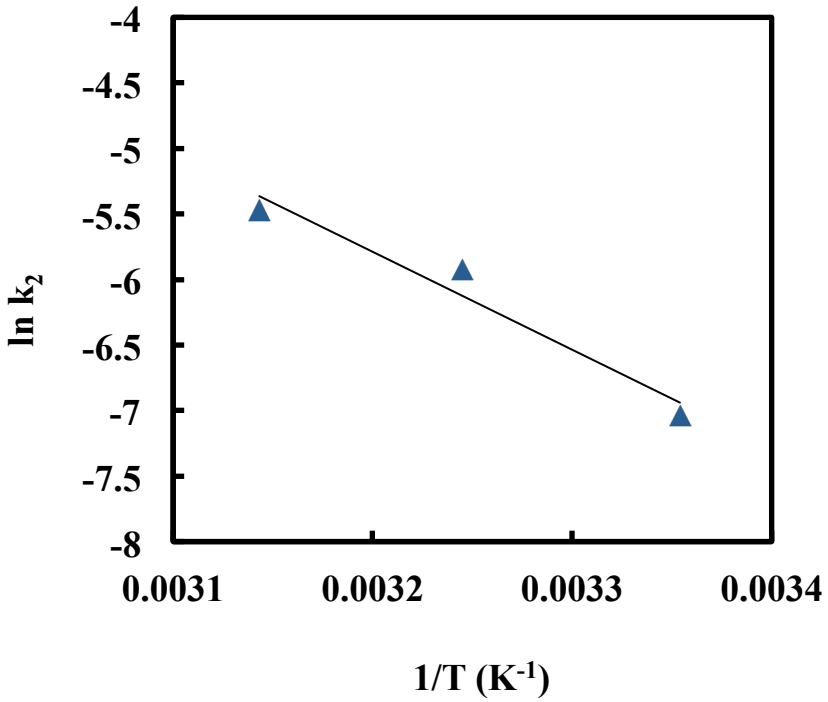

Figure 4.22 Arrhenius plot for the adsorption of mNA onto the optimized QCA.

The change in standard Gibbs free energy, $\Delta G°$, enthalpy, $\Delta H°$, and entropy, $\Delta S°$ of the system at equilibrium could be determined using the percent mNA removal at equilibrium for the system over the range of temperatures studied by plotting the inverse temperature against the natural logarithm of the equilibrium constant, K_c (Figure 4.22). The equilibrium constant may be defined by the following relationship:

$$K_c = \frac{C_o - C_e}{C_e} \tag{4.8}$$

where C_o is the initial adsorbate concentration (mg l^{-1}) and C_e is the adsorbate concentration at equilibrium (mg l^{-1}). At 25, 35, and 45ºC, the observed percent mNA removal during the batch kinetic adsorption experiment was 82.0%, 80.7%, and 80.0%, respectively. This

equates to K_c values of 4.54, 4.18, and 3.99. Therefore, as the temperature of the system increases, the amount of adsorbed mNA is observed to decrease.

The standard Gibbs free energy of the system may be defined by the following two equations:

$$\Delta G° = -RT \ln K_c \tag{4.9}$$

$$\Delta G° = \Delta H° - T\Delta S° \tag{4.10}$$

By substituting Equation 4.9 into Equation 4.10 and rearranging results in the following linear relationship:

$$\ln K_c = -\frac{\Delta H°}{R}\frac{1}{T} + \frac{\Delta S°}{R} \tag{4.11}$$

Linear regression of the data presented in Figure 4.23 allows for the calculation of $\Delta H°$ and $\Delta S°$. Substitution of these parameters into Equation 4.10 allows for the calculation of $\Delta G°$ at the three investigated temperatures. These values are presented below in Table 4.4.

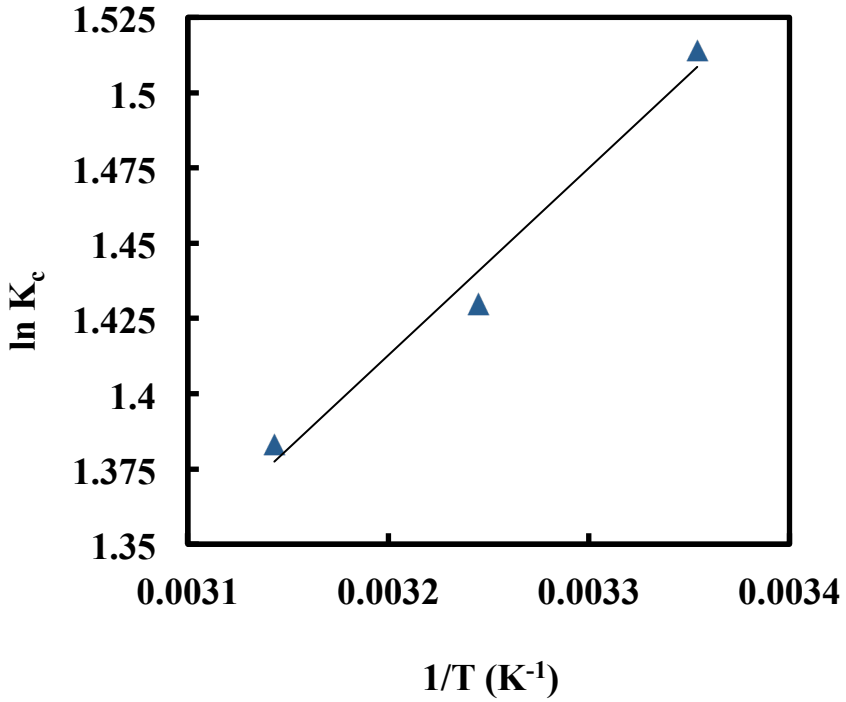

Figure 4.23 Plot of ln K_c against $1/T$ for the adsorption of mNA onto the optimized QCA for determining the thermodynamic parameters of the system.

Table 4.4 Thermodynamic parameters for the adsorption of mNA onto QCA.

Sample	$\Delta G°$ (kJ mol^{-1})			$\Delta H°$ (kJ mol^{-1})	$\Delta S°$ (J mol^{-1} K^{-1})
	298 K	308 K	318 K		
Optimized QCA	-3.74	-3.69	-3.64	-5.17	-4.80

The negative $\Delta H°$ indicates that the process of mNA adsorption on QCA is exothermic. This is often the case for ion exchange adsorption systems (Saha and Chowdhury 2011) (Inglezakis and Zorpas 2012) (Sowmya and Meenakshi 2013). The relatively low value observed for $\Delta H°$ (< |10-15| kJ mol^{-1}) further suggests that the adsorption process is driven by physical interactions (Inglezakis and Zorpas 2012), such as the electrostatic interaction

between the negatively charged carboxylate of mNA and the positively charged quaternary ammonium groups present on QCA. Congruently, an increase in the value of $\Delta G°$ is observed for increases in temperature from 25 to 45ºC. Therefore, the process becomes less spontaneous as the temperature of the system increases.

4.3.4 Regeneration of optimized adsorbent

The regeneration and reuse of the QCA was studied by eluting the adsorbed mNA by submerging the adsorbent material in a 50 mM NaCl solution. Because the adsorption of mNA onto the QCA is believed to be primarily electrostatic, saturation of the system with monovalent salts caused the adsorbed mNA to be replaced as the QCA counterion. This resulted in an increase in mNA concentration in the bulk, which could be detected by UV-vis absorption spectroscopy.

The concentration of mNA in the eluent is presented in Figure 4.24a as a function of time for five adsorption/desorption cycles. After inspection of the figure, it may be concluded that the mNA desorption process reached equilibrium within approximately 2 h. More than 95% of the equilibrium mNA concentration in the eluent had been achieved within the first 30 min of the desorption process. After the desorption process had reached equilibrium, the regenerated QCA were thoroughly washed with water and reused for mNA adsorption. This process was repeated for a total of 5 cycles. Figure 4.24b shows the mNA uptake and elution for each cycle. For each cycle, more than 80% of the mNA in a 1 mM solution was adsorbed onto the surface of the QCA. There was no observed reduction in the reusability of the adsorbents throughout the cycling. The elution process was able to remove over 90% of the adsorbed mNA for each cycle, implying that less than 10% of the

adsorbed mNA remained on the surface of the QCA. Again, this was repeatable throughout cycling.

These results demonstrate the ability of the QCA to be rapidly and efficiently regenerated for reuse by simply exposing the saturated adsorbent to a small volume of high ionic strength solution.

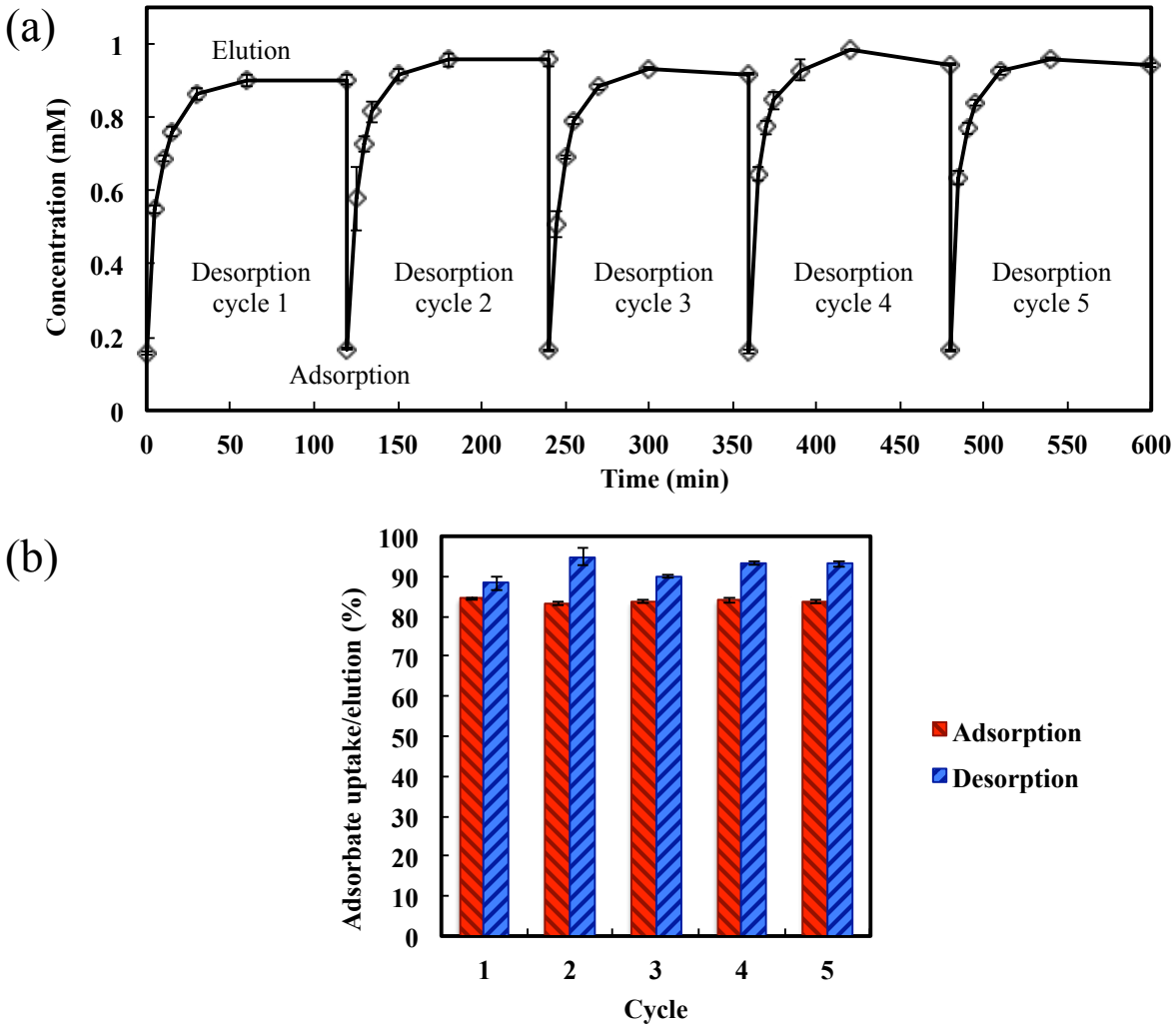

Figure 4.24 Adsorption/desorption cycling for mNA onto the QCA surface showing (a) the bulk concentration of mNA through multiple regeneration cycles and (b) the percent mNA uptake (red bars) and elution (blue bars) for each cycle.

CHAPTER 5

The development of novel quaternized cellulose nanocrystal-chitosan nanocomposite hydrogels for the adsorption of a model aromatic naphthenic acid from aqueous solution

5.1 Introduction

Throughout their useable lifespan, adsorbent materials endure a substantial amount of static and dynamic mechanical stresses (Shchukin, et al. 2006) (Antonyuk, et al. 2005). During manufacturing and packaging, contact with both handling equipment and other adsorbent particles introduces a number of shear stresses applied to the material. During operation, contact with the fluid phase, column wall, and neighbouring adsorbent particles also result in particle shearing. As well, for packed bed adsorption units, the gravitational force of higher packed adsorbents can present significant compressive stresses for particles nearer the bottom of the column. For relatively porous adsorbent materials, such as hydrogels, whose resistance to shear and compressive forces is minimal, this can pose as a significant limitation towards their industrial application (Breitbach, et al. 2002).

To combat this constraint, much work has been dedicated to improving the mechanical properties of hydrogel adsorbents (Liang, et al. 2012) (Wang, et al. 2012) (Güçlü, et al. 2010). One approach is to reinforce the material by using introducing a nanofiller that, through interaction with the hydrogel matrix, may help to better distribute applied stresses, reducing the risk of fracture (Park, Chen and Park 2001) (Wang, et al. 2008) (Zheng and Wang 2009) (Haraguchi 2007) (Kaşgöz and Durmus 2008). In most instances, certain mechanical properties, such as compressive strength, tensile strength, and Young's modulus, are observed to improve as a function of nanofiller loading, up until a certain point (J. Yang, C. -R. Han, et al. 2013).

Due to their inherently strong intermolecular interactions and natural abundance (Klemm, et al. 2005), cellulose-based nanofillers have been under frequent investigation for the improvement of hydrogel mechanical strength (Aouada, et al. 2011) (Eyholzer, et al. 2011) (Wang and Drzal 2012). Specifically, much interest has been directed towards the use of cellulose nanocrystals (CNC), whose high aspect ratio and easily functionalizable surface makes it a prime candidate as a reinforcing material in functional hydrogels (Yang, et al. 2013) (J. Yang, C. -R. Han, et al. 2013) (Abitbol, et al. 2011).

A recent report by Yang and coworkers (2013) discussed the incorporation of CNC into poly(ethylene glycol) hydrogels at loadings ranging from 0.2 to 1.8% v/v to improve the tensile properties of the material. The authors observed significant increases in the Young's modulus and fracture stress of the gels up to a loading of 1.4% v/v. Specifically, the Young's modulus increased from 7.5 ± 0.42 to 31.1 ± 2.3 kPa when increasing the CNC loading from 0 to 1.4% v/v. The fracture stress of the resulting material increased from 65 ± 3.8 to 375 ± 13.5 kPa for the same CNC loading. The authors suggested that the primary mechanism for reinforcement was the strong adsorption of the CNC particles into the PEG matrix, which behaved as physical crosslinks. Further increases in the CNC loading resulted in discontinuities within the hydrogel matrix, causing adverse effects to be observed for the tensile properties of the material.

Abitbol et al. (2011) investigated the reinforcement of poly(vinyl alcohol) hydrogels by incorporating CNC particles into the polymer matrix. CNC was added at loadings ranging from 0.75 to 3.0% w/w. The authors observed an increase in the swelling of the hydrogels, which they attributed to the increased overall hydrophilicity of the material after CNC

incorporation. The compressive strength of the hydrogels was observed to increase from approximately 0.75 kPa to approximately 3.7 kPa as the CNC loading increased from 0 to 1.5% w/w. Similar to the observations reported by Yang et al. (2013), further increase in the CNC loading yielded an overall reduction in the compressive strength, which Abitbol and coworkers also attributed to the disruption of the hydrogel network by the CNC particles.

In this study, CNC and quaternized CNC (QCNC) were used as reinforcing agents in quaternized chitosan hydrogel adsorbents (QCA). The resulting reinforced QCA (rQCA) specimens were applied as adsorbents for the removal of a model aromatic naphthenic acid (mNA), 2-naphthoxyacetic acid, from aqueous solution.

Naphthenic acids (NAs) are a family of aliphatic and alicyclic carboxylic acids naturally present in oil sands ore (Frank, et al. 2009). Upon the mining of this ore, NAs become highly concentrated in the process water used to mine and extract bitumen from the sand particles. Their presence results in a number of process-related and environmental issues, including corrosion of process equipment (Derungs 1956) (Schramm, Stasiuk and MacKinnon 2000) (Fan 1991) and toxicity towards several aquatic organisms (MacKinnon and Boerger 1986) (Schramm, Stasiuk and MacKinnon 2000) (Madill, et al. 2001) (Rogers, et al. 2002) (Frank, et al. 2009). Therefore, their removal from oil sands process-affected water is of primary concern for oil sands producers.

The quaternization of CNC was characterized by conductometric titration to determine the trimethylammonium content on the resulting QCNC material. Zeta potential analysis in

neutral aqueous solution was also used to confirm the charge reversal of desulfated and quaternized CNC.

CNC and QCNC were incorporated into the QCA at loadings of 0.1, 0.2, 0.3, and 0.6% w/w. The effect of adding CNC and QCNC to the hydrogels on the porosity of the hydrogels was characterized by measuring the swelling ratio of the resulting rQCA. The effect of CNC and QCNC loading on the mNA adsorption efficiency was studied by performing a series of batch equilibrium adsorption experiments for each loading. The Langmuir adsorption isotherm provided adequate characterization of the adsorption system. Lastly, the compressive strength of the hydrogel materials under the range of CNC and QCNC loadings was compared to investigate the overall changes in mechanical strength as a function of nanofiller type and loading.

5.2 Experimental section

5.2.1 Materials

Medium molecular weight chitosan (CS, 75-85% deacetylated), sodium hydroxide (NaOH, pellets, ≥ 99.0%), hydrochloric acid (HCl, 37%), glutaraldehyde (GA, 50% w/w in water), dimethylsulfoxide (DMSO, ≥ 99.0%), tetrabutylammonium hydroxide 30-hydrate (TBAH, ≥ 98.0%), glycidyltrimethylammonium chloride (GTMAC, ≥ 90%), silver nitrate (AgNO3, ≥ 99.0%), 2-naphthoxyacetic acid (mNA, ≥ 98.0%), and sodium chloride (NaCl, ≥ 99.0%) were purchased from Sigma-Aldrich and used without further purification. Water (≥ 18 MΩ cm) used in all procedures was filtered through a Millipore Milli-Q Purification System. CNC (CNC) were supplied by CelluForce, Inc.

5.2.2 Methods

5.2.2.1 Synthesis of quaternized CNC

The CNC, as supplied by the manufacturer, possess a negative surface charge attributed to the presence of sulfate ester groups on surface of the nanoparticles. The sulfate group is introduced during the sulfuric acid hydrolysis process used to isolate the CNC from bulk cellulose. Before a permanent positive charge was imparted on the CNC surface via trimethylammonium functionalization, the existing negative charge was removed using a modified procedure of previously published work (Scheme 5.1) (Feng, Esker and Roman 2010). 2 g CNC was added to 100 ml water in a 250 ml round bottom flask. The mixture was dispersed for 5 min at 15 000 rpm using a homogenizer, then sonicated for 10 minutes. 70 ml 5M NaOH was then added to the solution under stirring at 300 rpm and heated to 65ºC. After 5 h, the reaction product was allowed to cool and was dialyzed (12 kDa MWCO) against water for 3 days, with continual water change throughout. The desulfated CNC was then concentrated by centrifugation and lyophilized.

Scheme 5.1 Alkaline desulfation of CNC.

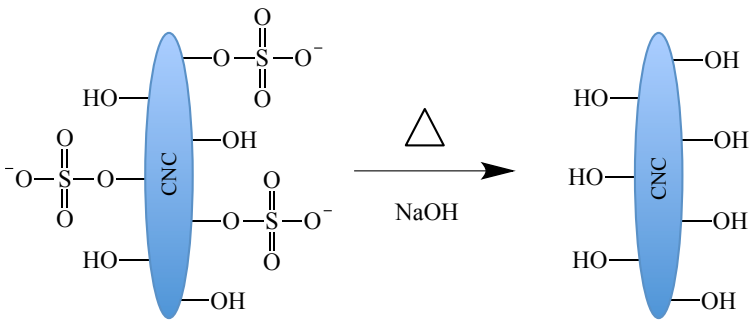

Quaternized CNC (QCNC) was prepared using a modified procedure of previously reported work (Scheme 5.2) (M. Hasani, E. D. Cranston, et al. 2008). 0.6 g desulfated CNC was dispersed in 60 DMSO. Next, 0.6 g TBAH and 2.5 ml water were added. The solution was then degassed using N_2 for 30 min under stirring at 300 rpm. 1.5 ml GTMAC was added to the stirring solution and the vessel was heated to 65ºC. After reacting for 5 h, the reaction product was allowed to cool and was then dialyzed (12 kDa MWCO) against water for 3 days, with continual water change throughout. The aqueous QCNC solution was then concentrated by centrifugation and lyophilized.

Scheme 5.2 CNC quaternization by reaction with GTMAC.

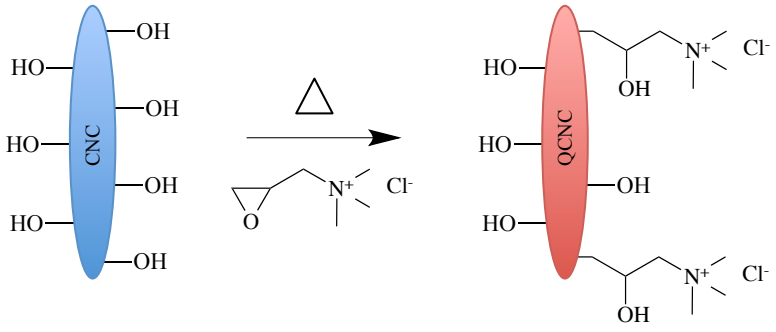

5.2.2.1 Synthesis of quaternized chitosan hydrogel adsorbents

The procedure for preparing the QCA was adapted from the recent work of Sowmya and Meenakshi (Sowmya and Meenakshi 2013). First, aqueous chitosan solutions were prepared by dissolving 300 mg CS in 19.52 to 19.7 ml 1% w/w HAc solution, depending on the desired CNC or QCNC loading (0 to 0.6% w/w). Then, 0 to 180 mg CNC or QCNC was added to the mixture. The solutions were shaken at 500 rpm on an orbital plate shaker for 1 h to ensure complete dissolution. Spherical CS-CNC nanocomposite hydrogels were

then prepared by slowly drop casting the mildly acidic CS-CNC solution into 100 ml of a gently stirring 0.5 M aqueous NaOH solution. A peristaltic pump was used to dispense the solution through a 22G hypodermic needle at a rate of approximately 2 drops per second. The tip of the needle was maintained at a height of 3 cm above the liquid surface. The hydrogels were stirred in the NaOH solution for 30 minutes to allow for complete coagulation. The beads were then carefully filtered from the NaOH solution and placed in 100 ml water to remove the NaOH from the pores of the beads. The beads were stirred for 5 minutes before carefully filtering them from the solution. This wash process was repeated until the pH of the water approached neutral values (pH 6-7) and remained consistent (approximately 5 to 7 total iterations).

The CS-CNC nanocomposite hydrogel beads were then added to 20 ml water in a 100 ml conical flask. Next, 100 µl GA was added and the solution was shaken at 250 rpm for 1 h to allow for the crosslinking reaction to occur, after which the beads were carefully filtered from the reaction solution and were washed using the previously described procedure.

The crosslinked CS-CNC nanocomposite hydrogel beads were then added to 30 ml water in a 100 ml round bottom flask. Next, 2.47 ml GTMAC was added. The contents were then heated to 55ºC under gentle stirring and allowed to react for 12 h. The resulting rQCR were then carefully filtered from the reaction solution and were washed using the previously described procedure. The beads were stored in their hydrated state.

5.2.3 Characterization

5.2.3.1 Conductometric titration

The quaternary amine content on the surface of QCNC was determined by conductometric titration with $AgNO_3$ using a Metrohm 809 Titrando autotitrator. 30 mg QCNC was dissolved in 50 ml water and stirred for 20 minutes at 25ºC to ensure complete dissolution prior to titration. 5 mM $AgNO_3$ was titrated into the solution at a rate of 0.05 ml min^{-1} under moderate stirring. The conductivity of the solution was measured as a function of titrant volume.

5.2.3.2 Zeta potential

To further confirm the presence of trimethylammonium moieties on the CNC surface of QCNC, the zeta potential was measured to compare the apparent surface charge of the CNC before and after surface modification. 0.1% w/w aqueous solutions of CNC and QCNC were prepared at neutral pH and were sonicated for 1 min immediately prior to testing. Zeta potential values were measured using a Malvern Zetasizer Nano ZS90 and a minimum of 10 measurements were reported.

5.2.3.3 Swelling ratio

The swelling ratio of the rQCA was determined gravimetrically. The hydrated beads were placed on cellulose filter paper to remove any excess water and the mass of 15 beads was measured. The beads were dried under vacuum pressure at room temperature for 12 h and the mass of the dehydrated beads was measured. The swelling ratio, *SR* (g g^{-1}), was determined as the ratio of hydrated mass, m_w (g), to dehydrated mass, m_d (g):

$$SR = \frac{m_w}{m_d} \tag{5.1}$$

Each measurement was recorded in triplicate.

5.2.3.4 Equilibrium adsorption

A 1 l stock solution of 1 mM mNA was prepared, with the pH adjusted to 8 using 0.1M NaOH to relate to the pH of OSPW. The same stock solution was used throughout the course of all adsorption experiments. UV-vis absorbance with a range in wavelength of 300-350 nm was used to measure the concentration of mNA in solution (Varian Cary 100 Bio). A calibration plot was prepared by diluting the stock mNA solution to five different concentrations using water (pH adjusted to 8) and measuring the corresponding peak UV-vis absorbance (325 nm) for each concentration. The same calibration plot was used throughout the course of all adsorption experiments.

10 mg dry CNC, QCNC or dry equivalent rQCA were added to a series of five 20 ml polypropylene vials. To each, certain volumes of mNA stock solution and water were added to a total volume of 10 ml and the vials were immediately placed on an orbital shaker and shaken at 300 rpm at 25ºC. After 4 h, equilibrium had been reached. The CNC and QCNC were separated from the system by centrifugation, while the rQCA were simply allowed to settle to the bottom of the vial. 2.5 ml aliquots of mNA solution were removed from each vial. The concentration of mNA was measured using UV-vis absorbance. Five initial adsorbate concentrations were studied: 0.2, 0.4, 0.6, 0.8, and 1.0 mM.

These experiments were used to determine the equilibrium adsorption characteristics for the rQCA under varying CNC and QCNC loadings. The equilibrium adsorption of mNA onto the various rQCA was modeled using the Langmuir isotherm (Langmuir 1916):

$$q_e = \frac{q_m k_l C_e}{1 + k_l C_e} \tag{5.2}$$

where q_e is the specific adsorption of an adsorbent at equilibrium (mg g^{-1}), q_m is the maximum specific adsorption of an adsorbent (mg g^{-1}), k_l is the Langmuir affinity coefficient (l mg^{-1}), and C_e is the concentration of the mNA in the bulk liquid at equilibrium (mg l^{-1}). q_e may be calculated using at equilibrium using the following relationship:

$$q_e = \frac{(C_o - C_e)V}{m} \tag{5.3}$$

where C_o is the initial mNA concentration, V is the volume of the system, and m is the adsorbent dosage.

The parameters to the Langmuir equation, q_m and k_l were evaluated nonlinearly using the MATLAB built-in function *nlinfit*.

5.2.3.5 Compression testing

To determine the effect of CNC and QCNC incorporation into the QCS hydrogel matrix on the mechanical properties of the beads, compression testing using a tension/compression instrument equipped with a 10 N load cell was completed. The hydrated beads were placed

on cellulose filter paper to remove any excess water and then uniaxially compressed between two parallel plates. The compression rate used was 0.05 mm s^{-1}. The engineering strain, σ_e (kPa), with respect to the initial cross-sectional area, A_o (m^2), of the spherical hydrogel beads, was measured in response to the applied stress.

$$\sigma_e = \frac{F}{A_o} \tag{5.4}$$

where F is the applied load (N). The compressive strength of each specimen corresponds to the observed engineering strain just prior to fracture, σ_e^*:

$$\sigma_e^* = \frac{F^*}{A_o} \tag{5.5}$$

Where F^* is the applied load just prior to fracture. The compressive strength measurements were replicated 10 times.

5.3 Results and discussion

5.3.1 CNC quaternization

5.3.1.1 Conductometric titration

The amount of quaternary ammonium groups present in cellulose-based materials has often been quantified by conductometric titration of chloride counterions using silver nitrate (M. Hasani, E. Cranston, et al. 2008) (Pei, et al. 2013). The titration data for QCNC is presented in Figure 5.1. For the titration, two clear stages separated by a conductivity minimum may be observed. The first stage shows a linear decrease in solution conductivity.

This is a result of free silver cations in solution binding with the chloride counterions of the quaternary ammonium groups on the QCNC sample to form silver chloride, which rapidly precipitates out of solution. The bulkier and less mobile nitrate anions that replace the chloride counterions are weaker conductors of electricity (Haynes 2014), thus resulting in the observed conductivity decrease. The second stage shows a sharp linear increase in solution conductivity, which results from the addition of free silver cations and nitrate anions into solution. The titration endpoints can be visually detected as the points of inflection between these two stages. Linear regression was used to model each of the two linear stages and the point of intersection between the two lines was used to determine the volume of silver nitrate titrant required to reach molar equivalence with the chloride ions and, thus, the quaternary ammonium groups. The quaternary ammonium content for the QCNC was 0.78 mmol g^{-1}.

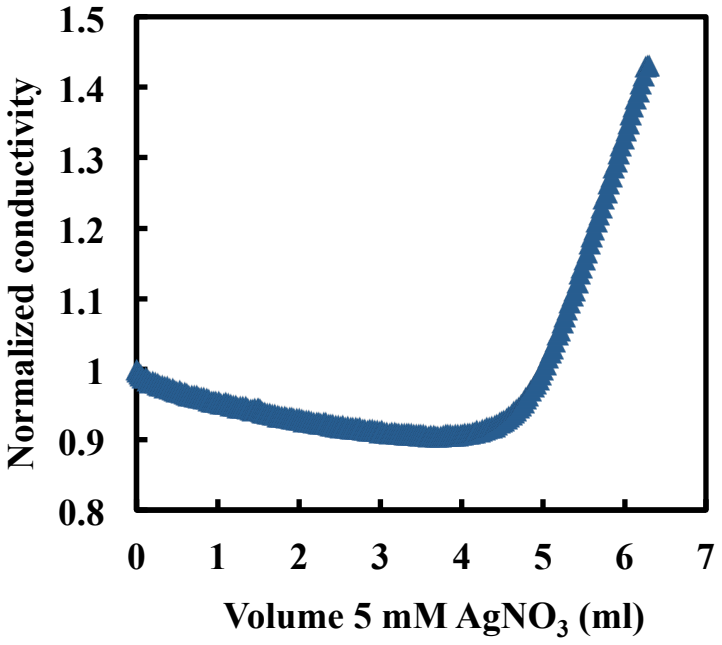

Figure 5.1 Conductometric titration of QCNC with $AgNO_3$.

5.3.1.2 Zeta potential

The zeta potential values displayed in Figure 5.2 help to further validate the presence of quaternary ammonium groups on QCNC. A complete charge reversal from -66.8 ± 9.51 to +76.1 ± 4.47 mV may be observed for the QCNC derivatives. This indicates the prominence of the positively charged species after desulfation and quaternization of CNC.

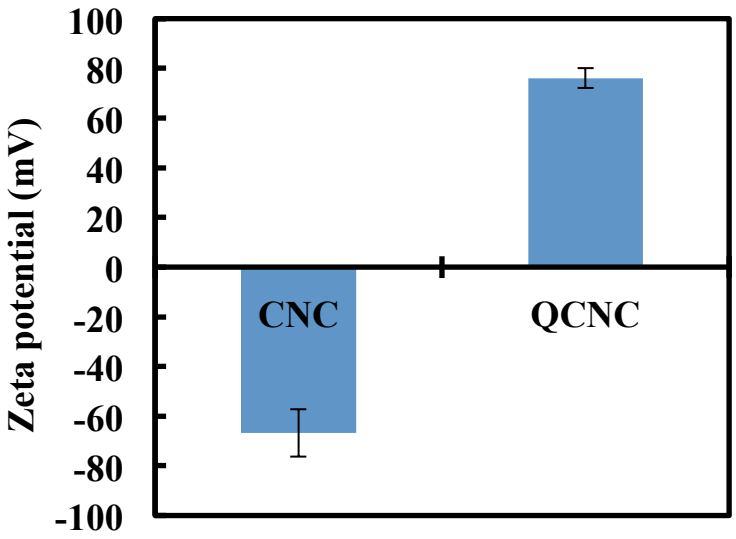

Figure 5.2 Zeta potential measurements for CNC and QCNC.

5.3.2 CNC and QCNC reinforced QCA

5.3.2.1 Swelling ratio

Figure 5.3 shows the effect of CNC and QCNC loading on the swelling properties of the resulting hydrogels. For both, a near-linear reduction in swelling ratio as a function of nanoparticle loading was observed. The swelling ratio for the QCA prior to reinforcement was 62.6 ± 0.37 g g^{-1}. Adding CNC and QCNC at solids loadings of 0.6% w/w yielded reduced swelling ratios of 39.4 ± 0.68 and 51.8 ± 1.62 g g^{-1}. The swelling ratio for the QCA

reinforced with CNC was reduced at an increased rate when compared to the QCNC reinforced QCA. The swelling ratio of hydrogels is a strong function of hydrogel hydrophilicity, material density, and degree of crosslinking for the gel. The CNC and QCNC reinforced materials may be expected to have the same overall hydrophilicity. Both nanofillers possessed charged surfaces and the overall QCS hydrogel matrix was very strongly positively charged, permitting both materials to absorb water molecules to a relatively high extent. Further, both the CNC and QCNC reinforced hydrogels were covalently crosslinked with the same amount of glutaraldehyde. Therefore, it is safe to assume that the degree of covalent crosslinking remains consistent regardless of the type of reinforcing agent. However, it is believed that the electrostatic interaction between the negatively charged sulfate ester moieties on CNC and the positively charged trimethylammonium groups on QCS result in the generation of physical crosslinking throughout the gel material. An increase in the CNC loading yields a greater degree of crosslinking, limiting the ability of the hydrogels to swell upon hydration. This electrostatic crosslinking is not observed for the QCNC reinforced material because the surface charge of QCNC is strongly positive. The trimethylammonium groups on QCNC repel those of QCS and so the QCNC particles are more loosely bound within the polymer gel network. Scheme 5.3 illustrates the effect of CNC and QCNC loading on the particle-matrix interactions that result in changes in hydrogel swelling. The slight reduction in swelling ratio upon increasing the QCNC loading, however, may be attributed to the overall density of the QCNC particles compared to the QCS hydrogel network. While the QCS exists as a loose, swollen polymer network upon hydration, the QCNC particles are composed of dense crystalline cellulose. While the water from within the polymer network may escape

during drying, the mass of the nanofiller material remains the same. Therefore, the mass of the dried hydrogels when reinforced with CNC or QCNC is larger than for the pristine QCA. This density effect also contributes to the observed reduction in swelling ratio upon increasing the nanofiller loading.

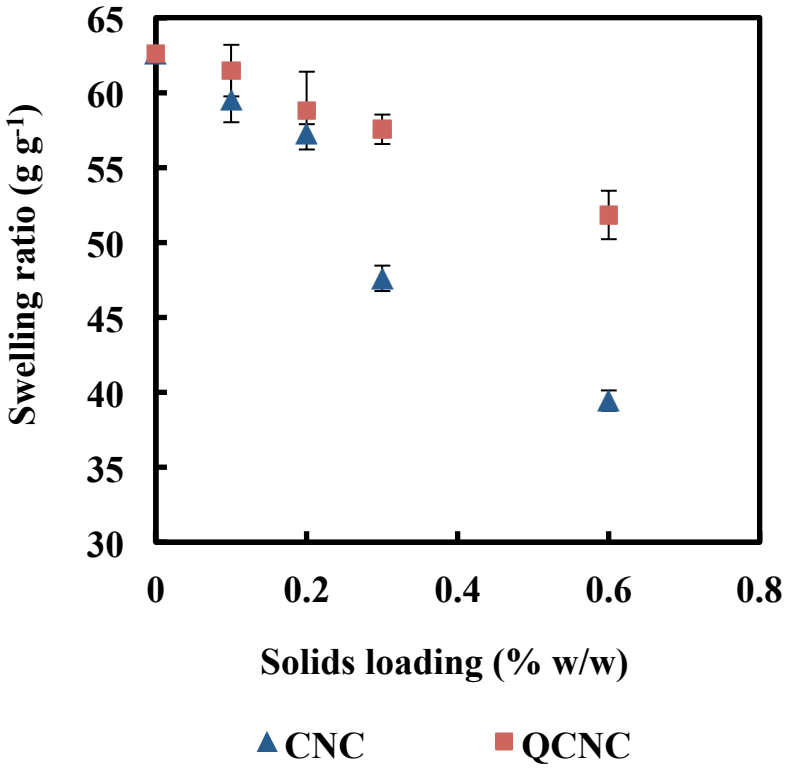

Figure 5.3 Swelling ratio for QCA reinforced with CNC (blue triangles) and QCNC (red squares).

Scheme 5.3 Hydrogel swelling behaviour as a result of CNC (blue) or QCNC (red) surface interactions with QCS matrix.

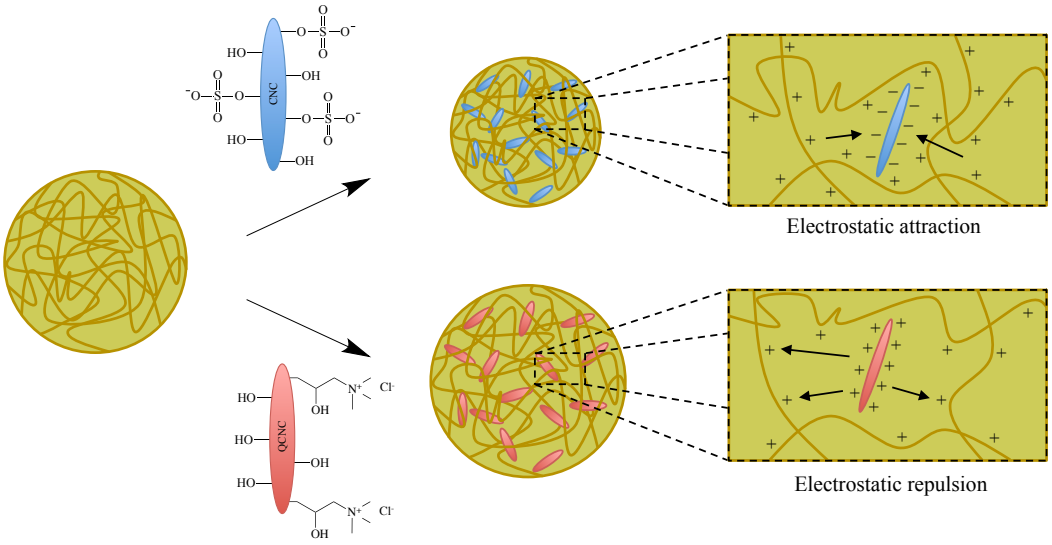

5.3.2.2 Equilibrium adsorption

The mNA adsorption efficiencies for CNC and QCNC as modeled by the Langmuir adsorption isotherm are presented in Figure 5.4. The Langmuir isotherm provided adequate fitting with $r^2 > 0.98$ for all experiments. For all experiments, adsorption equilibrium had been reached within 2 h under the conditions used.

The adsorption efficiency for QCNC was more than three-fold that of CNC. The adsorption efficiencies for CNC and QCNC were 43.4 and 144.5 mg g^{-1}, respectively. The strong positive surface charge of QCNC lends to its ability to electrostatically adsorb the negatively charged mNA molecules in solution. Meanwhile, the negative surface charge of CNC made it a poor adsorbent for the organic carboxylates. The low degree of adsorption observed, however, is attributed to hydrophobic interaction between the organic fraction of the mNA molecules and the cellulose material in sulfate ester-free domains.

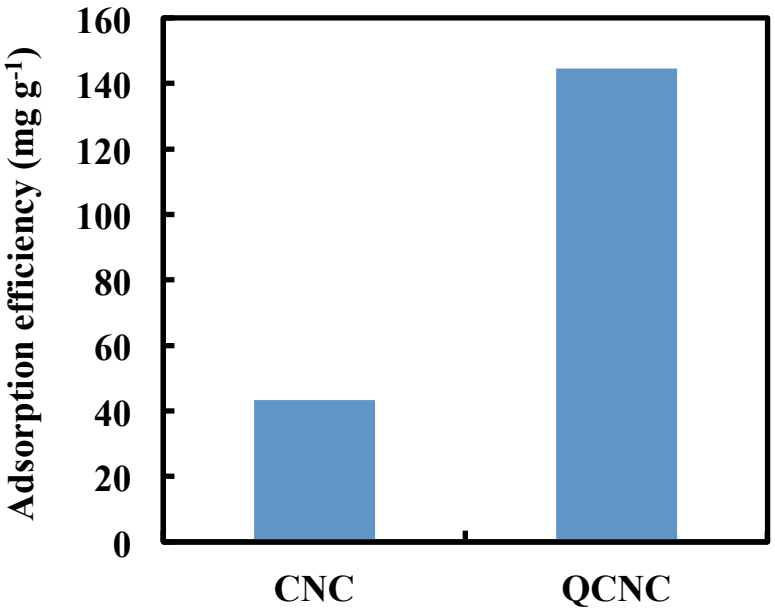

Figure 5.4 Langmuir adsorption efficiency for CNC and QCNC.

The mNA adsorption efficiencies for QCA reinforced with CNC and QCNC are displayed in Figure 5.5. As was observed with the swelling ratio of the hydrogel beads, the adsorption efficiency of both is observed to decay exponentially with an increase in nanofiller loading. The adsorption efficiency for the QCA without reinforcement was 314.9 mg g^{-1}. Addition of CNC and QCNC at a loading of 0.6% w/w yielded significantly reduced adsorption efficiencies of 192.7 and 228.0 mg g^{-1}. The electrostatic crosslinking between the QCS and CNC is believed to be a primary cause for the observed reduction in adsorption efficiency upon increasing addition of CNC. By introducing negatively charged functional groups to bind the positively charged groups of QCS, the number of available sites for mNA adsorption is reduced. By increasing the amount of CNC present in the hydrogel matrix, the number of potential sites for adsorption is reduced. Further, the CNC material contributes to the overall mass of the adsorbent material. However, the CNC

material does not contribute significantly to the adsorption of mNA. Since the adsorption efficiency is normalized by the mass of the adsorbent material, an overall reduction may be observed when increasing the amount of CNC. A similar inference may be made for the QCNC rQCA. While the QCNC contributes significantly to the overall mass of the adsorbent, it does not contribute to the adsorption of mNA to the same degree as the QCS hydrogel network. Therefore, an overall reduction in the adsorption efficiency is observed while increasing the QCNC loading.

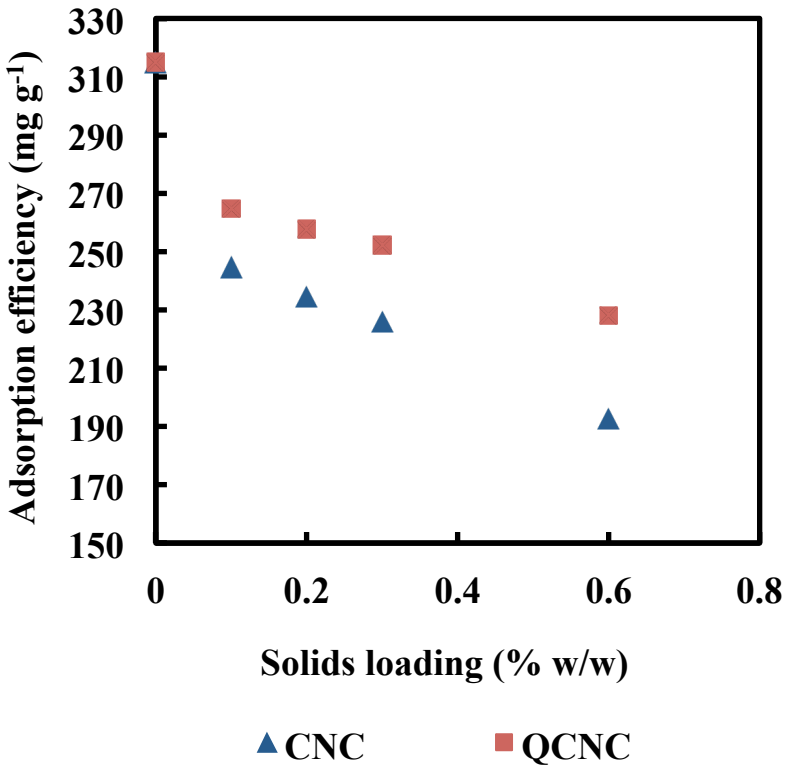

Figure 5.5 Langmuir adsorption efficiency for QCA reinforced with CNC (blue triangles) and QCHC (red squares).

Similar observations were reported by Zheng and Wang for their study of the incorporation of rectorite clay particles into the matrix of a chitosan-poly(acrylic acid) dual

polymer hydrogel adsorbent system to reduce the overall cost of the material. The material was used to remove ammonium from aqueous solution. While the hydrogel matrix alone reportedly possessed an adsorption efficiency of 40.61 mg g^{-1}, the rectorite particles were much weak adsorbents, with an adsorption efficiency of 1.54 mg g^{-1}. Upon addition of the rectorite into the hydrogel adsorbent system, the adsorption efficiency was observed to decrease to as low as 17.3 mg g^{-1} with a loading of 50% w/w.

Therefore, the adsorption efficiency of a composite adsorbent material may in some cases be considered to be additive of the adsorption efficiencies of each individual component, based their relative compositions. However, the effects of particle-matrix interactions may yield deviations from this generalization.

5.3.2.3 Compression testing

The compressive strengths of the rQCA are shown in Figure 5.6. The series of stress-strain curves for each formulation are shown in Appendix B (Figures B1 to B9). For both the CNC and QCNC reinforced hydrogels, a very clear increase in compressive strength may be observed. The compressive strength of the non-reinforced QCA was 5.56 ± 1.57 kPa. Adding CNC at solid loadings of 0.1, 0.2, 0.3, and 0.6% w/w resulted in highly improved compressive strengths of 8.10 ± 0.71, 9.14 ± 1.15, 10.08 ± 2.43, and 15.06 ± 0.78 kPa, respectively. The addition of QCNC at solid loadings of 0.1, 0.2, 0.3, and 0.6% w/w yielded slightly more modest, but still improved compressive strengths of 7.21 ± 0.67, 7.94 ± 1.86, 7.96 ± 0.57, and 12.17 ± 1.22 kPa, respectively. At the highest solids loading (0.6% w/w), the addition of CNC and QCNC to the QCA material resulted increases in compressive strength of 171% and 119%, respectively.

Typically, nanofiller materials provide structural reinforcement to hydrogels through the even distribution of applied stresses throughout the bulk of the material, reducing the risk to crack nucleation at specific sites within the material. The ability for nanofiller materials to do so, however, hinges on their interfacial adhesion with the neighbouring polymers and their uniform dispersion throughout the matrix material. A number of studies reporting on the reinforcement of materials by CNC incorporation attribute the observed improvement in mechanical properties to the interfacial interactions between the matrix material and the CNC surface (Fox, et al. 2012) (Yang, et al. 2013) (Azouz, et al. 2012) (J. Yang, C. -H. Han, et al. 2014). For the presently reported CNC reinforced QCA, the interfacial adhesion is likely greater due to the high degree of electrostatic gel points that exist between the negatively charged CNC and positively charged QCS. It is believed that, under compressive strain, this improved interactivity yields superior force displacement from the relatively weak hydrogel matrix to the tougher nanorods. For the QCNC reinforced QCA, the electrostatic repulsion that exists between the positively charged QCNC particles and QCS matrix is believed to yield poorer interfacial adhesion. However, modest improvements in the compressive strength of the resulting hydrogels were still observed. Although it was not observed under the solids loadings used in this study, it is possible for the addition of nanofiller beyond a certain point to hinder the mechanical properties of the bulk material. Such a phenomenon is typically attributed to nanofiller aggregation with the continuous phase.

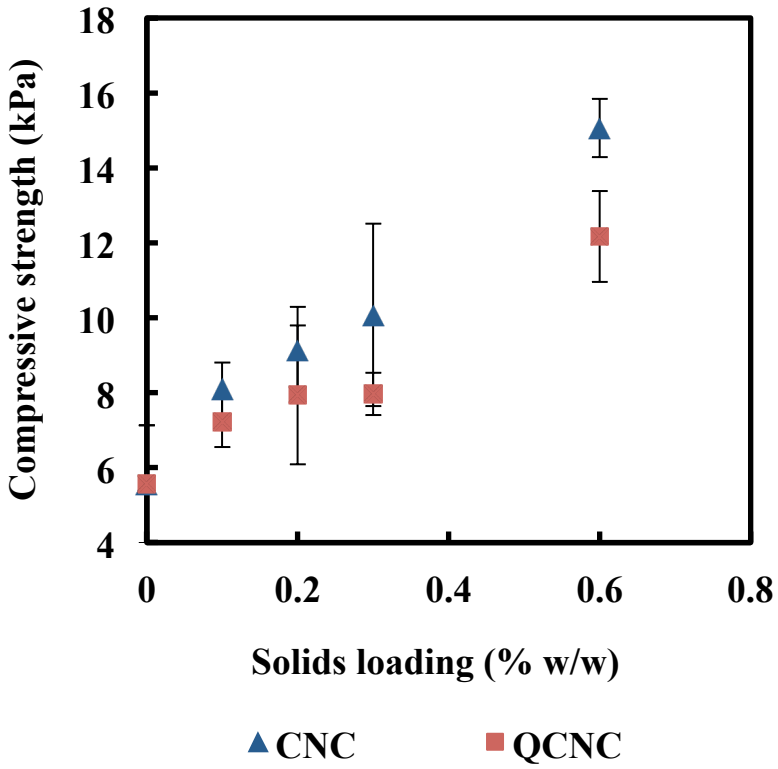

Figure 5.6 Compressive strength for QCA reinforced with CNC (blue triangles) and QCHC (red squares).

CHAPTER 6

Conclusions and engineering significance

6.1 Conclusions for the work presented in Chapter 4

Covalently crosslinked quaternized chitosan hydrogels were prepared using a modified method of Sowmya and Meenakshi (2013). The resulting hydrogels were applied as adsorbents for the removal of 2-naphthoxyacetic acid, a model NA (mNA), from aqueous solution. The effects of varying three processing parameters on the swelling behaviour and adsorption efficiency of the hydrogels were investigated. The parameters studied were the density of the chitosan polymer in the hydrogels, the amount of glutaraldehyde used for covalent crosslinking of the hydrogels, and the amount of GTMAC used to impart quaternary ammonium functionality to the hydrogels.

The swelling ratios of the resulting hydrogels, which provide insight into the extent of gelation and resulting porosity of the hydrogels, were measured gravimetrically. The maximum efficiency with which the mNA was adsorbed onto the resulting hydrogels was estimated by modeling a series of batch equilibrium adsorption experiments using the Langmuir adsorption isotherm.

The swelling ratio of the hydrogels was observed to decrease at a linear rate from 57.0 ± 2.55 g g^{-1} to 30.0 ± 0.94 g g^{-1} when the chitosan density increased from 1 to 2% w/v. Meanwhile, the adsorption efficiency remained relatively unchanged for changes in chitosan density. The predicted adsorption efficiencies varied from 181.8 to 197.3 mg g^{-1}, but without any observable trend. This result indicated that although the porosity of the hydrogels decreased with increasing polymer density, the ability of the material to remove

the mNA from water did not suffer. This leads to the conclusion that the equilibrium adsorption process is not hindered by diffusive limitations.

Increasing the amount of crosslinking agent used to gel the chitosan polymer resulted in near linear decreases for both the swelling ratio and adsorption efficiency of the adsorbent. The swelling ratio decreased sharply from 77.6 ± 2.43 g g^{-1} to 57.4 ± 0.72 g g^{-1} when the molar ratio of aldehyde on glutaraldehyde to amine on chitosan was increased from 0.5 to 1. A modest reduction in swelling ratio from 57.4 ± 0.72 g g^{-1} to 46.6 ± 0.49 g g^{-1} was observed when the ratio was further increased from 1 to 2.5. The adsorption efficiency decreased linearly from 185.3 to 159.6 mg g^{-1} when the ratio was increased from 0.5 to 2.5. It is believed that by increasing the extent of crosslinking, the number of potential sites for adsorption is reduced. This is because the amine groups that participate in the crosslinking reaction are also hosts for the future quaternization reaction, which provides the quaternary amine groups necessary for adsorbing the negatively charged mNA. The limited adsorption efficiency for highly crosslinked hydrogels is not believed to be a result of limited mass transfer.

A swelling ratio of 49.5 ± 1.43 g g^{-1} was detected for hydrogels produced using a molar ratio of GTMAC to amine group equal to 5, while an increased swelling ratio of 59.1 ± 0.67 g g^{-1} was observed when the ratio was increased to 17.5. This was believed to be a result of increased hydrophilicity of the hydrogels and electrostatic repulsion between cationic groups. A sharp improvement in the adsorption efficiency from 107.3 to 227.8 mg g^{-1} was observed as the ratio increased from 5 to 12.5. Further increase in the amount of quaternizing agent resulted in only a minor improvement in adsorption efficiency, from

227.8 to 266.4 mg g^{-1}. This saturation is believed to correspond to a maximal degree of quaternization, wherein all available primary amine groups on chitosan have undergone quaternization.

Using the results of the parameter study, an optimized quaternized chitosan hydrogel adsorbent (QCA) was prepared, with an adsorption efficiency of 315 mg g^{-1}. When compared with other adsorbent materials reported in the literature, the adsorption efficiency of the presently reported material was on par if not superior.

Studying the effects of various process parameters on the adsorption kinetics of the mNA onto the optimized QCA showed that initial adsorbent concentration, adsorbent dosage, agitation rate, pH, ionic strength, and temperature were all of significance. Increasing the initial adsorbate concentration from 0.2 to 1.0 mM resulted in a reduction in the initial rate of adsorption and the overall percent removal. Increasing the adsorbent dosage from 5 to 15 mg dry equivalent caused the initial rate of adsorption and overall percent removal to increase. Increasing the agitation rate from 100 to 300 rpm resulted in a drastic improvement in the initial adsorption rate. Further increase to 500 rpm did not result in any further significant improvements. The overall percent removal at all three rates did not vary significantly. The effect of pH was only prominent in highly acidic and basic environments when charge screening due to ionic strength is more prevalent. The initial rate of adsorption and percent removal were very drastically reduced at pH 2. Increasing the monovalent ionic strength from 0 to 40 mM caused the initial rate of adsorption to decrease. The percent removal was also observed to decay exponentially. This was likely a result of charge screening and competitive adsorption. Increasing the temperature of the

system from 25 to 45ºC caused a very slight increase in the initial rate of adsorption. However, the percent removal at equilibrium showed a slight reduction. The standard changes in Gibbs free energy, enthalpy, and entropy for the adsorption process at 25ºC were -3.74 kJ mol^{-1}, -5.17 kJ mol^{-1}, and -4.80 J mol^{-1} K^{-1}, indicating that the adsorption of the mNA onto the QCA was spontaneous and exothermic.

Regeneration of the adsorbent by contacting the hydrogels with NaCl solution was simple and efficient. After five cycles, the adsorbents maintained the same ability to remove the mNA from aqueous solution.

To the best of our knowledge, this work is one of very few studies to investigate the adsorption of NAs using polymeric resins and is first to report the use of biopolymer based hydrogels for this application. We believe that the thorough investigation of the processing parameters involved in the preparation of these hydrogel adsorbents will be of significant value to those looking to prepare similar materials.

6.2 Conclusions for the work presented in Chapter 5

Cellulose nanocrystals (CNC) and quaternized CNC (QCNC) were used as reinforcing agents in QCA. The resulting reinforced QCA (rQCA) were applied as adsorbents for the removal of 2-naphthoxyacetic acid, a model aromatic naphthenic acid (mNA), from aqueous solution.

QCNC were successfully prepared by the method of Feng and coworkers (2010). Desulfation was used to remove the existing negative surface charge of the particles and a positive charge was introduced by reaction with GTMAC. The quaternary ammonium

content of the particles, as determined by conductometric titration, was 0.78 mmol g^{-1}. The charge reversal was verified by comparing the zeta potentials of the pristine unreacted particles and the particles after desulfation and quaternization. The zeta potential was observed to change from -66.8 ± 9.51 to +76.1 ± 4.47 mV.

The adsorption of the mNA onto CNC and QCNC was studied using batch equilibrium adsorption experiments. The maximum adsorption efficiencies for the two nanomaterials, as estimated using the Langmuir adsorption isotherm, were 43.4 and 144.5 mg g^{-1}. It is believed that the adsorption efficiency of the quaternized cellulose nanocrystal provided enhanced adsorption due to the strong electrostatic attraction that exists between the anionic adsorbate molecules and the cationic trimethylammonium functionality of the material.

The swelling ratio of the rQCA was observed to decrease linearly with the addition of CNC or QCNC into the hydrogel matrix. The swelling ratio for the adsorbent prior to reinforcement was 62.6 ± 0.37 g g^{-1}. Adding CNC and QCNC at solids loadings of 0.6% w/w yielded reduced swelling ratios of 39.4 ± 0.68 and 51.8 ± 1.62 g g^{-1}. The drastic reduction upon addition of CNC may be attributed to the generation of new physical gel points, which limits the ability of the hydrogels to swell when hydrated.

The adsorption of the mNA onto the QCA prior to the addition of CNC or QCNC was 315 mg g^{-1}, as previously reported. Addition of CNC and QCNC at a loading of 0.6% w/w yielded significantly reduced adsorption efficiencies of 192.7 and 228.0 mg g^{-1}. The observed reductions were attributed to the weaker ability of the nanofiller material to adsorb the mNA.

For both the CNC- and QCNC-rQCA, a very clear increase in compressive strength may be observed. The compressive strength of the non-reinforced QCA was 5.56 ± 1.57 kPa. Adding CNC at solid loadings of 0.1, 0.2, 0.3, and 0.6% w/w resulted in highly improved compressive strengths of 8.10 ± 0.71, 9.14 ± 1.15, 10.08 ± 2.43, and 15.06 ± 0.78 kPa, respectively. The addition of QCNC at solid loadings of 0.1, 0.2, 0.3, and 0.6% w/w yielded slightly more modest, but still improved compressive strengths of 7.21 ± 0.67, 7.94 ± 1.86, 7.96 ± 0.57, and 12.17 ± 1.22 kPa, respectively. At the highest solids loading (0.6% w/w), the addition of CNC and QCNC to the rQCA resulted increases in compressive strength of 171% and 119%, respectively.

To the best of our knowledge, this is the first report to demonstrate the enhanced mechanical properties of quaternized chitosan hydrogels upon addition of CNC. These findings help to demonstrate the applicability of CNC and derivatives thereof as a reinforcing material in hydrogels.

CHAPTER 7

Recommendations

7.1 Recommendations for the work presented in Chapter 4

To improve the practical applicability of the QCA towards the removal of NAs from OSPW, the following recommendations are made for future studies:

1. *Investigate the ortho-quaternization of chitosan to increase the quaternary ammonium content of the adsorbent.*

A recent study by Gruškienė and coworkers (2013) reported on the *ortho*-quaternization of chitosan by reacting both the C_2 primary amine and C_6 hydroxyl moieties with GTMAC under alkaline conditions in aqueous media. Doing so increased the degree of quaternization of the polymer from 68% to 95%. According to the authors, only the amine groups of chitosan are nucleophilic enough to induce ring opening of the epoxy groups on GTMAC under acidic and neutral conditions. However, under alkaline conditions, the hydroxyl groups may also react with GTMAC, yielding *ortho*-quaternized chitosan. It is believed that this approach may help to increase the overall cationic charge density of the QCA presented in this study, effectively increasing the number of potential naphthenic acid adsorption sites without requiring additional chitosan material. Unfortunately, the authors reported increased hydrolysis of the GTMAC under alkaline conditions. Therefore, for the reaction to successfully increase the degree of quaternization, GTMAC was required in extreme excess. An alternative solution to aid in reducing GTMAC consumption might be to perform the reaction in DMSO, as has been investigated for the quaternization of cellulose-based material (M. Hasani, E. D. Cranston, et al. 2008), to eliminate the water hydrolysis side reaction.

2. *Investigate the adsorption of native NAs from real OSPW samples.*

It is well known that real OSPW contains a very broad range of naphthenic acid structures and is often highly concentrated in suspended solid material (Schramm, Stasiuk and MacKinnon 2000). Further, the concentration of dissolved salts is, in most cases, very high (Allen 2008). By investigating the adsorption of native NAs from real OSPW samples onto the presently reported QCA, the relative adsorption of NAs of different structures may be revealed. This may aid in understanding the underlying factors that affect the adsorption process for this system. As well, one may more realistically study the effects of charge screening on naphthenic acid adsorption due to the presence of monovalent and divalent ionic species. Lastly, the effects of fouling on the overall effectiveness and lifetime of the QCA may be studied.

7.2 Recommendations for the work presented in Chapter 5

To further enhance the compressive strength of the rQCA, the following recommendations are made for future studies:

1. *Investigate the covalent crosslinking of amine-functionalized CNC into the quaternized chitosan hydrogel matrix.*

Recent work by Hemraz and coworkers (Hemraz, Boluk and Sunasee 2013) reports on the surface functionalization of CNC with primary amine moieties under aqueous conditions. By adding similarly prepared amine-functionalized CNC into the chitosan-based hydrogels prior to gelation and quaternization, the CNC particles may be covalently crosslinked into the hydrogel matrix. It is believed that the glutaraldehyde crosslinking

reaction that binds together amine groups on chitosan (Argüelles-Monal, et al. 1998) may also react with the amine groups present on the nanofiller to help strengthen the interfacial adhesion between the nanofiller and polymer matrix phases. Since this interfacial interaction is paramount in the translation of applied forces from the matrix to the reinforcing material and vice-versa (Fox, et al. 2012) (Yang, et al. 2013) (Azouz, et al. 2012) (J. Yang, C. -H. Han, et al. 2014), the covalent gelation of the CNC into the hydrogel matrix is expected to yield an adsorbent material with a much improved compressive strength. Further, it is hypothesized that the amine-functionalization of CNC will allow for quaternization of the CNC surface while simultaneously quaternizing the primary amine groups of chitosan through reaction with GTMAC.

2. *Investigate the reinforcement QCA with cellulose nanofibrils (CNF).*

When compared to CNC, the aspect ratio of CNF is much greater (Iwamoto, Lee and Endo 2014). Many studies have demonstrated that nanofiller materials with increased aspect ratios often result in significant improvements in mechanical properties (Thomas, et al. 2013). Therefore, it is hypothesized that by using CNF as a nanofiller material instead of CNC, further improved compressive strength of the QCA may result. However, due to the amorphous cellulose regions present within CNF fibers, they are, generally, less rigid than their shorter, fully crystalline CNC counterparts (Klemm, et al. 2005). It would be interesting to investigate how the mechanical properties of the individual nanofiller particles affect the mechanical properties of the bulk nanocomposite. Ultimately, this might shed more light on the nanofiller reinforcement mechanism in the presently reported hydrogel adsorbents.

REFERENCES

Abitbol, T., T. Johnstone, T. M. Quinn, and D. G. Gray. "Reinforcement with cellulose nanocrystals of poly(vinyl alcohol) hydrogels prepared by cyclic freezing and thawing." *Soft Matter* 7 (2011): 2373-2379.

Afzal, A., P. Drzewicz, L. A. Perez-Estrada, Y. Chen, J. W. Martin, and M. Gamal El-Din. "Effect of molecular structure on the relative reactivity of naphthenic acids in the UV/H2O2 advanced oxidation process." *Environ. Sci. Technol.* 46 (2012): 10727-10734.

Allen, E. W. "Process water treatment in Canada's oil sands industry: I. Target pollutants and treatment objectives." *J. Environ. Eng. Sci.* 7 (2008): 123-138.

Allen, E. W. "Process water treatment in Canada's oil sands industry: II. A review of emerging technologies." *J. Environ. Eng. Sci* 7 (2008): 499-524.

Alpatova, A., E. S. Kim, S. Dong, N. Sun, P. Chelme-Ayala, and M. Gamal El-Din. "Treatment of oil sands process-affected water with ceramic ultrafiltration membrane: Effects of operating conditions on membrane performance." *Sep. Purif. Technol.* 122 (2014): 170-182.

Andreozzi, R., V. Caprio, A. Insola, and R. Marotta. "Advanced oxidation processes (AOP) for water purification and recovery." *Catal. Today* 53 (1999): 51-59.

Antonyuk, S., J. Tomas, S. Heinrich, and L. Mörl. "Breakage behaviour of spherical granulates by compression." *Chem. Eng. Sci.* 60 (2005): 4031-4044.

Aouada, F. A., M. R. de Moura, W. J. Orts, and L. H. C. Mattoso. "Preparation and characterization of novel micro- and nanocomposite hydrogels containing cellulosic fibrils." *J. Agric. Food Chem.* 59 (2011): 9433-9442.

Argüelles-Monal, W., F. M. Goycoolea, C. Peniche, and I. Higuera-Ciapara. "Rheological study of the chitosan/glutaraldehyde chemical gel system." *Polym. Gels Netw.* 6 (1998): 429-440.

Armstrong, S. A. *Dissipation and Phytotoxicity of Oil Sands Naphthenic Acids in Wetland Plants.* Doctoral Thesis, Saskatoon, SK: University of Saskatchewan, 2008, 173.

Arrhenius, S. A. "Über die Dissociationswärme und den Einflusß der Temperatur auf den Dissociationsgrad der Elektrolyte." *Z. Physik. Chem.* 4 (1889): 96-116.

Azouz, K. B., E. C. Ramires, W. Van den Fonteyne, N. El Kissi, and A. Dufresne. "Simple method for the melt extrusion of a cellulose nanocrystal reinforced hydrophobic polymer." *ACS Macro Lett.* 1 (2012): 236-240.

B., E. Mirzaei, A. Ramazani S. A., M. Shafiee, and M. Danaei. "Studies on glutaraldehyde crosslinked chitosan hydrogel properties for drug delivery systems." *Int. J. Polym. Mater. Polym. Biomater.* 62 (2013): 605-611.

Baysal, K., A. Z. Aroguz, Z. Adiguzel, and B. M. Baysal. "Chitosan/alginate crosslinked hydrogels: Preparation, characterization and application for cell growth purposes." *Int. J. Biol. Macromol.* 59 (2013): 342-348.

Bendoraitiene, J., R. Kavaliauskaite, R. Klimaviciute, and A. Zemaitaitis. "Peculiarities of starch cationization with glycidyltrimethylammonium chloride." *Starch* 58 (2006): 623-631.

Berger, J., M. Reist, J. M. Mayer, O. Felt, N. A. Peppas, and R. Gurny. "Structure and interactions in covalently and ionically crosslinked chitosan hydrogels for biomedical applications." *Eur. J. Pharm. Biopharm.* 57 (2004): 19-34.

Berlin, A., and O. Myroshynchenko. Remediation of naphthenic acid contamination. U.S. Patent 20130319948 A1. 2013.

Bjornen, K. K. Electrocoagulation for removal of dissolved naphthenic acids from water. U.S. Patent 8658014. 2014.

Breitbach, M., D. Bathen, H. Schmidt-Traub, and H. Ebener. "Stability of adsorber resins under mechanical compression and ultrasonication." *Polym. Adv. Technol.* 13 (2002): 391-400.

Brient, J. A., P. J. Wessner, and M. N. Doyle. *Naphthenic acids.* Vol. 16, in *Kirk-Othmer Encyclopedia of Chemical Technology*, edited by J. I. Kroschwitz, 1017-1029. New York, NY: Wiley, 1995.

Butler, M. F., Y. F. Ng, and P. D. A. Pudney. "Mechanism and kinetics of the crosslinking reaction between biopolymers containing primary amine groups and genipin." *J. Polym. Sci. A1* 41 (2003): 3941-3953.

Cecen, F., and Ö. Aktas. *Activated Carbon for Water and Wastewater Treatment: Integration of Adsorption and Biological Treatment.* Weinheim: Wiley-VCH, 2012.

Chakravarti, R., B. N. Patrick, M. Barney, G. Kusinski, and T. M. Devine. "Toward the mechanism of corrosion in crude oil: a study using vibrational spectroscopic techniques at elevated temperatures." *Energy Fuels* 27, no. 12 (2013): 7905-7914.

Chatterjee, S., M. W. Lee, and S. H. Woo. "Adsorption of congo red by chitosan hydrogel beads impregnated with carbon nanotubes." *Biores. Technol.* 101, no. 6 (2010): 1800-1806.

Chen, Y., L. Chen, H. Bai, and L. Li. "Graphene oxide–chitosan composite hydrogels as broad-spectrum adsorbents for water purification." *J. Mater. Chem. A* 1 (2013): 1992-2001.

Chiou, M. -S., P. -Y. Ho, and H. -Y. Li. "Adsorption of anionic dyes in acid solutions using chemically cross-linked chitosan beads." *Dyes Pigm.* 60 (2004): 69-84.

Clemente, J. S., and P. M. Fedorak. "A review of the occurrence, analyses, toxicity, and biodegradation of naphthenic acids." *Chemosphere* 60 (2005): 585-600.

Clemente, J. S., M. D. MacKinnon, and P. M. Fedorak. "Aerobic biodegradation of two commercial naphthenic acids preparations." *Environ. Sci. Technol.* 38 (2004): 1009-1016.

Clemente, J. S., N. G. N. Prasad, M. D. MacKinnon, and P. M. Fedorak. "A statistical comparison of naphthenic acids characterized by gas chromatography-mass spectrometry." *Chemosphere* 50 (2003): 1265-1274.

Conrad Environmental Aquatics Technical Advisory Group (CEATAG). "Naphthenic acids background information discussion report." Alberta Department of Energy, Edmonton, AB, 1998.

Davis, W. M. *Physical Chemistry: A Modern Introduction.* 2nd. Boca Raton, FL: CRC, 2012.

De Philippis, R., and E. Micheletti. *Heavy Metals in the Environment.* Edited by L. K. Wang, J. P. Chen, Y. T. Hung and N. K. Shammas. Boca Raton, FL: CRC, 2009.

Del Rio, L., A. Hadwin, L. Pinto, M. MacKinnon, and M. Moore. "Degradation of naphthenic acids by sediment micro-organisms." *J. Appl. Microbiol.* 101 (2006): 1049-1061.

Derungs, W. A. "Naphthenic acid corrosion - an old enemy of the petroleum industry." *Corrosion* 12, no. 12 (1956): 617-622.

Domard, A., M. Rinaudo, and C. Terrassin. "New method for quaternization of chitosan." *Int. J. Bio. Macromol.* 8 (1986): 105-107.

Espinosa-García, B. M., W. M. Argüelles-Monal, J. Hernández, L. Félix-Valenzuela, N. Acosta, and F. M. Goycoolea. "Molecularly imprinted chitosan-genipin hydrogels with recognition capacity toward o-xylene." *Biomacromol.* 8 (2007): 3355-3364.

Eyholzer, C., et al. "Biocomposite hydrogels with carboxymethylated, nanofibrillated cellulose powder for replacement of the nucleus pulposus." *Biomacromol.* 12 (2011): 1419-1427.

Fan, T. -P. "Characterization of naphthenic acids in petroleum by fast atom bombardment mass spectrometry." *Energy Fuels* 5 (1991): 371-375.

Faust, S. D., and O. M. Aly. *Adsorpton Processes for Water Treatment.* Stoneham, MA: Butterworth, 1987.

Feng, J., A. R. Esker, and M. Roman. "Acid-catalyzed and solvytic desulfation of H2SO4-hydrolyzed cellulose nanocrystals." *Langmuir* 26, no. 23 (2010): 17919-17925.

Foo, K. Y., and B. H. Hameed. "Insights into the modeling of adsorption isotherm systems." *Chem. Eng. J.* 156 (2010): 2-10.

Fox, J., et al. "High-strength healable, supramolecular polymer nanocomposites." *J. Am. Chem. Soc.* 134 (2012): 5362-5368.

Frank, R. A., et al. "Effect of carboxylic acid content on the acute toxicity of oil sands naphthenic acids." *Environ. Sci. Technol.* 43, no. 2 (2009): 266-271.

Freundlich, H. M. F. "Over the adsorption in solution." *J. Phys. Chem.* 57A (1906): 385-470.

Güçlü, G., S. Al, S. Emik, T. B. İyim, and S. Özgümüş. "Removal of Cu2+ and Pb2+ ions from aqueous solutions by starch-graft-acrylic acid/montmorillonite superabsorbent nanocomposite hydrogels." *Polym. Bull.* 65 (2010): 333-346.

Gaikar, V. G., and D. Maiti. "Adsorptive recovery of naphthenic acids using ion-exchange resins." *React. Funct. Polym.* 31 (1996): 154-166.

Gong, X., and J. Yao. Naphthenic acid removal and conversion. U.S. Patent 8137565. 2012.

Grady, C. P. L., G. T. Daigger, and H. C. Lim. *Biological Wastewater Treatment.* 2nd. New York, NY: Marcel Dekker, 1999.

Gruškienė, R., R. Deveikytė, and R. Makuška. "Quaternization of chitosan and partial destruction of the quaternized derivatives making them suitable for electrospinning." *Chemija* 24 (2013): 325-334.

Gutzeit, J. "Naphthenic acid corrosion in oil refineries." *Mater. Perform.* 16, no. 10 (1977): 24-35.

Han, X., A. C. Scott, P. M. Fedorak, M. Bataineh, and J. W. Martin. "Influence of molecular structure on the biodegradability of naphthenic acids." *Environ. Sci. Technol.* 42 (2008): 1290-1295.

Han, X., M. D. MacKinnon, and J. W. Martin. "Estimating the in situ biodegradation of naphthenic acids in oil sands process waters by HPLC/HRMS." *Chemosphere* 76 (2009): 63-70.

Haraguchi, K. "Nanocomposite hydrogels." *Curr. Opin. Solid St. M.* 11 (2007): 47-54.

Hasani, M., E. Cranston, G. Westman, and D. G. Gray. "Cationic surface functionalization of cellulose nanocrystals." *Soft Matter* 4 (2008): 2238-2244.

Hasani, M., E. D. Cranston, G. Westman, and D. G. Gray. *Soft Matter* 4 (2008): 2238-2244.

Havre, T. E., J. Sjöblom, and J. E. Vindstad. "Oil/water-partitioning and interfacial behaviour of naphthenic acids." *J. Disper. Sci. Technol.* 24, no. 6 (2003): 789-801.

Havre, T., M. H. Ese, J. Sjöblom, and A. M. Blokhus. "Langmuir films of naphthenic acids at different pH and electrolyte concentrations." *Colloid and Polymer Science* 280, no. 7 (2002): 647-52.

Haynes, W. M., ed. *CRC Handbook of Chemistry and Physics.* Vol. 95. Boca Raton, FL: CRC, 2014.

Headley, J. V., and D. W. McMartin. "A review of the occurence and fate of naphthenic acids in aquatic environments." *J. Environ. Sci. Heal. A* 39 (2004): 1989-2010.

Hein, F. J., D. Leckie, S. Larter, and J. R. Suter. *Heavy-oil and oil-sand petroleum systems in Alberta and beyond.* Calgary, AB: American Association of Petroleum Geologists, 2013.

Hemraz, U. D., Y. Boluk, and R. Sunasee. "Amine-decorated nanocrystalline cellulose surfaces: synthesis, characterization, and surface properties." *Can. J. Chem.* 91 (2013): 974-981.

Hendricks, D. *Fundamentals of Water Treatment Unit Processes: Physical, Chemical, and Biological.* Boca Raton, FL: CRC, 2011.

Ho, Y. S. "Citation review of Lagergren kinetic rate equation on adsorption reactions." *Scientomet.* 59, no. 1 (2004): 171-177.

Ho, Y. S., and G. McKay. "Pseudo-second order model for sorption processes." *Proc. Biochem.* 34 (1999): 451-465.

Ho, Y. S., and G. McKay. "The kinetics of sorption of basic dyes from aqueous solution by sphagnum moss peat." *Can. J. Chem. Eng.* 76, no. 4 (1998): 822-827.

Hoch, G., A. Chauhan, and C. J. Radke. "Permeability and diffusivity for water transport through hydrogel membranes." *J. Membrane Sci.* 214 (2003): 199-209.

Hoffman, A. S. "Hydrogels for biomedical applications." *Adv. Drug Deliver. Rev.* 54 (2002): 3-12.

"Adsorption and Ion Exchange." In *Principles of Water Treatment*, by K. J. Howe, D. W. Hand, J. C. Crittenden, R. R. Trussell and G. Tchobanoglous. Hoboken, N.J.: Wiley, 2012.

Hudson, S. M., and D. W. Jenkins. "Chitin and Chitosan." In *Encyclopedia of Polymer Science and Technology*, by H. F. Mark. Wiley, 2004.

Humphries, M. "Oil Sands Production Process." In *North American Oil Sands: History of Development, Prospects for the Future*, 4-18. Washington, D.C.: Congressional Research Service, 2008.

Inglezakis, V. J., and A. A. Zorpas. "Heat of adsorption, adsorption energy, and activation energy in adsorption and ion exchange systems." *Desal. Water Treatm.* 39 (2012): 149-157.

Inglezakis, V., and S. Poulopoulos. *Adsorption, Ion Exchange, and Catalysis: Design of Operations and Environmental Applications.* Amsterdam: Elsevier, 2006.

Internation Organization for Standardization (ISO). "ISO 14001:2004 Environmental Management Systems - Requirements with Guidance for Use." 2004.

Iranmanesh, S., T. Harding, J. Abedi, F. Seyedeyn-Azad, and D. B. Layzell. "Adsorption of naphthenic acids on high surface area activated carbons." *J. Environ. Sci. Heal. A* 49, no. 8 (2014): 913-922.

Islam, M. S., T. Dong, Z. Sheng, Y. Zhang, Y. Liu, and M. Gamal El-Din. "Microbial community structure and operational performance of a fluidized bed biofilm reactor treating oil sands process-affected water." *Int. Biodeterior. Biodegrad.* 91 (2014): 111-118.

Islam, M. S., Y. Zhang, K. N. McPhedran, Y. Liu, and M. Gamal El-Din. "Granular activated carbon for simultaneous adsorption and biodegradation of toxic oil sands process-affected water organic compounds." *J. Environ. Manage.* 152 (2015): 49-57.

Israelachvilli, J. N. *Intermolecular and Surface Forces.* 3rd. Oxford: Academic Press, 2011.

Iwamoto, S., S. -H. Lee, and T. Endo. "Relationship between aspect ratio and suspension viscosity of wood cellulose nanofibers." *Polym. J.* 46 (2014): 73-76.

Jintapattanakit, A., S. Mao, T. Kissel, and V. B. Junyaprasert. "Physicochemical properties and biocompatibility of N-trimethyl chitosan: Effect of quaternization and dimethylation." *Eur. J. Pharm. Biopharm.* 70 (2008): 563-571.

Jones, D., C. E. West, A. G. Scarlett, R. A. Frank, and S. J. Rowland. "Isolation and estimation of the 'aromatic' naphthenic acid content of an oil sands process-affected water extract." *J. Chromatog. A* 1247 (2012): 171-175.

Kaşgöz, H., and A. Durmus. "Dye removal by a novel hydrogel-clay nanocomposite with enhanced swelling properties." *Polym. Adv. Technol.* 19 (2008): 838-845.

Kannel, P. R., and T. Y. Gan. "Naphthenic acids degradation and toxicity mitigation in tailings wastewater systems and aquatic environments: A review." *J. Environ. Sci. Heal. A* 47 (2012): 1-21.

Klemm, D., B. Heublein, H. -P. Fink, and A. Bohn. "Cellulose: fascinating biopolymer and sustainable raw material." *Angew. Chem. Int. Ed.* 44 (2005): 3358-3393.

Kumar, K. V. "Linear and non-linear regression analysis for the sorption kinetics of methylene blue onto activated carbon." *J. Hazard. Mater.* 137 (2006): 1538–1544.

Kumar, M. N. V. R. "A review of chitin and chitosan application." *React. Funct. Polym.* 46, no. 1 (2000): 1-27.

Lagergren, S. "Zur theorie der sogenannten adsorption gelöster stoffe." *K. Sven. Vetenskapsakad. Handl.* 24, no. 4 (1898): 1-39.

Lai, J. Y. "Biocompatibility of genipin and glutaraldehyde cross-linked chitosan materials in the anterior chamber of the eye." *Int. J. Mol. Sci.* 13 (2012): 10970-10985.

Langmuir, I. "The constitution and fundamental properties of solids and liquids Part I: Solids." *J. Am. Chem. Soc.* 38, no. 11 (1916): 2221-2295.

Legrini, O., E. Oliveros, and A. M. Braun. "Photochemical processes for water treatment." *Chem. Rev.* 93, no. 2 (1993): 671-698.

Li, N., and R. Bai. "A novel amine-shielded surface cross-Llnking of chitosan hydrogel beads for enhanced metal adsorption performance." *Ind. Eng. Chem. Res.* 44 (2005): 6692-6700.

Li, P., P. F. Gomes, J. M. Loureiro, and A. E. Rodrigues. "Protein separation and purification by expanded bed adsorption and simulated moving bed technology." In *Continous Processing in Pharmaceutical Manufacturing*, edited by G. Subramanian. Weinheim: Wiley-VCH, 2014.

Liang, H. -W., Q. -F. Guan, L. -F. Chen, Z. Zhu, W. -J. Zhang, and S. -H. Yu. "Macroscopic-scale template synthesis of robust carbonaceous nanofiber hydrogels and aerogels and their applications." *Angew. Chem. Int. Ed.* 51 (2012): 5101-5105.

Lim, S. -H., and S. M. Hudson. "Synthesis and antimicrobial activity of a water-soluble chitosan derivative with a fiber-reactive group." *Carbohyd. Res.* 339 (2004): 313-319.

Liu, Y., Y. Zheng, and A. Wang. "Enhanced adsorption of Methylene Blue from aqueous solution by chitosan-g-poly(acrylic acid)/vermiculite hydrogel composites." *J. Environ. Sci.* 22 (2010): 486-493.

Lochte, H. L., and E. R. Littmann. *The Petroleum Acids and Bases.* New York, NY: Chemical Publishing Company, 1955.

MacKinnon, M. D., and H. Boerger. "Description of two treatment methods for detoxifying oil sands process water." *Wat. Poll. Res. J. Can.* 21 (1986): 496-512.

Madill, R. E. A., M. T. Orzechowski, G. Chen, B. G. Brownlee, and N. J. Bunce. "Preliminary risk assessment of the wet landscape option for reclamation of oil sands mine tailings: Bioassays with mature fine tailings pore water." *Environ. Toxicol.* 16, no. 3 (2001): 197-208.

Mapolelo, M. M., R. P. Rodgers, G. T. Blakney, A. T. Yen, S. Asomaning, and A. G. Marshall. "Characterization of naphthenic acids in crude oils and naphthenates by electrospray ionization FT-ICR mass spectrometry." *Int. J. Mass. Spectrom.* 300, no. 2-3 (2011): 149-157.

Mi, F. L., H. W. Sung, and S. S. Shyu. "Synthesis and characterization of a novel chitosan-based network prepared using naturally occurring crosslinker." *J. Polym. Sci. A* 38, no. 15 (2000): 2804-2814.

Migneault, I., C. Dartiguenave, M. J. Bertrand, and K. C. Waldron. "Glutaraldehyde: behavior in aqueous solution, reaction with proteins, and application to enzyme crosslinking." *Biotechniques* 37 (2004): 790-802.

Mohamed, M. H., L. D. Wilson, J. V. Headley, and K. M. Peru. "Novel materials for environmental remediation of tailing pond waters containing naphthenic acids." *Process Saf. Environ.* 86 (2008): 237-243.

Mohamed, M. H., L. D. Wilson, J. V. Headley, and K. M. Peru. "Sequestration of naphthenic acids from aqueous solution using b-cyclodextrin-based polyurethanes." *Phys. Chem. Chem. Phys.* 13 (2011): 1112-1122.

Mohamed, M. H., L. D. Wilson, K. M. Peru, and J. V. Headley. "Colloidal properties of single component naphthenic acids and complex naphthenic acid mixtures." *J. Colloid Interface Sci.* 395 (2013): 104-110.

Monteiro, O. A. C., and C. Airoldi. "Some studies of crosslinking chitosan–glutaraldehyde interaction in a homogeneous system." *Int. J. Bio. Macromol.* 26 (1999): 119-128.

Muñoz, I., J. Rieradevall, F. Torrades, J. Peral, and X. Doménech. "Environmental assessment of different solar driven advanced oxidation processes." *Sol. Energy* 79 (2005): 369-375.

Muzzarelli, R. A. A. "Genipin-crosslinked chitosan hydrogels as biomedical and pharmaceutical aids." *Carbohyd. Polym.* 77 (2009): 1-9.

Neyens, E., and J. Baeyens. "A review of classic Fenton's peroxidation as an advanced oxidation technique." *J. Hazard. Mater. B* 98 (2003): 33-50.

Oller, I., S. Malato, and J. A. Sánchez-Pérez. "Combination of advanced oxidation processes and biological treatments for wastewater decontamination - A review." *Sci. Total Environ.* 409 (2011): 4141-4166.

Park, K., J. Chen, and H. Park. Hydrogel composites and superporous hydrogel composites having fast swelling, high mechanical strength, and superabsorbent properties. U.S. Patent 6271278. 2001.

Patel, H., and R. T. Vashi. *Wastewater Engineering: Advanced Wastewater Treatment Systems.* Edited by H. A. Aziz and A. Mojiri. Penang: IJSR Publications, 2014.

Pei, A., N. Butchosa, L. A. Berglund, and Q. Zhou. "Surface quaternized cellulose nanofibrils with high water absorbency and adsorption capacity for anionic dyes." *Soft Matter* 9 (2013): 2047-2055.

Peng, H., K. Volchek, M. MacKinnon, W. P. Wong, and C. E. Brown. "Application of nanofiltration to water management options for oil sands operations." *Desalination* 170 (2004): 137-150.

Perez-Estrada, L. A., X. Han, P. Drzewicz, M. Gamal El-Din, P. M. Fedorak, and J. W. Martin. "Structure-reactivity of naphthenic acids in the oxonation process." *Environ. Sci. Technol.* 45 (2011): 7431-7437.

Pourrezaei, P., et al. "The impact of metallic coagulants on the removal of organic compounds from oil sands process-affected water." *Environ. Sci. Technol.* 45 (2011): 8452-8459.

Pyhälä, E. "Zur Kenntnis der hochmolekularen Naphthensäuren des Bakuer Erdöls." *Angew. Chem.* 27, no. 52 (1914): 407.

Qin, C., Y. Du, Z. Zhang, Y. Liu, L. Xiao, and X. Shi. "Adsorption of chromium (VI) on a novel quaternized chitosan resin." *J. App. Polym. Sci.* 90 (2003): 505-510.

Riffat, R. *Fundamentals of Wastewater Treatment and Engineering.* Boca Raton, FL: CRC, 2013.

Rinaudo, M. "Chitin and chitosan: Properties and applications." *Prog. Polym. Sci.* 31, no. 7 (2006): 603-632.

Roberts, G. A. F., and K. E. Taylor. "The formation of gels by reaction of chitosan with glutaraldehyde." *Macromol. Chem. Physic.* 190 (1989): 951-960.

Roelofsen, P. A., and I. Hoette. "Chitin in the cell walls of yeast." *A. Van. Leeuw. J. Microb.* 17, no. 1 (1951): 297-313.

Rogers, V. V., M. Wickstrom, K. Liber, and M. D. MacKinnon. "Acute and subchronic mammalian toxicity of naphthenic acids from oil sands tailings." *Toxicol. Sci.* 66, no. 2 (2002): 347-355.

Rowland, S. J., C. E. West, D. Jones, A. G. Scarlett, R. A. Frank, and L. M. Hewitt. "Steroidal aromatic 'naphthenic acids' in oil sands process-affected water: Structural comparisons with environmental estrogens." *Environ. Sci. Technol.* 45, no. 22 (2011): 9806-9815.

Ruihua, H., Y. Bingchao, D. Zheng, and B. Wang. "Preparation and characterization of a quaternized chitosan." *J. Mater. Sci.* 47 (2012): 845-851.

Sah, S. L. *Encyclopaedia of Petroleum Science and Engineering.* Delhi: Kalpaz Publications, 2003.

Saha, P., and S. Chowdhury. "Insight into adsorption thermodynamics." In *Themodynamics*, edited by M. Tadashi. InTech, 2011.

Sanford, E. C. "Processability of Athabasca oil sand: Interrelationship between oil sand fine solid, process aids, mechanical energy, and oil sand age after mining." *Can. J. Chem. Eng.* 61 (1983): 554-67.

Sarkar, B. *Adsorption of single-ring model naphthenic acid from oil sands tailings pond water using petroleum coke-derived activted carbon.* Masters Thesis, Toronto: University of Toronto, 2013.

Schiffman, J. D., and C. L. Schauer. "Cross-linking chitosan nanofibers." *Biomacromol.* 8 (2007): 594-601.

Schramm, L. L., and R. G. Smith. Control of process aid used in hot water process for extraction of bitumen from tar sand. U.S. Patent 4462892. 1984.

Schramm, L. L., E. N. Stasiuk, and D. Turner. "The influence of interfacial tension in the hot-water process for recovering bitumen from Athabasca oil sands." *Canadian International Petroleum Conference.* Calgary, 2001.

Schramm, L. L., E. N. Stasiuk, and M. D. MacKinnon. "Surfactants in the Athabasca Oil Sands Slurry Conditioning, Flotation Recovery, and Tailings Processes." In *Surfactants: Fundamentals and Applications in the Petroleum Industry*, by L. L. Schramm, 365-460. Cambridge: Cambridge University Press, 2000.

Schramm, L. L., R. G. Smith, and J. A. Stone. "The influence of natural surfactant concentration on the hot water process for removing bitumen from the Athabasca oil sands." *AOSTRA J. Res.* 1 (1984): 5-14.

Scott, A. C., M. D. MacKinnon, and P. M. Fedorak. "Naphthenic acids in Athabasca oil sands tailings waters are less biodegradable than commercial naphthenic acids." *Environ. Sci. Technol.* 39 (2005): 8388-8394.

Shchukin, E. D., et al. "Effects of adsorption-active media on the mechanical properties of catalysts and adsorbents." *Colloid Surface A* 282-283 (2006): 287-297.

Small, C. C., Z. Hashisho, and A. C. Ulrich. "Preparation and characterization of activated carbon from oil sands coke." *Fuel* 92, no. 1 (2012): 69-76.

Smith, B. E., C. A. Lewis, S. T. Belt, C. Whitby, and S. J. Rowland. "Effect of alkyl chain branching on the biotransformation of naphthenic acids." *Environ. Sci. Technol.* 42 (2008): 9323-9328.

Sowmya, A., and S. Meenakshi. "An efficient and regenerable quaternary amine modified chitosan beads for the removal of nitrate and phosphate anions." *J. Environ. Chem. Eng.* 1 (2013): 906-915.

Takamura, K. "Microscopic structure of athabasca oil sand." *Can. J. Chem. Eng.* 60, no. 4 (1982): 538-545.

Taylor, J. S., and S. J. Duranceau. *Membrane Technology in Water and Wastewater Treatment.* Edited by P. Hillis. Cambridge: RSC, 2000.

Temkin, M. I., and V. Pyzhev. "Kinetics of ammonia synthesis on promoted iron catalyst." *Acta Physiochim. U.R.S.S.* 12 (1940): 327-356.

Teng, W. L., E. Khor, T. K. Tan, L. Y. Lim, and S. C. Tan. "Concurrent production of chitin from shrimp shells and fungi." *Carbohyd. Res.* 332, no. 3 (2001): 305-316.

Tharanathan, R. N., and F. S. Kittur. "Chitin - The undesputed biomolecule of great potential." *CRC Cr. Rev. Food. Sci.* 43, no. 1 (2003): 61-87.

Thomas, S., K. Joseph, S. K. Malhotra, K. Goda, and M. S. Sreekala. *Polymer Composites.* Weinheim: Wiley-VCH, 2013.

Wang, N., et al. "High-strength hydrogel as a reusable adsorbent of copper ions." *J. Hazard. Mater.* 213-214 (2012): 258-264.

Wang, T., and L. T. Drzal. "Cellulose-nanofiber-reinforced poly(lactic acid) composites prepared by a water-based approach." *ACS Appl. Mater. Interface* 4 (2012): 5079-5085.

Wang, X., Y. Du, J. Yang, Y. Tang, and J. Luo. "Preparation, characterization, and antimicrobial activity of quaternized chitosan/organic montmorillonite nanocomposites." *J. Biomed. Mater. Res. A* 84 (2008): 384-390.

Watson, J. S., D. M. Jones, R. P. J. Swannell, and A. C. T. van Duin. "Formation of carboxylic acids during aerobic biodegradation of crude oil and evidence of microbial oxidation of hopanes." *Organ. Geochem.* 33 (2002): 1153-1169.

Weber, W. J., and J. C. Morris. "Kinetics of adsorption on carbon from solution." *J. San. Eng. Div.* 89, no. 2 (1963): 31-60.

Worch, E. *Adsorption Technology in Water Treatment: Fundamental, Processing, and Modeling.* Berlin: Walter de Gruyter, 2012.

Yan, W. L., and R. Bai. "Adsorption of lead and humic acid on chitosan hydrogel beads." *Water Res.* 39 (2005): 688-698.

Yang, J., C. -H. Han, Z. -M. Zhang, F. Xu, and R. -C. Sun. "Cellulose nanocrystals mechanical reinforcement in composite hydrogels with multiple cross-links: correlations between dissipation properties and deformation mechanics." *Macromol.* 47 (2014): 4077-4086.

Yang, J., C. -R. Han, J. -F. Duan, F. Xu, and R. -C. Sun. "Mechanical and viscoelastic properties of cellulose nanocrystals reinforced poly)ethylene glycol) nanocomposite hydrogels." *ACS Appl. Mater. Interface* 5 (2013): 3199-3207.

Yang, X., E. Bakaic, T. Hoare, and E. D. Cranston. "Injectable polysaccharide hydrogels reinforced with cellulose nanocrystals: morphology, rheology, degradation, and cytotoxicity." *Biomacromol.* 14 (2013): 4447-4455.

Yao, K., J. Li, F. Yao, and Y. Yin, . *Chitosan-Based Hydrogels: Functions and Applications.* Boca Raton, FL: CRC, 2012.

Zaman, M., H. Xiao, F. Chibante, and Y. Ni. "Synthesis and characterization of cationically modified nanocrystalline cellulose." *Carbohyd. Polym.* 89 (2012): 163-170.

Zhang, W., C. Sun, Y. Zhao, and X. Lu. "One-pot synthesis and characterization of cross-linked quaternized chitosan microspheres as protein adsorbent." *Int. J. Biol. Macromol.* 49 (2011): 688-692.

Zheng, Y., and A. Wang. "Evaluation of ammonium removal using a chitosan-g-poly(acrylic acid)/rectorite hydrogel composite." *J. Hazard. Mater.* 171 (2009): 671-677.

Zou, L., B. Han, H. Yan, K. L. Kasperski, Y. Xu, and L. G. Hepler. "Enthalpy of adsorption and isotherms for adsorption of naphthenic acids onto clays." *J. Colloid Interface Sci.* 190 (1997): 472-475.

APPENDIX A

Optimized adsorption of a model aromatic naphthenic acid from aqueous solution using sustainable quaternized chitosan hydrogel adsorbents

---

Table A1 Batch equilibrium adsorption data for mNA using QCA samples A1 to A5.

Sample	C_o (mg l^{-1})	C_e (mg l^{-1})	UV abs at 325 nm	q_e (mg g^{-1})	Fractional removal
A1	40.44	7.05	0.05	36.18	0.83
	80.88	20.43	0.15	65.67	0.75
	121.33	35.11	0.26	93.42	0.71
	161.77	55.25	0.41	114.48	0.66
	202.21	80.94	0.59	131.30	0.60
A2	40.44	7.21	0.05	30.11	0.82
	80.88	18.77	0.14	56.80	0.77
	121.33	33.71	0.25	79.71	0.72
	161.77	51.33	0.38	99.96	0.68
	202.21	70.12	0.51	120.38	0.65
A3	40.44	6.67	0.05	33.31	0.84
	80.88	18.05	0.13	61.45	0.78
	121.33	31.22	0.23	88.29	0.74
	161.77	49.40	0.36	110.13	0.69
	202.21	72.82	0.53	128.87	0.64
A4	40.44	7.76	0.06	32.61	0.81
	80.88	20.77	0.15	60.38	0.74
	121.33	37.17	0.27	84.77	0.69
	161.77	57.98	0.43	104.78	0.64
	202.21	76.84	0.56	126.30	0.62
A5	40.44	5.90	0.04	33.89	0.85
	80.88	15.85	0.12	64.71	0.80
	121.33	28.72	0.21	90.98	0.76
	161.77	47.06	0.35	114.45	0.71
	202.21	69.19	0.51	130.21	0.66

Table A2 Batch equilibrium adsorption data for mNA using QCA samples B1 to B5.

Sample	C_o (mg l^{-1})	C_e (mg l^{-1})	UV abs at 325 nm	q_e (mg g^{-1})	Fractional removal

B1	40.44	7.92	0.06	32.44	0.80
	80.88	18.96	0.14	61.91	0.77
	121.33	35.23	0.26	86.34	0.71
	161.77	56.13	0.41	106.51	0.65
	202.21	77.60	0.57	125.70	0.62
B2	40.44	8.10	0.06	31.81	0.80
	80.88	21.02	0.15	59.32	0.74
	121.33	38.95	0.29	83.06	0.68
	161.77	57.63	0.42	105.15	0.64
	202.21	81.57	0.60	122.19	0.60
B3	40.44	8.11	0.06	32.34	0.80
	80.88	23.52	0.17	57.34	0.71
	121.33	41.01	0.30	80.09	0.66
	161.77	60.01	0.44	101.18	0.63
	202.21	84.48	0.62	116.51	0.58
B4	40.44	9.41	0.07	30.88	0.77
	80.88	26.04	0.19	54.57	0.68
	121.33	46.88	0.34	74.01	0.61
	161.77	65.84	0.48	95.36	0.59
	202.21	89.99	0.66	110.46	0.55
B5	40.44	11.14	0.08	27.20	0.72
	80.88	27.46	0.20	48.89	0.66
	121.33	49.73	0.36	66.97	0.59
	161.77	70.71	0.52	84.74	0.56
	202.21	96.91	0.71	98.24	0.52

Table A3 Batch equilibrium adsorption data for mNA using QCA samples C1 to C6.

Sample	C_o (mg l^{-1})	C_e (mg l^{-1})	UV abs at 325 nm	q_e (mg g^{-1})	Fractional removal
C1	40.44	12.38	0.09	28.01	0.69
	80.88	30.40	0.22	50.39	0.62
	121.33	54.28	0.40	66.92	0.55
	161.77	86.01	0.63	75.62	0.47

	202.21	118.53	0.87	83.53	0.41
C2	40.44	9.32	0.07	30.65	0.77
	80.88	23.15	0.17	57.84	0.71
	121.33	40.55	0.30	80.43	0.67
	161.77	61.20	0.45	99.39	0.62
	202.21	86.88	0.64	113.21	0.57
C3	40.44	7.52	0.06	32.92	0.81
	80.88	18.57	0.14	62.28	0.77
	121.33	35.13	0.26	85.94	0.71
	161.77	53.72	0.39	108.03	0.67
	202.21	77.21	0.57	125.57	0.62
C4	40.44	4.79	0.04	35.53	0.88
	80.88	12.67	0.09	68.39	0.84
	121.33	23.37	0.17	97.63	0.81
	161.77	36.80	0.27	125.05	0.77
	202.21	53.87	0.39	148.69	0.73
C5	40.44	5.05	0.04	35.13	0.88
	80.88	12.54	0.09	67.85	0.84
	121.33	23.11	0.17	97.68	0.81
	161.77	34.87	0.26	124.79	0.78
	202.21	47.73	0.35	152.31	0.76
C6	40.44	4.62	0.03	35.60	0.89
	80.88	12.26	0.09	69.22	0.85
	121.33	22.90	0.17	97.91	0.81
	161.77	34.22	0.25	127.35	0.79
	202.21	47.69	0.35	154.48	0.76

Table A4 Batch equilibrium adsorption data for mNA using the optimized QCA.

Sample	C_o (mg l^{-1})	C_e (mg l^{-1})	UV abs at 325 nm	q_e (mg g^{-1})	Fractional removal
Optimized QCA	40.44	3.67	0.03	35.89	0.91
	80.88	10.31	0.08	70.83	0.87
	121.33	18.53	0.14	101.62	0.85

	161.77	28.45	0.21	131.81	0.82
	202.21	38.31	0.28	165.68	0.81

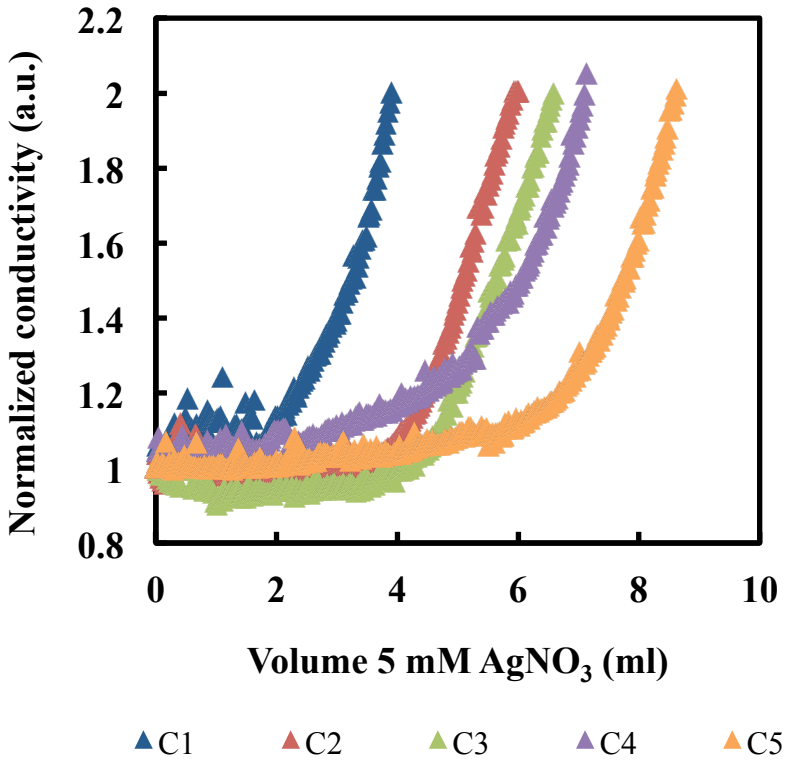

Figure A1 $AgNO_3$ titration curves for QCA samples C1 to C5.

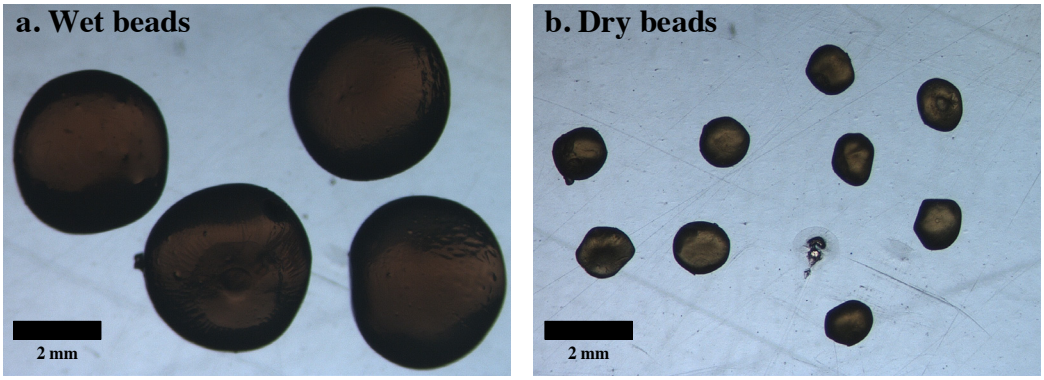

Figure A2 Optical microscope images of (a) hydrated and (b) dehydrated QCA.

APPENDIX B

Mechanically reinforced quaternized cellulose nanocrystal-chitosan nanocomposite hydrogels for the adsorption of a model aromatic naphthenic acid from aqueous solution

---

Table B1 Batch equilibrium adsorption data for mNA using the CNC and QCNC.

Sample	C_o (mg l^{-1})	C_e (mg l^{-1})	UV abs at 325 nm	q_e (mg g^{-1})	Fractional removal
CNC	40.44	30.59	0.22	9.87	0.24
	80.88	63.90	0.47	16.93	0.21
	121.33	98.85	0.72	22.21	0.19
	161.77	138.76	1.02	23.24	0.14
	202.21	174.75	1.28	28.31	0.14
QCNC	40.44	7.23	0.05	33.30	0.82
	80.88	19.49	0.14	57.86	0.76
	121.33	37.11	0.27	85.19	0.69
	161.77	57.47	0.42	99.81	0.64
	202.21	81.96	0.60	123.07	0.59

Table B2 Batch equilibrium adsorption data for mNA using the QCA-CNC nanocomposites.

Sample	C_o (mg l^{-1})	C_e (mg l^{-1})	UV abs at 325 nm	q_e (mg g^{-1})	Fractional removal
QCA 0.1% w/w CNC	40.44	5.98	0.04	35.38	0.85
	80.88	14.71	0.11	67.91	0.82
	121.33	24.12	0.18	99.89	0.80
	161.77	37.97	0.28	124.49	0.77
	202.21	56.75	0.42	149.41	0.72
QCA 0.2% w/w CNC	40.44	6.51	0.05	32.57	0.84
	80.88	15.87	0.12	64.68	0.80
	121.33	25.81	0.19	94.25	0.79
	161.77	40.78	0.30	119.02	0.75
	202.21	61.00	0.45	140.35	0.70
QCA 0.3% w/w CNC	40.44	7.11	0.05	33.29	0.82
	80.88	16.77	0.12	63.81	0.79
	121.33	26.48	0.19	95.49	0.78
	161.77	41.54	0.30	119.30	0.74

	202.21	64.62	0.47	136.62	0.68
QCA 0.6% w/w CNC	40.44	8.27	0.06	32.13	0.80
	80.88	20.09	0.15	61.43	0.75
	121.33	35.29	0.26	86.31	0.71
	161.77	52.72	0.39	107.95	0.67
	202.21	76.64	0.56	124.15	0.62

Table B3 Batch equilibrium adsorption data for mNA using the QCA-QCNC nanocomposites.

Sample	C_o (mg l^{-1})	C_e (mg l^{-1})	UV abs at 325 nm	q_e (mg g^{-1})	Fractional removal
QCA 0.1% w/w QCNC	40.44	4.53	0.03	35.86	0.89
	80.88	11.11	0.08	69.40	0.86
	121.33	20.47	0.15	101.02	0.83
	161.77	30.98	0.23	130.72	0.81
	202.21	43.61	0.32	158.40	0.78
QCA 0.2% w/w QCNC	40.44	4.95	0.04	35.34	0.88
	80.88	11.99	0.09	69.36	0.85
	121.33	21.16	0.16	99.63	0.83
	161.77	33.22	0.24	129.04	0.79
	202.21	47.23	0.35	155.00	0.77
QCA 0.3% w/w QCNC	40.44	6.08	0.04	34.70	0.85
	80.88	14.04	0.10	67.32	0.83
	121.33	24.86	0.18	96.96	0.80
	161.77	38.70	0.28	124.21	0.76
	202.21	53.25	0.39	147.62	0.74
QCA 0.6% w/w QCNC	40.44	6.92	0.05	33.75	0.83
	80.88	15.85	0.12	64.50	0.80
	121.33	29.49	0.22	92.51	0.76
	161.77	45.05	0.33	117.83	0.72
	202.21	62.67	0.46	140.13	0.69

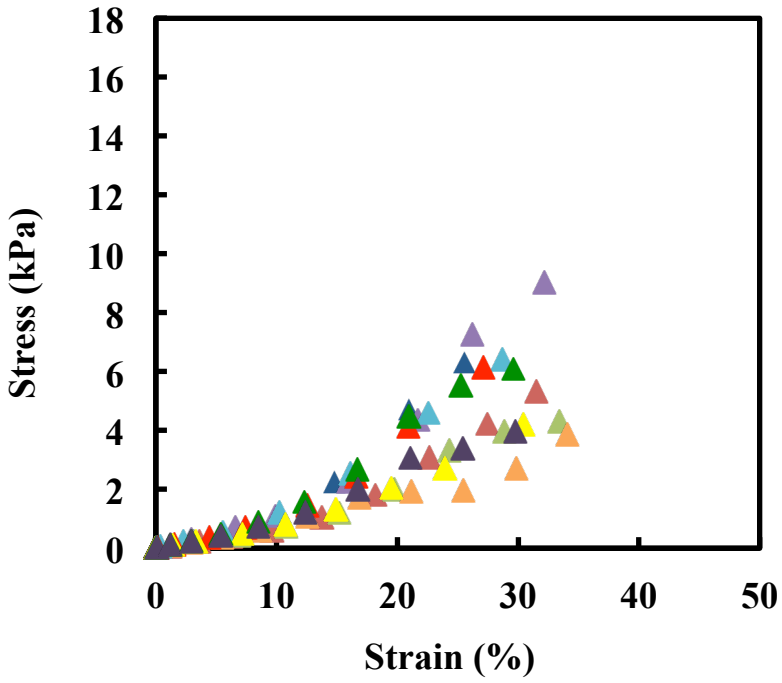

Figure B1 Stress-strain curves for the uniaxial compression of QCA (n = 10).

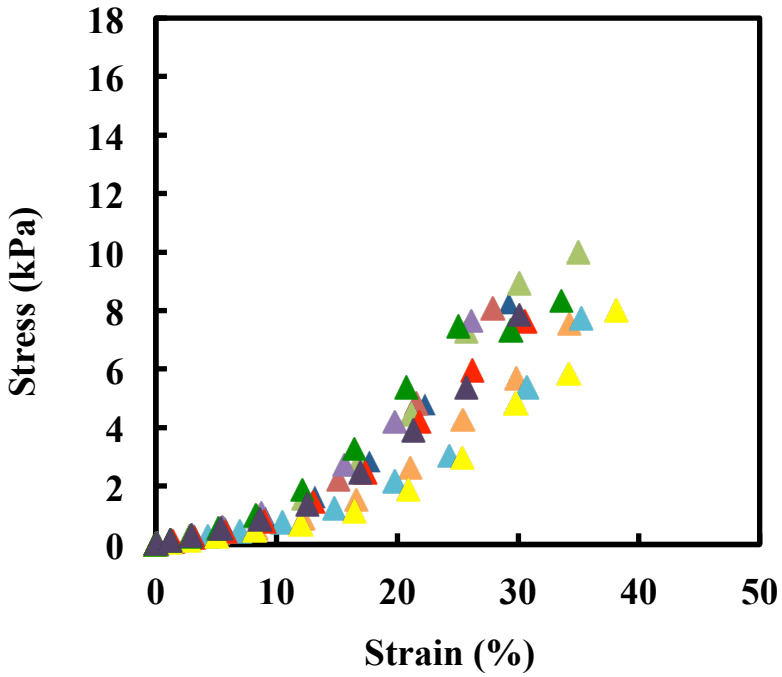

Figure B2 Stress-strain curves for the uniaxial compression of 0.1% w/w CNC QCA nanocomposites (n = 10).

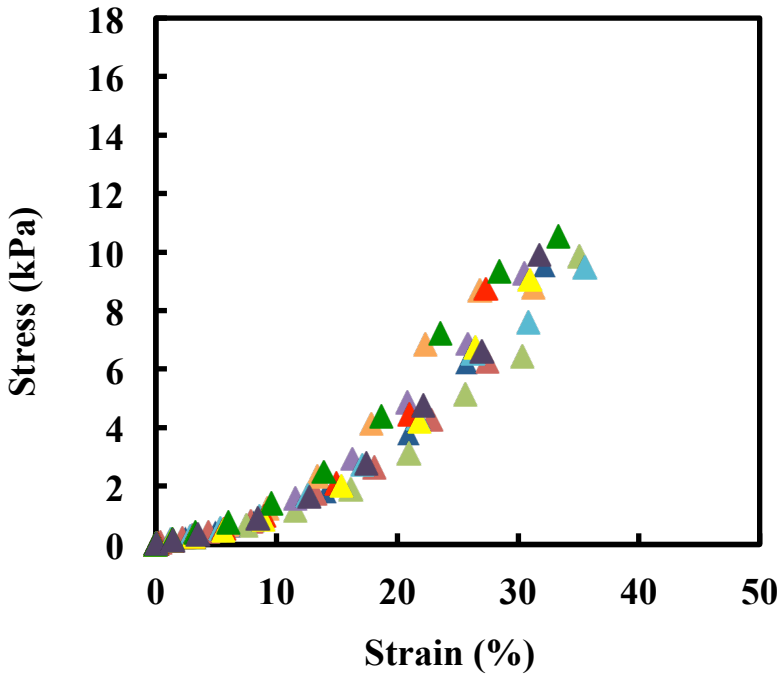

Figure B3 Stress-strain curves for the uniaxial compression of 0.2% w/w CNC QCA nanocomposites (n = 10).

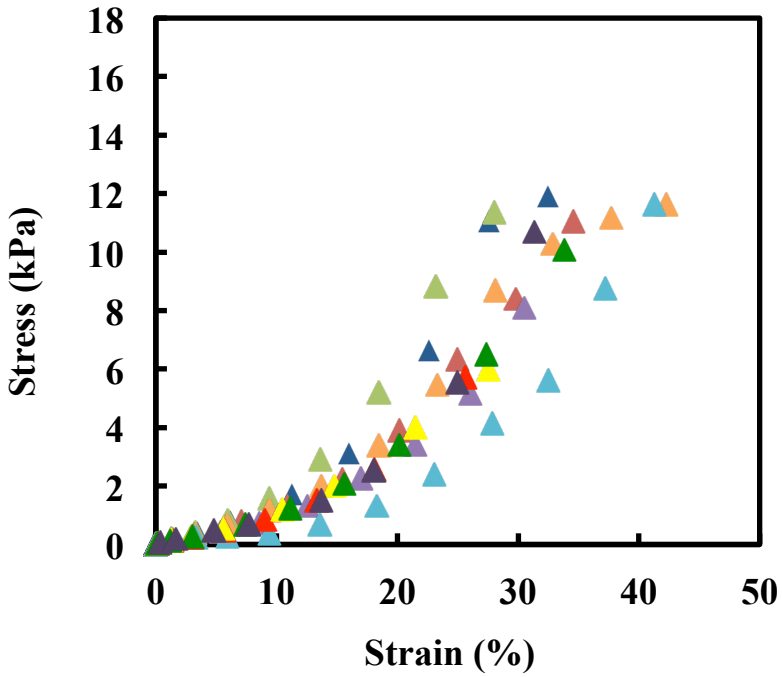

Figure B4 Stress-strain curves for the uniaxial compression of 0.3% w/w CNC QCA nanocomposites (n = 10).

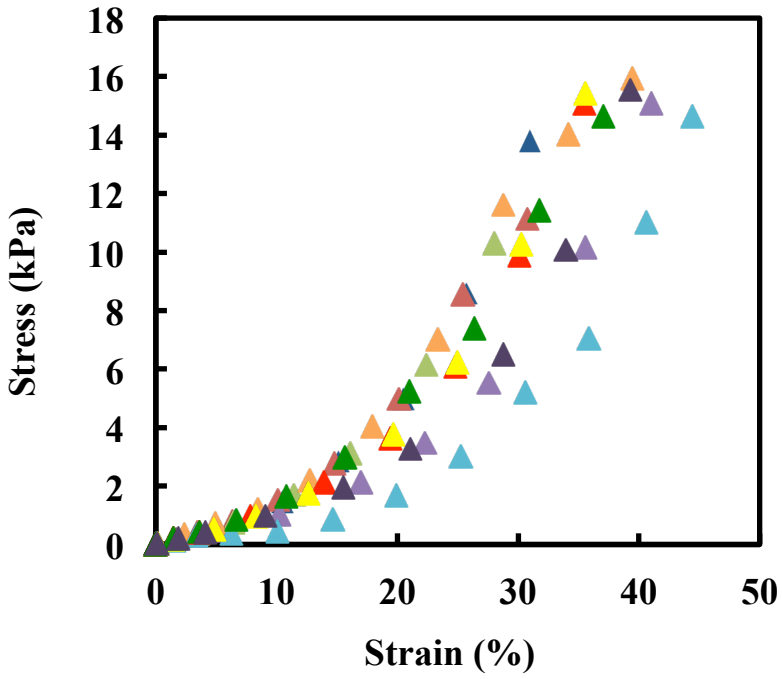

Figure B5 Stress-strain curves for the uniaxial compression of 0.6% w/w CNC QCA nanocomposites (n = 10).

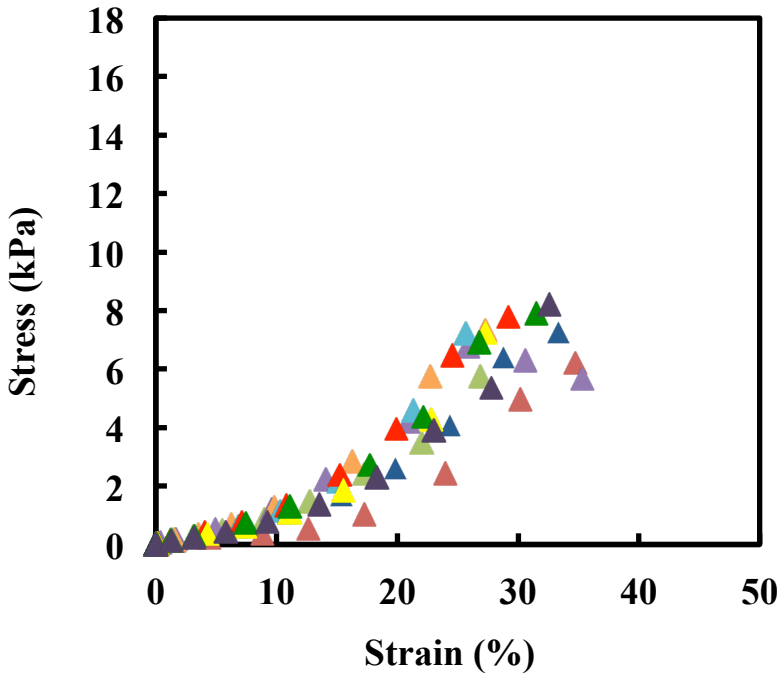

Figure B6 Stress-strain curves for the uniaxial compression of 0.1% w/w QCNC QCA nanocomposites (n = 10).

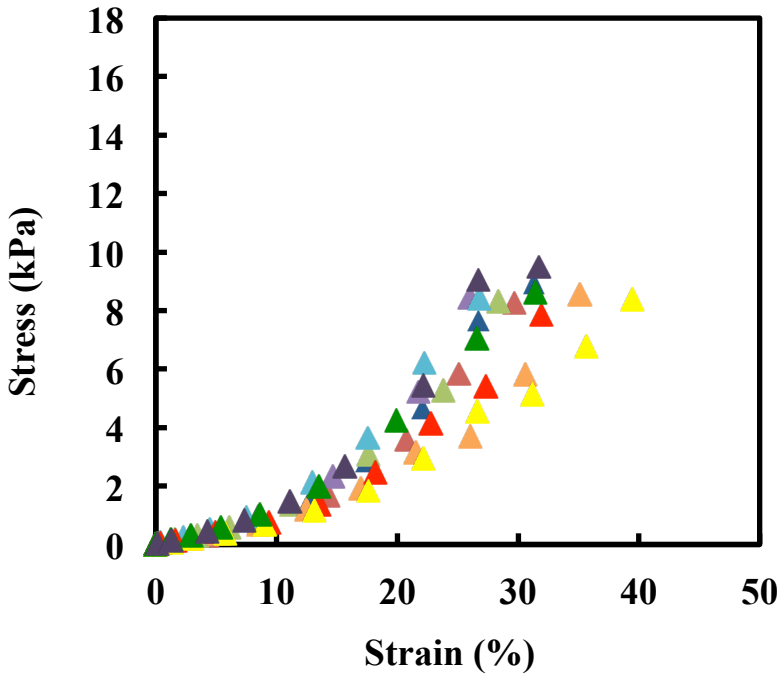

Figure B7 Stress-strain curves for the uniaxial compression of 0.2% w/w QCNC QCA nanocomposites (n = 10).

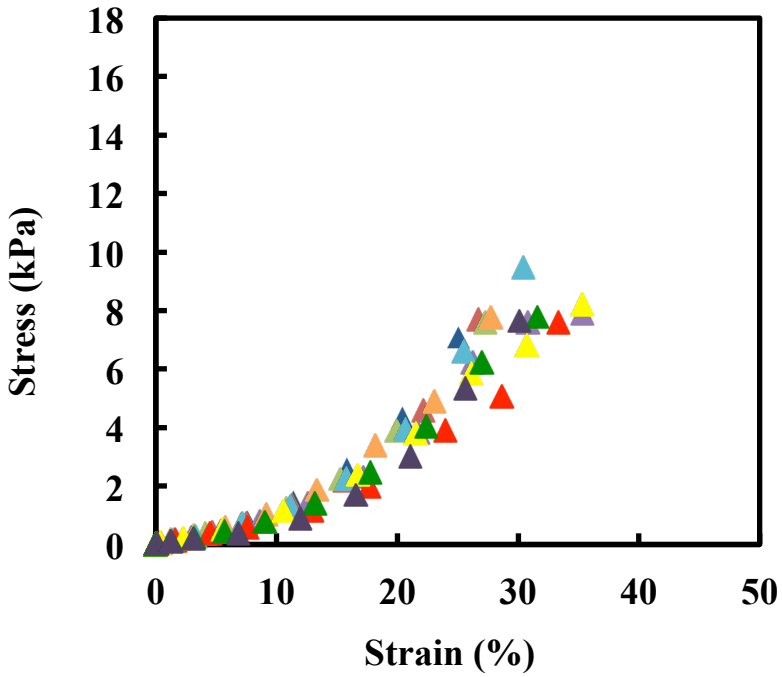

Figure B8 Stress-strain curves for the uniaxial compression of 0.3% w/w QCNC QCA nanocomposites (n = 10).

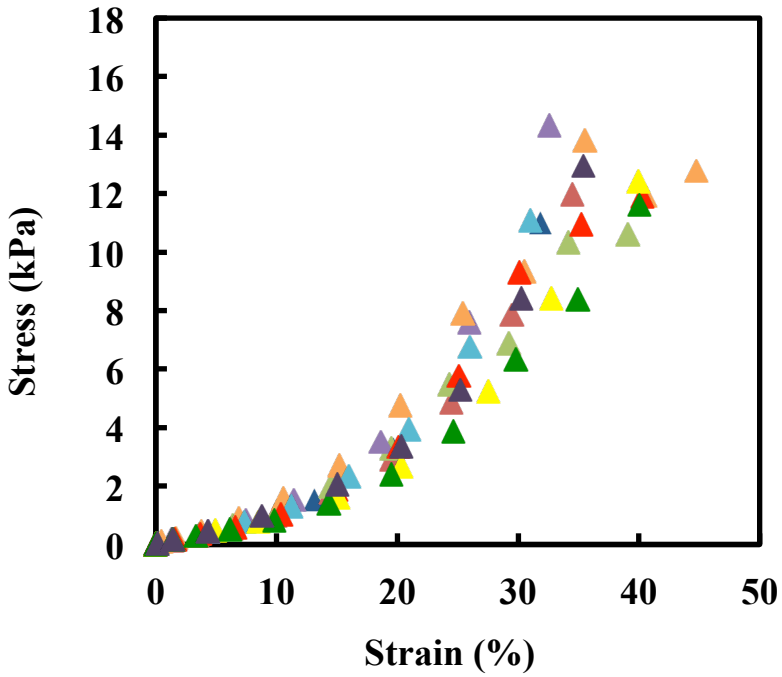

Figure B9 Stress-strain curves for the uniaxial compression of 0.6% w/w QCNC QCA nanocomposites (n = 10).